

SENSITIZER-LINKED SUBSTRATES AS
PROBES OF HEME ENZYME STRUCTURE
AND CATALYSIS

Thesis by

Alexander R. Dunn

In Partial Fulfillment of the Requirements for the
degree of

Doctor of Philosophy

CALIFORNIA INSTITUTE OF TECHNOLOGY

Pasadena, California

2003

(Defended 15 May, 2003)

© 2003

Alexander R. Dunn

All Rights Reserved

ACKNOWLEDGEMENTS

Caltech provided both my undergraduate and graduate education. Accordingly, I have a few more people to thank than usual. Bob Grubbs offered me (a freshman with few qualifications) a spot in his lab the first time we met, and has been incredibly supportive ever since. Geoff Coates was a dedicated and patient teacher, who taught me organic synthesis, and more importantly, to do “simple things that work.” John Bercaw, Dennis Dougherty, and Barbara Imperiali all taught inspiring courses that provided a large fraction of my scientific knowledge.

Harry Gray has been a fantastic advisor. I’ve benefited greatly from his generosity with his time, resources, and ideas, and enjoyed a unique degree of freedom in my research. I was (and am) particularly appreciative for the opportunity to work in his research group following my return to Caltech. Jay Winkler provided valuable help with time-resolved spectroscopy and data analysis. Doug Rees allowed me to use his laboratory equipment and taught me a great deal about protein structure. Our collaborators at Scripps, Anna-Maria Hays, Dave Goodin, Libby Getzoff, and Dave Stout, helped broaden my research horizons and have been a great bunch of people to work with.

I’ve been fortunate to work with many brilliant and kind fellow students and postdocs during my time in the Gray group. Ivan Dmochowski was an ideal mentor for a beginning graduate student. Brian Crane and Alex Bilwes were likewise generous with their time in teaching me protein crystallography. I’ve had a great time working (and not working) with Wendy Belliston, Brian Leigh, and Steve Contakes. In addition, I greatly appreciate the friendship of Libby Mayo, Jeremiah Miller, Xenia Amashukeli, Jeremy

Weaver, and Will Wehbi. During the past year of traveling back and forth between Stanford and Caltech, I've been hosted and treated royally by Brian, Wendy, Xenia, Libby, Jeremy, and Will. Thanks!

I thank those who had little to do with my research, but everything to do with my success. Kathryn Todd's help in proofreading this thesis is only the most recent example of the support and understanding she has given me during the past 5 years. My parents instilled in me an appreciation of knowledge and culture. My uncle, Michael Dunn, introduced me to research science by inviting me to work in his lab at UCR. Finally, I thank my grandfather, Fred Dunn, a self-taught archaeologist, geologist, and historian, whose example inspired his children and grandchildren to be curious about the world around them.

ABSTRACT

Ruthenium-diimine sensitizers (Ru-wires) with the structure $[\text{Ru}(\text{L}_2)\text{L}]^{2+}$, where L' is a perfluorobiphenyl bridge connecting 4,4'-dimethylbipyridine to the substrate adamantane or the heme ligand imidazole, bind to cytochrome P450cam with micromolar dissociation constants. Ru-wires can be used to trigger redox reactions on timescales faster than those achievable using conventional stopped-flow techniques: photoinduced heme reduction with an imidazole-terminated Ru-wire occurs in 40 ns. The large variation in ET rates among the Ru-diimine:P450 conjugates strongly supports a through-bonds model of Ru:heme electronic coupling.

The Ru-wires also bind the murine inducible nitric oxide synthase (NOS) oxidase domain, both in the active site and to the hydrophobic surface patch that interacts with the NOS reductase domain. Rhenium-diimine probes with the structure $[\text{Re}(4,7\text{-dimethyl phenanthroline})(\text{CO})_3\text{L}]^+$, where L = imidazole- C_{12}F_8 -imidazole (Re-im) or imidazole- C_{12}F_9 (Re-F₉bp), bind in the NOS active site. Re-im ($K_d = 6$ nM) ligates the heme iron. Re-F₉bp ($K_d = 3.4$ μM) produces a partial low- to high-spin conversion of the heme. Compounds with properties similar to the Ru- and Re-diimine probes may provide novel means of NOS inhibition.

Luminescent dansyl probes were designed to target cytochrome P450cam. D-4-Ad (dansyl- C_4 -adamantane) luminescence is quenched by Förster energy transfer upon binding ($K_d = 0.83$ μM), but is restored when the probe is displaced from the active site by camphor. In contrast, D-8-Ad ($K_d \sim 0.02$ μM) is not displaced from the enzyme even in the presence of a large excess of camphor. Probes with properties similar to those of D-4-Ad potentially could be useful for screening P450 inhibitors.

Crystal structures of P450cam bound to ruthenium diimine and dansyl probes reveal an open enzyme conformation that allows substrate access to the active center via a 22-Å deep channel. Interactions of the probes with the channel illustrate the importance of exploiting protein dynamics in inhibitor design. Movements of the F, G and B' helices couple to conformational changes in active site residues implicated in proton pumping and dioxygen activation. Common conformational states among P450cam and homologous enzymes indicate that the structural flexibility of the F/G helix region allows the 54 human P450s to oxidize diverse substrates.

TABLE OF CONTENTS

Acknowledgements.....	iii
Abstract.....	v
Table of Contents.....	vi
Chapter 1: Introduction.....	1
Background.....	5
Förster Energy Transfer.....	5
Electron Transfer.....	6
Ruthenium <i>tris</i> -bipyridine.....	10
Ligand-protein Interactions.....	10
Cytochromes P450.....	13
Cytochrome P450 Reaction Mechanism.....	17
Nitric Oxide Synthase.....	20
NOS Reaction Mechanism.....	21
Previous and Concurrent Work.....	24
Ru-wires for Cytochrome P450cam.....	24
Dual SLS and Enzyme Engineering: Cytochrome <i>c</i> Peroxidase.....	29
Electrochemistry at a Deeply Buried Active Site: Amine Oxidase.....	38
References.....	41
Chapter 2: Nanosecond Photoreduction of Cytochrome P450cam by	
Channel-Specific Ru-diimine Electron Tunneling Wires.....	49
Abstract.....	50
Introduction.....	51
Materials and Methods.....	56
General.....	56
Reduction of P450cam.....	56
Transient Spectroscopy.....	57
Binding Constants.....	58
ET Rate Constants.....	59
Förster Energy Transfer.....	63
Calculation of Buried Surface Area.....	63

Results.....	64
Synthesis.....	64
Binding.....	64
Electron Transfer.....	69
Discussion.....	77
ET kinetics.....	82
Concluding Remarks.....	87
Acknowledgement.....	88
References and Notes.....	90
Chapter 3: Probing the Open State of Cytochrome P450cam with	
Ruthenium-linker Substrates.....	97
Abstract.....	98
Introduction.....	99
Materials and Methods.....	100
Crystallization and Data Collection.....	100
Structure Determination of P450:RuF ₈ bp-Ad.....	101
Results and Discussion.....	102
Ru-substrate Binding Reveals a Substrate Access Channel	
in P450cam.....	102
Interactions of Ru-substrates with P450cam.....	114
Ru-F ₈ bp-Ad Interactions.....	115
Ru-C ₉ -Ad Interactions.....	118
F/G loop Movement Affects the P450cam Active Site.....	120
Solvation Changes Important for Substrate Binding and Catalysis...126	
Structural Flexibility makes Cytochrome P450 a	
Versatile Catalyst.....	127
Acknowledgement.....	128
References.....	129
Chapter 4: Fluorescent Probes for Cytochrome P450 Structural	
Characterization and Inhibitor Screening.....	134
Abstract.....	135

Introduction.....	136
Materials and Methods.....	143
Results and Discussion.....	143
Concluding Remarks.....	152
References and Notes.....	153
Chapter 5: Ruthenium- and Rhenium-diimine luminescent probes	
for Nitric Oxide Synthase.....	156
Abstract.....	157
Introduction.....	159
Materials and Methods.....	160
Results.....	161
Ru-wires.....	161
Re-wires.....	172
Discussion.....	184
Concluding Remarks.....	188
Acknowledgement.....	188
References and Notes.....	189
Appendix A: Synthesis and Characterization of Ru-wires.....	193
Syntheses.....	194
References.....	200
Appendix B: Dansyl Probe Syntheses and Characterization and	
D-8-Ad:P450cam Structure Determination.....	201
Syntheses.....	202
P450cam:D-8-Ad Crystallization and Data Collection.....	205
Structure Determination.....	205
Crystal data table.....	207
References.....	208
Appendix C: Matlab Deconvolution Scripts.....	209
Introduction.....	210
Matlab Scripts.....	211
References.....	216

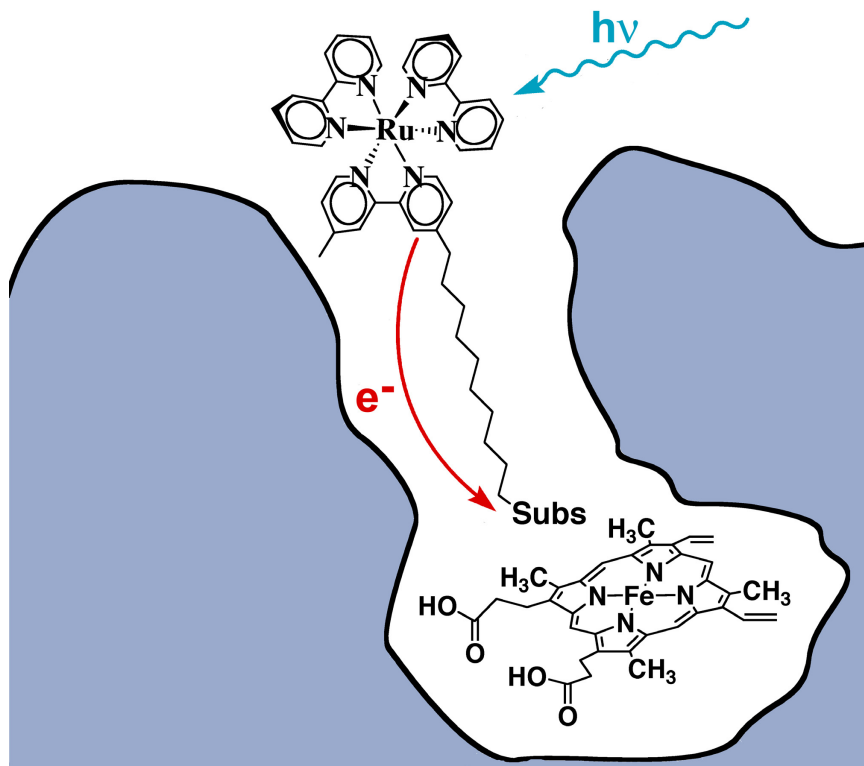
Chapter 1

Introduction

This thesis describes the use of photoactive molecules to study heme enzyme reaction mechanisms and structural dynamics. Our approach has been to attach a photosensitizer to an enzyme substrate by a covalent tether (Figure 1.1). The substrate provides the binding energy and specificity to bring the sensitizer to the target enzyme. Once the sensitizer is bound, a variety of photophysical and photochemical processes may be used to detect the presence of the enzyme, characterize its structure and dynamics, or trigger reactions within it.

Sensitizer-linked substrates (SLS) help to span the orders of magnitude between our sensory experience and chemically relevant lengths (cm vs. nm), times (s vs. ps), and numbers (moles vs. molecules). Förster energy transfer (FET) and photo-triggered electron transfer (ET) occur over nanometer distances, luminescence decay occurs on the pico- to microsecond timescales, and the detection of single fluorescent molecules is now a well-established technique.¹ In addition, the association of the sensitizer with the target enzyme through a substrate or inhibitor has several useful aspects. The sensitizer can act as a spectroscopic probe to characterize the interactions of the target enzyme with small molecules. In addition, the specificity of the enzyme:SLS interaction can potentially provide binding selectivity in chemically complex environments. Because preassociation of the enzyme and sensitizer circumvents the time restraints inherent to bimolecular diffusive reactions, SLS probes can be used to photochemically trigger reactions on the

Figure 1.1. A schematic representation of an SLS:enzyme conjugate. In this example, a ruthenium *tris*-bipyridyl photosensitizer reduces the heme upon excitation with 470 nm light. The substrate moiety (subs) mediates the binding of the SLS to the target enzyme. The linker serves both to connect the sensitizer to the substrate and to mediate electron tunneling from the Ru-diimine to the heme.



submicrosecond timescale. Unlike covalently labeled proteins, the SLS:enzyme conjugate can be formed immediately prior to the experiment, thus circumventing potential complications due to degradation of the enzyme:photosensitizer conjugate.

The remainder of the Introduction serves two purposes. The Background section contains information taken for granted in the remainder of the thesis. The topics covered are: Förster energy transfer, electron transfer theory, ruthenium *tris*-bipyridine photochemistry, enzyme-small molecule interactions, cytochrome P450, and nitric oxide synthase. The section entitled Previous and Concurrent Work describes SLS research that preceded or occurred simultaneously with the research described in the following chapters.

BACKGROUND

Förster energy transfer. Förster energy transfer (FET) is one form of radiationless transfer of energy from one molecule to another.^{2,3} In order for this process to occur the donor emission and acceptor absorption spectra must overlap. FET is modeled as the interaction of the donor and acceptor dipoles, and so has an r^6 distance dependence. This process is characterized by the equations (Eqns. 1-3):

$$k_E = k_0 \left(\frac{R_0}{r} \right)^6 \quad (1)$$

$$R_0^6 = 8.8 \cdot 10^{-5} (\kappa^2 n^{-4} \phi_0 J) \quad (2)$$

$$J = \frac{\int_0^\infty F_0(\lambda)E_A(\lambda)\lambda^4 d\lambda}{\int_0^\infty F_0(\lambda)d\lambda} \quad (3)$$

Here k_E is the rate of energy transfer, k_0 is the intrinsic decay rate of the donor, r is the donor-acceptor distance, R_0 is the characteristic distance of the Förster pair, κ^2 is an orientation factor (2/3 for a freely rotating donor or acceptor), n is the index of refraction, φ_0 is the donor luminescence quantum yield, λ is wavelength (nm), $F_0(\lambda)$ is the fluorescence emission spectrum, and $E_A(\lambda)$ is the acceptor absorption spectrum ($\text{M}^{-1}\text{cm}^{-1}$).

R_0 ranges from 10 to 70 Å, a lengthscale that corresponds nicely with the dimensions of typical proteins. R_0 increases with φ_0 and the overlap integral J . J in turn increases with the overlap of the donor and acceptor emission and absorption spectra, the strength of the acceptor absorption, and λ^4 . R_0 is thus easily tailored: Blue emission, weak absorption, and a small φ_0 produce a short R_0 , while red emission, strong absorption, and a large φ_0 produce a long R_0 .

Electron Transfer. Electron transfer (ET) through a protein can occur over distances of up to 20 Å. The rate of ET can be modeled in several ways. The most general treatment is (Eqn. 4):^{4,5}

$$k_{ET} = \left(\frac{4\pi^3}{h^2 \lambda k_B T} \right)^{1/2} \mathbf{H}_{AB}^2 \exp \left[\frac{-(\Delta G^\circ + \lambda)^2}{4\lambda k_B T} \right] \quad (4)$$

The key elements influencing the ET rate are the thermodynamic driving force ΔG , the reorganization energy λ , and the electronic coupling H_{AB} . The term λ is a measure of how much the electron donor and acceptor and their surroundings must distort in order for ET to occur. Hydrophobic solvents are insensitive to changes in charge distribution, and so lead to small λ 's; polar solvents result in large λ 's. Note that the rate of ET is maximized when $\Delta G = \lambda$.

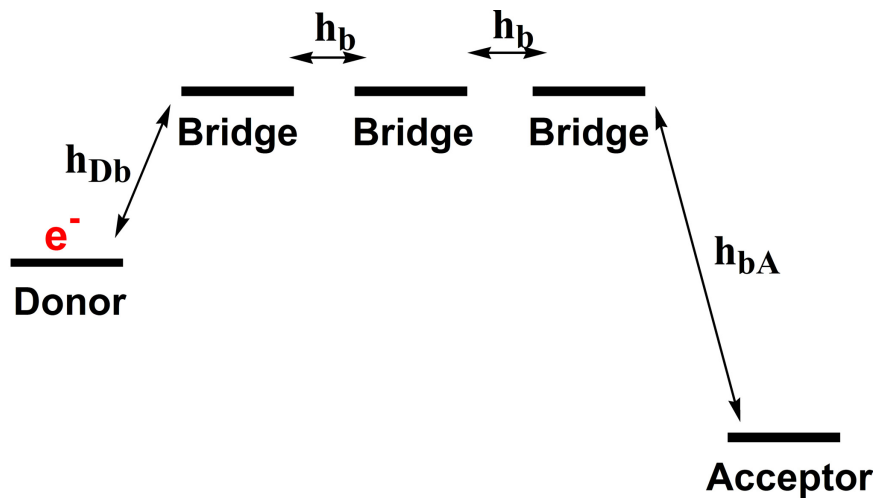
H_{AB} corresponds to the degree of electronic interaction between the donor and acceptor. In general, H_{AB} decreases exponentially with donor-acceptor spacing. Over larger distances the electronic coupling between the electron donor and acceptor is mediated by the intervening medium (Figure 1.2). It is useful to look at H_{AB} as resulting from communication across n identical bridging units (BU's), where $\Delta\varepsilon$ is the energetic gap between the donor and the unoccupied orbitals of the bridge, and h_{Db} , h_b and h_{bA} are couplings across the donor-bridge, bridge-bridge, and bridge-acceptor junctions (Eqn. 5):⁶⁻⁸

$$H_{AB} = \frac{h_{Db}}{\Delta\varepsilon} \left(\frac{h_b}{\Delta\varepsilon} \right)^{n-1} h_{bA} \quad (5)$$

Breaks in conjugation define BU boundaries. For spatially extended alkyl⁹⁻¹¹ and aromatic oligomers^{12,13} each BU decreases the ET rate by roughly a factor of 5 when $\Delta\varepsilon$ is large compared to $k_B T$. However, this simple behavior begins to break down when the

Figure 1.2. Schematic representation of superexchange-mediated electron tunneling.

The vertical dimension corresponds to the energetic potential experienced by the tunneling electron. In this simple model the bridging units are identical, and thus have identical bridge-bridge couplings and energies.

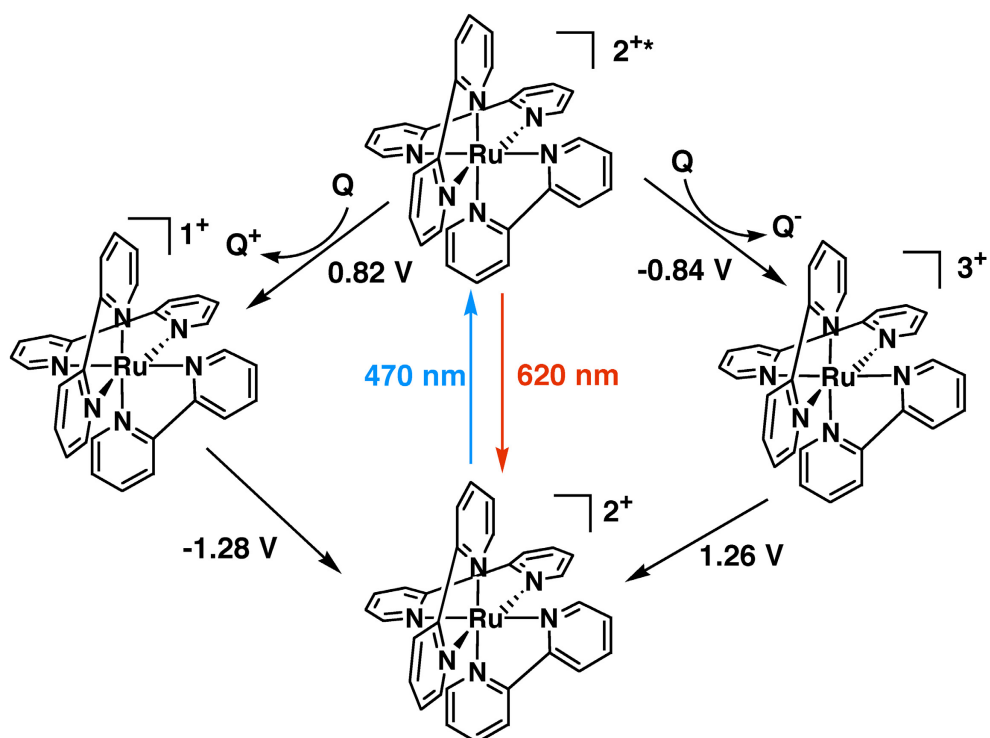


bridge is highly conjugated,^{14,15} structural dynamics control ET rates,¹⁶ or $\Delta\epsilon$ is small enough for the charge to “hop” along the bridge.¹⁷

Ruthenium tris-bipyridine. No Gray group thesis would be complete without a discussion of $[\text{Ru}(\text{bpy})_3]^{2+}$ ($\text{Ru}(\text{bpy})_3$) photophysics and chemistry (Figure 1.3). Excitation of $\text{Ru}(\text{bpy})_3$ with 470 nm light results in the promotion of an electron from the ruthenium atom to the bipyridyl ligands. This excited state has a lifetime of about a microsecond, and decays with the emission of a red photon (~620 nm) with a quantum yield of 0.042.¹⁸ The $\text{Ru}(\text{bpy})_3$ excited state is both a good oxidant (0.82 V NHE) and reductant (-0.84 V NHE). This remarkable property can be rationalized by considering the excited state to be a combination of Ru^{3+} and a bipyridine radical anion. The excited state can be intercepted with biomolecular quenchers to generate the longer-lived oxidant $[\text{Ru}(\text{bpy})_3]^{3+}$ or the reductant $[\text{Ru}(\text{bpy})_2\text{bpy}^-]^+$. Because of these photochemical properties, $\text{Ru}(\text{bpy})_3$ derivatives have been used extensively to study ET in proteins,⁵ and also to deliver holes and electrons to the active sites of the enzymes horseradish peroxidase¹⁹ and cytochrome *c* oxidase.^{20,21}

Ligand-protein interactions. The design of a molecule that will bind to a protein of interest may at first seem like a daunting task. However, over the past 5 years members of our research group have produced probes that bind cytochrome P450, nitric oxide synthase, amine oxidase, cytochrome *c* peroxidase, and myeloperoxidase, demonstrating

Figure 1.3. Ru(bpy)₃ photochemistry. Bimolecular reaction with a quencher (Q) can be used to generate [Ru(bpy)₃]³⁺ (1.26 V NHE) or [Ru(bpy)₂(bpy)⁻]¹⁺ (-1.28 V NHE).

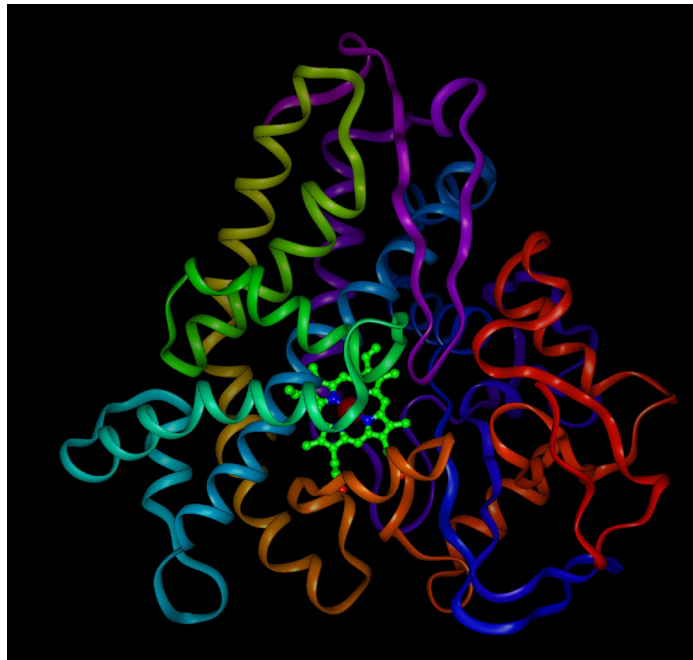


that the production of enzyme-binding photochemical probes is feasible. The simplest way to design an SLS is to elaborate upon a known substrate or inhibitor. If the crystal structure of the target enzyme is known, simple modeling greatly improves the chances of producing a probe molecule that binds to the target enzyme. While more sophisticated methods may be useful, manual docking of the proposed SLS into the active site has thus far been sufficient to uncover obvious deficiencies in probe design. Experience suggests that an iterative SLS design process is effective. It has proven far more efficient to synthesize multiple rounds of simple probe molecules than to attempt the synthesis of a more complex “optimal” SLS.

Once a functioning probe molecule exists, x-ray crystallographic determination of the structure of the probe:enzyme conjugate has proven to be very valuable. Structural characterization is helpful both in interpreting solution-phase spectroscopy and in the design of second and third generation probes. As will be discussed (Chapter 3), the structures of the probe-bound enzymes have also proven to be intrinsically interesting.

Cytochromes P450. Cytochromes P450 comprise a superfamily of heme monooxygenases characterized by a conserved fold and a cysteine-ligated heme (Figure 1.4). In particular, the ability of P450s to hydroxylate aliphatic carbon by generating a reactive heme-oxygen species has stimulated much research ($R-H + O_2 + 2H^+ + 2e^- \rightarrow R-OH + H_2O$).²² Bacteria, eukaryotes and archaeobacteria all express cytochrome P450s.²³

Figure 1.4. Ribbon diagram of cytochrome P450cam.²⁴ The fold is unique to cytochromes P450, and is highly conserved among all structurally characterized P450s despite low sequence similarities.



Cytochrome P450 genes make up a sizable fraction of expressed genes in known genomes: 0.63% in *Drosophila* (86 known genes), about 1.0% in *Arabidopsis* (270 known genes) and about 0.2% in humans (54 known genes).^{25,26}

Over 22,000 papers concerning P450 enzymes have been written in the past 10 years. This prolixity stems largely from the medical importance of these enzymes. Substrate-specific cytochromes P450 play major roles in steroid and eicosanoid biosynthesis, and thus constitute important drug design targets.²⁷⁻³¹ Inhibitors of aromatase (P450 19) have passed phase III trials in the treatment of breast cancer.²⁹ Cytochrome P450 14-sterol demethylases (CYP51) are drug targets for both antifungal agents and cholesterol lowering drugs.^{30,31}

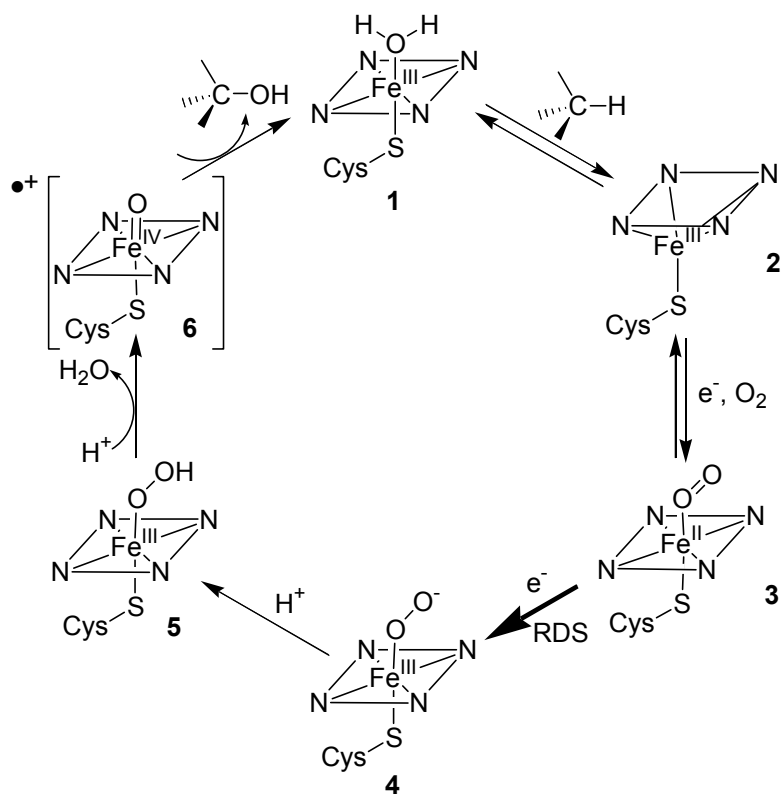
In contrast, hepatic P450s help metabolize a wide range of foreign compounds, including environmental contaminants and drugs. P450 3A4 metabolizes about half of all drugs in use.³² Although the total amount of P450's expressed varies only 3-fold in individuals, expression levels of individual P450 isozymes can vary by 1-3 orders of magnitude, leading to dramatic differences in the metabolism of xenobiotics.^{33,34} Adverse drug reactions, for instance, to Prozac,³⁵ result from individual variations in hepatic P450s.³⁶ The reactions catalyzed by cytochromes P450 are not always benign:

P450 1A2 N-hydroxylates aromatic heterocycles found in cigarette smoke and charred food, converting them into potent carcinogens.³⁷

Cytochrome P450 reaction mechanism. Both this thesis and the majority of mechanistic P450 studies employ cytochrome P450cam, a prototypical P450 from the soil bacterium *Pseudomonas putida*. The canonical P450 mechanism is shown in Figure 1.5. The steps through intermediate **3** are well established: Substrate binding displaces water from the heme iron, converting it from low-spin, six-coordinate to high-spin, five-coordinate (**2**).³⁸ The spin shift is accompanied by a change in the ferric heme reduction potential from -150 to -300 mV, which makes its reduction by putidaredoxin (Putd) thermodynamically feasible.³⁹ Dioxygen binds to the reduced heme, producing a well-characterized ferrous-dioxygen intermediate (**3**).⁴⁰

The addition of the second reducing equivalent by Putd is the last kinetically resolvable step in the catalytic cycle under biological conditions. Low-temperature ENDOR measurements indicate that reduction of **3** results in a ferric-peroxy intermediate, which rapidly protonates (**5**).⁴¹ In these experiments the next observed species is hydroxylated camphor and the resting enzyme. Based on the mechanisms of many other heme oxidases, it is assumed that the active, hydroxylating species is a ferryl cation radical (**6**) known as compound I.⁴² Recent results show that compound I can

Figure 1.5. The canonical cytochrome P450 catalytic cycle. ET constitutes the rate determining step (RDS) in catalysis under biologically relevant conditions.



indeed be generated using organic peracids.^{43,44} However, debate persists as to whether compound I, the peroxy intermediate **5**, or other species constitute the key oxidizing intermediate. Some evidence suggests that the oxidizing intermediate may be substrate and isozyme dependent.⁴⁵

Nitric oxide synthase. Nitric oxide (NO) is recognized as a ubiquitous biological second messenger, acting in a myriad of circumstances that include neuronal development, regulation of blood pressure, apoptosis, neurotransmission, and immunological response.⁴⁶⁻⁵² These diverse functions depend on the production of NO by nitric oxide synthase (NOS), an enzyme that catalyzes the transformation $L\text{-Arg} + 2\text{O}_2 + 3/2(\text{NADPH} + \text{H}^+) \rightarrow L\text{-citrulline} + \text{NO} + 2\text{H}_2\text{O} + 3/2 \text{NADP}^+$.⁵³ Like cytochrome P450, the NOS active site contains a cysteine-ligated heme. However, the active site also contains a tetrahydrobiopterin cofactor (H₄B) that is essential for catalysis.

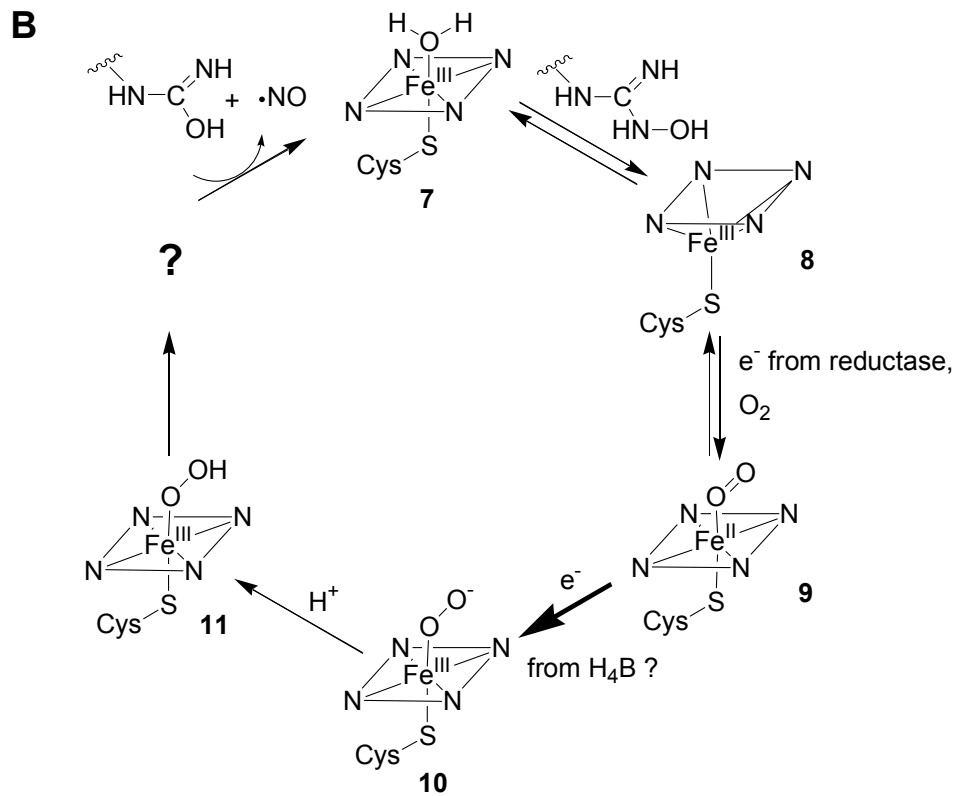
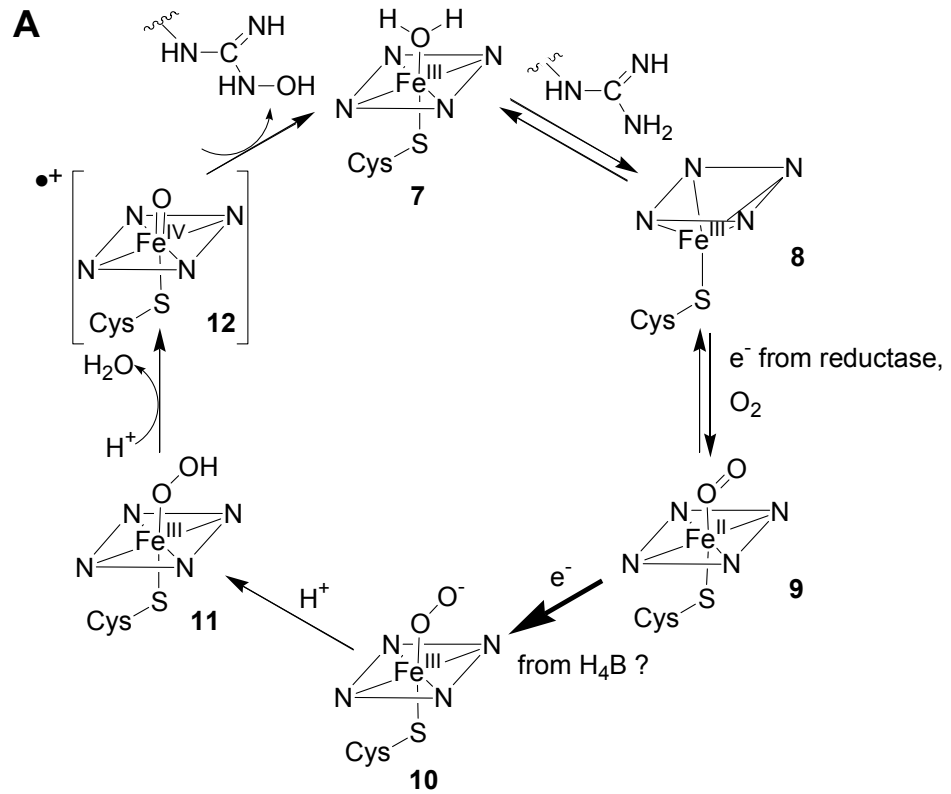
NOS was isolated independently from neuronal (nNOS), endothelial (eNOS), and immune system cells (iNOS).⁵⁴⁻⁵⁸ A more distantly related NOS has also been isolated from the bacterium *Bacillus subtilis*.⁵⁹ Subsequent research has shown that the mammalian NOS isozymes occur with a complex distribution in a wide variety of tissues. Abnormal nNOS activity has been implicated in a variety of diseases, including both Parkinson's and Alzheimer's disease.^{49,60} The isozyme eNOS is expressed in smooth muscles, including those lining blood vessels.⁴⁷ Local production of NO triggers the

relaxation of the vascular tissue, leading to a reduction in blood pressure. In addition to vasodilation, eNOS also modulates angiogenesis.⁶¹ iNOS is thought to be essential in fighting tuberculosis,⁶² but is also involved in the often destructive inflammation response to infection or injury.⁵¹

NOS reaction mechanism. The complete NOS enzyme consists of a heme-containing oxidase domain and an FMN- and FAD-containing reductase domain that are connected by a calmodulin-binding linker.^{54,63,64} The reductase domain binds NADPH and shuttles electrons into the oxidase domain. NOS functions as a dimer, with the reductase domain from one half providing electrons to the oxidase domain of the second half.^{65,66}

The catalytic mechanism of NOS is thought to be analogous to that of cytochrome P450 in many respects (Figure 1.6). Like P450, a compound I species is thought to catalyze the conversion of arginine to N-hydroxyarginine.⁶⁷ However, current evidence does not rule out other potential hydroxylating intermediates, notably ferric-peroxy species.⁶⁸ The mechanism for the oxidation of N-hydroxyarginine to citrulline and NO has been proposed to be catalyzed by ferric-peroxy or superoxy species.⁶⁸ Intriguingly, the conversion of N-hydroxyarginine to NO and citrulline formally requires oxidation by only one electron. This unusual stoichiometry has led some to suggest that the nitroxyl anion (NO^-) may be the initial product formed.⁶⁴ Current evidence suggests that H_4B

Figure 1.6. NOS catalytic mechanism. Arginine hydroxylation (A) is thought to follow a mechanism similar to that of P450. Current evidence suggests that H₄B acts as a temporary electron donor, and is presumably re-reduced by the reductase domain after catalysis is complete. The production of NO from N-hydroxyarginine (B) is poorly understood. Numerous mechanisms involving the reaction of intermediates **9**, **10**, **11** or **12** with N-hydroxyarginine have been proposed. The observation of a pterin radical during single turnover experiments suggests that a two-electron reduced oxygen intermediate such as **10**, **11** or **12** plays some part in the mechanism.



donates an electron during both catalytic cycles.⁶⁹ Despite this clear catalytic role, it is not clear why NOS requires H₄B while cytochrome P450 does not.

PREVIOUS AND CONCURRENT WORK

Ru-wires for P450cam. The original impetus for the creation of sensitizer-linked substrates was the desire to observe the fleeting intermediates in P450 catalysis (Figure 1.5). In order to observe intermediates **5** and **6**, Ivan Dmochowski *et al.* sought to use Ru(bpy)₃-functionalized P450cam substrates (Ru-wires) to rapidly reduce the ferrous dioxygen intermediate **3**, thus replacing the sluggish reduction by Putd with a rapid photochemical trigger. The initial Ru-wires investigated consist of a Ru(bpy)₃ moiety connected to adamantane, imidazole, or ethylbenzene by an alkyl linker of varying length (Figure 1.7).⁷⁰ The Ru-wires bind P450cam with micromolar K_d's, as evidenced by changes to the heme absorption spectrum and FET from the Ru-diimine excited state to the heme Q-bands (Table 1.1).⁷¹ Interestingly, neither the adamantyl nor imidazole groups are necessary for binding: Ru-wires terminating in an alkyl chain bind to the enzyme, suggesting that interactions of the enzyme with the Ru-diimine and linker moieties provide the bulk of the binding energy.

The crystal structure of Ru-C₉-Ad bound to P450cam was determined to 1.55 Å resolution by Ivan Dmochowski and Brian Crane.⁷¹ Preliminary analysis showed that a

Figure 1.7. First generation Ru-wires. The $\text{Ru}(\text{bpy})_3$ photosensitizer is connected to adamantane, ethylbenzene, or the heme ligand imidazole through an alkyl chain of varying length.

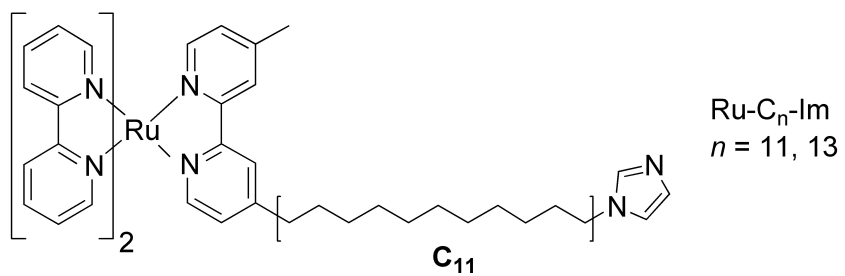
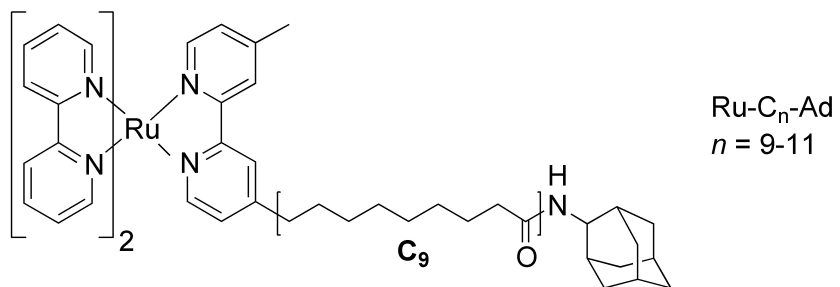
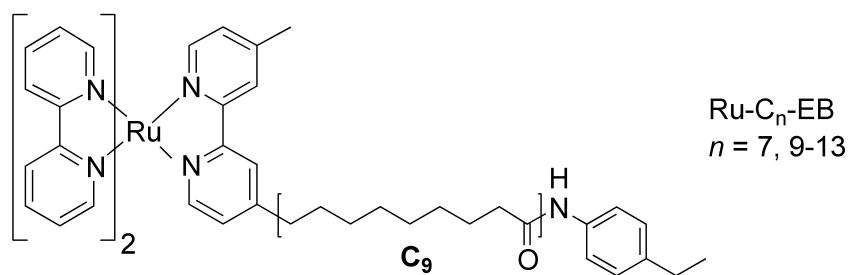


Table 1.1. Ru-wire dissociation constants and Ru-Fe distances derived from FET measurements.

Compound	K_d , μM	Ru-Fe, \AA
Ru-C ₁₃ -EB	1.7 ± 0.4	20.6 ± 0.2
Ru-C ₁₂ -EB	1.5 ± 0.3	20.5 ± 0.2
Ru-C ₁₁ -EB	0.9 ± 0.4	20.1 ± 0.3
Ru-C ₁₀ -EB	0.9 ± 0.4	19.9 ± 0.1
Ru-C ₉ -EB	0.7 ± 0.1	19.4 ± 0.1
Ru-C ₇ -EB	6.5 ± 1.3	19.5 ± 0.1
Ru-C ₉ -Ad	0.8 ± 0.3	21.0 ± 0.3
Ru-C ₁₁ -Ad	0.7 ± 0.2	21.4 ± 0.2
Ru-C ₁₃ -Im	4.1 ± 1.1	21.2 ± 0.1
Ru-C ₁₁ -Im	> 50	NA

conformational change opens a 21-Å deep channel in order to allow Ru-C₉-Ad access to the active site. The Ru-Fe distance seen in the crystal structure agrees well with that calculated from the rate of energy transfer observed in solution, demonstrating the utility of FET calculations for characterizing SLS:enzyme interactions.

The FET-derived Ru-heme distances for a series of ethylbenzene Ru-wires remains roughly constant for varying alkyl chain lengths (Table 1.1), indicating that an optimal Ru-heme distance exists in the Ru-wire:P450 conjugate.⁷¹ In contrast, Ru-C₁₃-Im binds P450cam ($K_d = 4.1 \mu\text{M}$), while Ru-C₁₁-Im does not. Evidently, the imidazole tip must ligate the heme iron in order for binding to occur, suggesting a substantial energetic penalty for its sequestration in the hydrophobic P450 active site. This result demonstrates that sensitive binding discrimination is possible with properly designed probe molecules.

As synthesized, the Ru-wires consist of a racemic mixture of Δ and Λ stereoisomers. However, the Δ and Λ forms of Ru-C₉-Ad were successfully separated using chiral chromatography. The isomers bind P450cam with similar dissociation constants ($K_d(\Delta) = 190 \text{ nM}$; $K_d(\Lambda) = 90 \text{ nM}$), corresponding to a difference in binding energies of $0.46 \text{ kcal mol}^{-1}$.⁷² Detailed analysis shows that the apparent K_d for the racemate is not the average of the stereoisomer K_d 's.⁷³

P450cam hydroxylates Ru-C₉-Ad when supplied with electrons via the natural NADH/putidaredoxin reductase/Putd reduction relay.⁷⁴ Ru-C₉-Ad hydroxylation occurs

at only 1.6% the rate of camphor hydroxylation, and only 10% of the electrons supplied by NADH go to product formation. Presumably the rest are diverted to the formation of reduced oxygen species such as superoxide or hydrogen peroxide.⁷⁵ The ability of P450cam to hydroxylate a molecule so structurally different from camphor is remarkable. As discussed in Chapter 3, Ru-wire turnover supports the hypothesis that the structural flexibility inherent in the P450 fold allows cytochromes P450 to hydroxylate structurally diverse substrates.

Photochemically reduced or oxidized Ru-wires transfer electrons or holes to the P450cam ferric heme with time constants of around 50 μ s (Figures 1.8, 1.9),⁷⁰ rates that are typical for ET through saturated bonds over comparable distances. These results demonstrate that it is in principle possible to trigger reactions in the buried active sites of proteins on the sub-millisecond timescale.

Dual SLS and enzyme engineering: cytochrome *c* peroxidase. The removal of the residues thought to mediate ET to the heme of cytochrome *c* peroxidase (CCP) results in a ligand-binding channel (Figure 1.10).⁷⁶ Hays *et al.* describe a dansyl-functionalized peptide that binds within this channel (Figure 1.11).⁷⁷ Partial unfolding and renaturation of the CCP mutant in the presence of **13** or **14** results in the kinetic trapping of the peptide within the channel. In contrast to cytochrome P450, peptide binding depends crucially on the replication of hydrogen bonding and salt bridging interactions present in

Figure 1.8. The flash-quench sequence for delivering electrons or holes into the active site of P450cam. The Ru-wire is excited with 470 nm light (Ru*), and intercepted with either $\text{Co}(\text{NH}_3)_6^{3+}$ or *para*-methoxy-N,N-dimethylaniline (PMDA) to generate the oxidized (Ru³⁺) or reduced (Ru¹⁺) Ru-wire. The photochemically generated hole or electron tunnels to the heme on the millisecond timescale, forming a heme cation radical or ferrous heme.

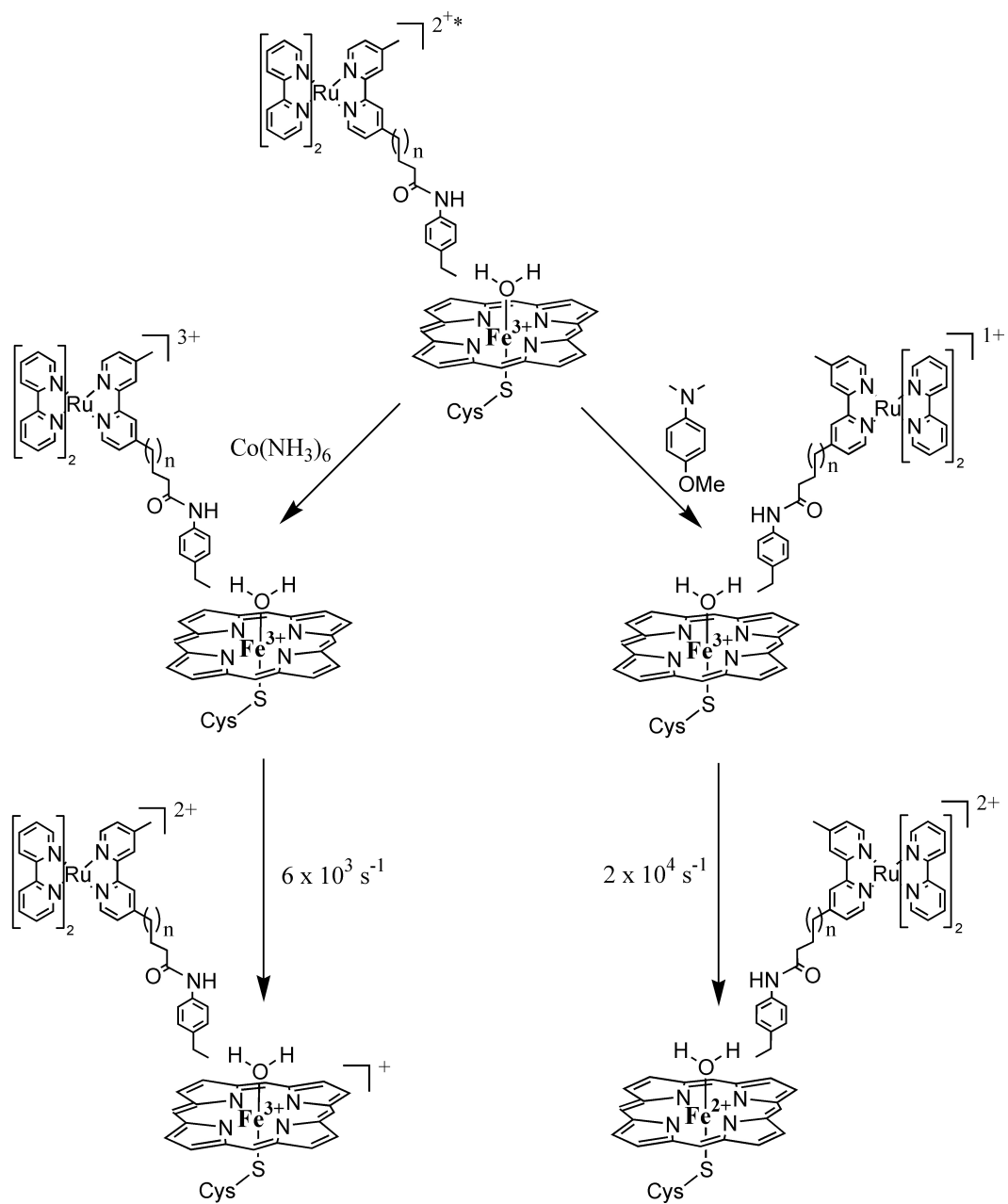


Figure 1.9. Transient absorption difference kinetics showing the reduction of P450cam by photochemically generated $[\text{Ru}^{\text{I}}\text{-C}_{13}\text{-Im}]^+$ (10 μM Ru-C₁₃-Im, 20 μM P450cam, 20 mM PMDA). Figure from ref. 73 (used with permission).

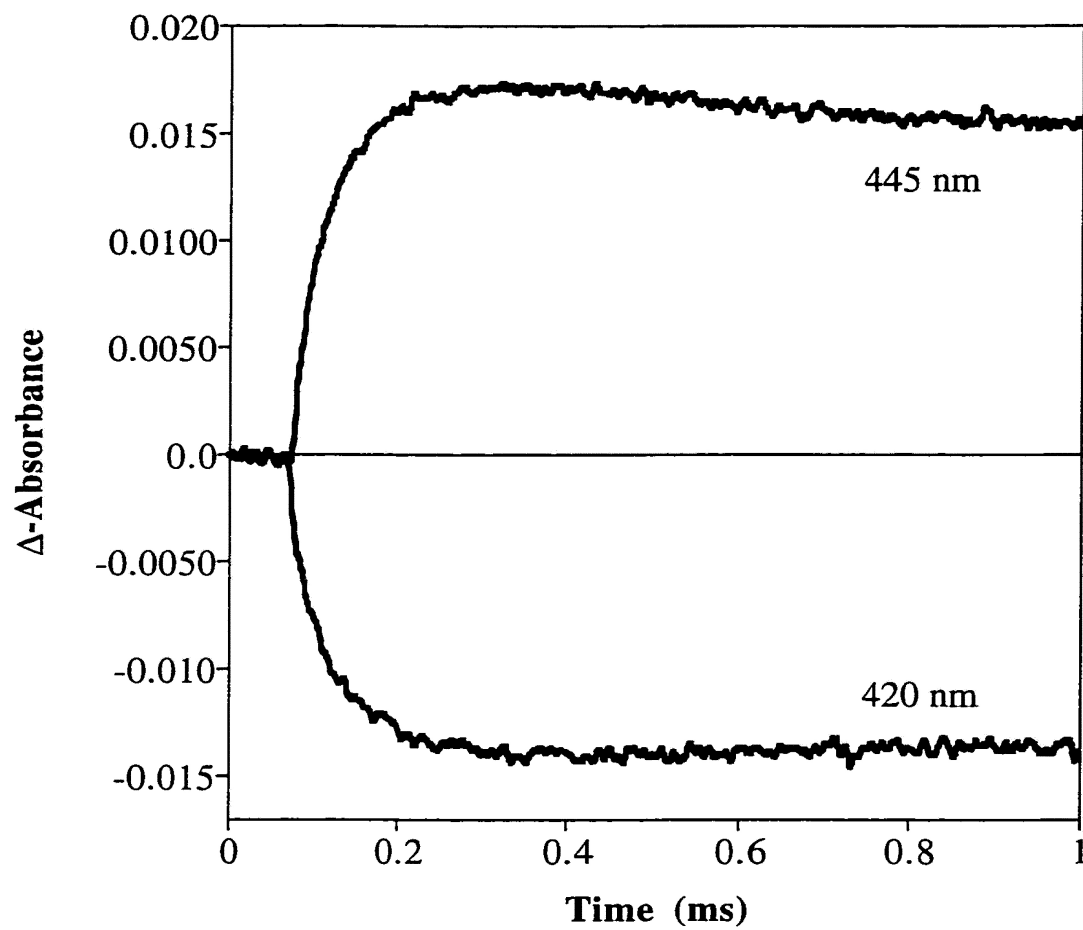


Figure 1.10. Crystal structure of the channel-containing CCP mutant (blue) overlaid with wild-type CCP (white). The mesh shows the surface of the protein, including the channel that reaches deep into the enzyme. The deleted residues are shown in cyan.

Figure provided by Anna-Maria A. Hays.

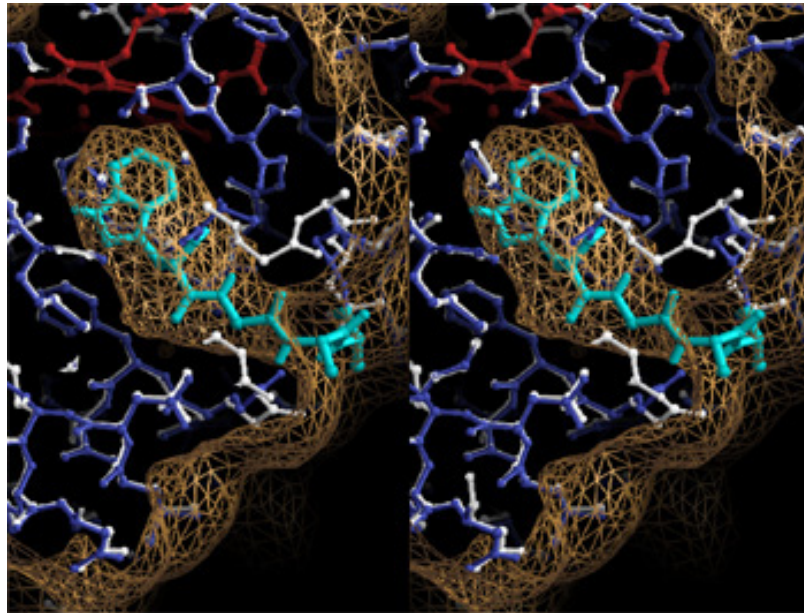
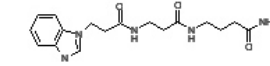
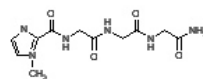
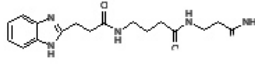
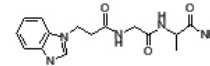
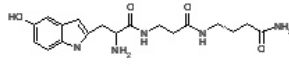
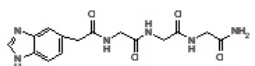
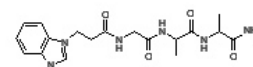
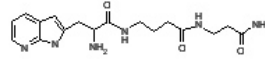
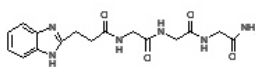
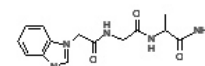
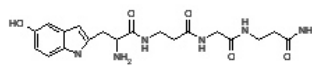
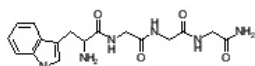
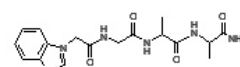
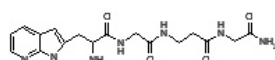
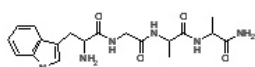
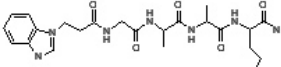
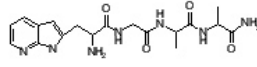
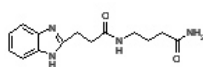


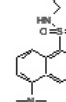
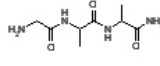
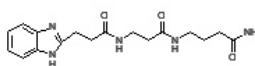
Figure 1.11. Amide oligomers designed to bind in the artificial CCP channel. Only **13** and **14**, which mimic the hydrogen-bonding pattern of the native peptide, bind to the enzyme. Figure provided by Anna-Maria A. Hays.



13



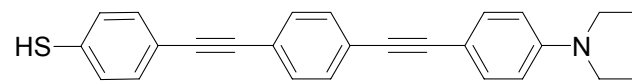
14



the native enzyme. These observations demonstrate that not all enzymes possess the structural flexibility of cytochrome P450 (Chapter 3).

Electrochemistry at a deeply buried active site: amine oxidase. The enzyme amine oxidase (AO) catalyzes the conversion of amines to aldehydes and ammonia using an active site that contains both copper and a topoquinone cofactor. The catalytic role of copper (if any) in catalysis remains a matter of persistent debate. The potentials of the deeply buried topoquinone and copper cannot be accurately measured using conventional electrochemical techniques. Instead, Hess *et al.* measured the topoquinone potential using gold electrodes functionalized with a phenyl-alkynyl bridge designed to bind in the AO active site, thus providing an ET conduit from the electrode to the topoquinone (Figure 1.12).⁷⁸ The topoquinone potential was found to be -360 mV, and no copper electrochemistry was observed. However, it is not clear whether the copper potential is anomalously low or if it could not be measured due to weak electronic coupling with the phenyl-alkynyl bridge.

Figure 1.12. The highly conjugated molecular “wire” used to electronically couple the active site of amine oxidase to a gold electrode. N,N-diethylaniline is a known inhibitor of amine oxidase.



REFERENCES

- (1) Moerner, W. E.; Orrit, M. *Science* **1999**, *283*, 1670-1676.
- (2) Wu, P. G.; Brand, L. *Anal. Biochem.* **1994**, *218*, 1-13.
- (3) Foerster, T. *Ann. Phys.-Berlin* **1948**, *2*, 55-75.
- (4) Marcus, R. A. *J. Chem. Phys.* **1956**, *24*, 966-978.
- (5) Gray, H. B.; Winkler, J. R. *Annu. Rev. Biochem.* **1996**, *65*, 537-561.
- (6) McConnell, H. *J. Chem. Phys.* **1961**, *35*, 508-515.
- (7) Davis, W. B.; Wasielewski, M. R.; Ratner, M. A.; Mujica, V.; Nitzan, A. *J. Phys. Chem. A* **1997**, *101*, 6158-6164.
- (8) Davis, W. B.; Ratner, M. A.; Wasielewski, M. R. *Chem. Phys.* **2002**, *281*, 333-346.
- (9) Yonemoto, E. H.; Saupe, G. B.; Schmehl, R. H.; Hubig, S. M.; Riley, R. L.; Iverson, B. L.; Mallouk, T. E. *J. Am. Chem. Soc.* **1994**, *116*, 4786-4795.
- (10) Smalley, J. F.; Feldberg, S. W.; Chidsey, C. E. D.; Linford, M. R.; Newton, M. D.; Liu, Y. P. *J. Phys. Chem.* **1995**, *99*, 13141-13149.
- (11) Paddon-Row, M. N.; Oliver, A. M.; Warman, J. M.; Smit, K. J.; De Haas, M. P.; Oevering, H.; Verhoeven, J. W. *J. Phys. Chem.* **1988**, *92*, 6958-6962.
- (12) Helms, A.; Heiler, D.; McLendon, G. *J. Am. Chem. Soc.* **1992**, *114*, 6227-6238.

- (13) Creager, S.; Yu, C. J.; Bamdad, C.; O'Connor, S.; MacLean, T.; Lam, E.; Chong, Y.; Olsen, G. T.; Luo, J. Y.; Gozin, M.; Kayyem, J. F. *J. Am. Chem. Soc.* **1999**, *121*, 1059-1064.
- (14) Sikes, H. D.; Smalley, J. F.; Dudek, S. P.; Cook, A. R.; Newton, M. D.; Chidsey, C. E. D.; Feldberg, S. W. *Science* **2001**, *291*, 1519-1523.
- (15) Davis, W. B.; Svec, W. A.; Ratner, M. A.; Wasielewski, M. R. *Nature* **1998**, *396*, 60-63.
- (16) Davis, W. B.; Ratner, M. A.; Wasielewski, M. R. *J. Am. Chem. Soc.* **2001**, *123*, 7877-7886.
- (17) Kilsa, K.; Kajanus, J.; Macpherson, A. N.; Martensson, J.; Albinsson, B. *J. Am. Chem. Soc.* **2001**, *123*, 3069-3080.
- (18) Roundhill, D. M. *Photochemistry and Photophysics of Metal Complexes*; Plenum Press: New York, 1994.
- (19) Berglund, J.; Pascher, T.; Winkler, J. R.; Gray, H. B. *J. Am. Chem. Soc.* **1997**, *119*, 2464-2469.
- (20) Zaslavsky, D.; Kaulen, A. D.; Smirnova, I. A.; Vygodina, T.; Konstantinov, A. A. *FEBS Lett.* **1993**, *336*, 389-393.
- (21) Zaslavsky, D.; Sadoski, R. C.; Wang, K. F.; Durham, B.; Gennis, R. B.; Millett, F. *Biochemistry* **1998**, *37*, 14910-14916.

- (22) Ortiz de Montellano, P. R., Ed. *Cytochrome P450: Structure, Mechanism, and Biochemistry*; Plenum Press: New York, 1995.
- (23) McLean, M.; Maves, S.; Weiss, K. E.; Krepich, S.; Sligar, S. G. *Biochem. Biophys. Res. Commun.* **1998**, *252*, 166-172.
- (24) Poulos, T. L.; Finzel, B. C.; Howard, A. J. *J. Mol. Biol.* **1987**, *195*, 867-700.
- (25) Nelson, D. R. *Arch. Biochem. Biophys.* **1999**, *369*, 1-10.
- (26) Nelson, D. R. (2002) Cytochrome P450 homepage:
<http://drnelson.utmem.edu/CytochromeP450.html>
- (27) Kagawa, N.; Waterman, M. R. In *Cytochrome P450: Structure, Mechanism, and Biochemistry*; Ortiz de Montellano, P. R., Ed.; Plenum Press: New York, 1995, pp 419-442.
- (28) Capdevila, J. H.; Zeldin, D.; Makita, K.; Karara, A.; Falck, J. R. In *Cytochrome P450: Structure, Mechanism and Biochemistry*; Ortiz de Montellano, P. R., Ed.; Plenum Press: New York, 1995, pp 443-472.
- (29) Goss, P. E.; Strasser, K. *J. Clin. Oncol.* **2001**, *19*, 881-894.
- (30) Frye, L. L.; Leonard, D. A. *Crit. Rev. Biochem. Mol. Biol.* **1999**, *34*, 123-140.
- (31) Sheehan, D. J.; Hitchcock, C. A.; Sibley, C. M. *Clin. Microbiol. Rev.* **1999**, *12*, 40-79.
- (32) Guengerich, F. P. *Annu. Rev. Pharmacol. Toxicol.* **1999**, *39*, 1-17.

- (33) Disterath, L. M.; Guengerich, F. P., Eds. *Enzymology of Human Liver Cytochromes P-450*; CRC Press: Boca Raton, FL, 1987; Vol. 1.
- (34) Guengerich, F. P. In *Cytochrome P450: Structure, Mechanism and Biochemistry*; Ortiz de Montellano, P. R., Ed.; Plenum Press: New York, NY, 1995, pp 473-536.
- (35) Otton, S. V.; Wu, D. F.; Joffe, R. T.; Cheung, S. W.; Sellers, E. M. *Clin. Pharm. Ther.* **1993**, *53*, 401-409.
- (36) Li, A. P., Ed. *Drug-drug interactions: scientific and regulatory perspectives*; Academic Press: New York, 1997.
- (37) Lang, N. P.; Butler, M. A.; Massengill, J.; Lawson, M.; Stotts, R. C.; Hauerjensen, M.; Kadlubar, F. F. *Cancer Epidemiol. Biomarkers Prev.* **1994**, *3*, 675-682.
- (38) Sligar, S. G. *Biochemistry* **1976**, *15*, 5399-5406.
- (39) Sligar, S. G.; Gunsalus, I. C. *Proc. Natl. Acad. Sci. U.S.A.* **1976**, *73*, 1078-1082.
- (40) Schlichting, I.; Berendzen, J.; Chu, K.; Stock, A. M.; Maves, S. A.; Benson, D. E.; Sweet, R. M.; Ringe, D.; Petsko, G. A.; Sligar, S. G. *Science* **2000**, *287*, 1615-1622.
- (41) Davydov, R.; Makris, T. M.; Kofman, V.; Werst, D. E.; Sligar, S. G.; Hoffman, B. M. *J. Am. Chem. Soc.* **2001**, *123*, 1403-1415.
- (42) Groves, J. T.; McClusky, G. A.; White, R. E.; Coon, M. J. **1978**, *81*, 154-160.
- (43) Kellner, D. G.; Hung, S. C.; Weiss, K. E.; Sligar, S. G. *J. Biol. Chem.* **2002**, *277*, 9641-9644.

- (44) Egawa, T.; Shimada, H.; Ishimura, Y. *Biochem. Biophys. Res. Commun.* **1994**, *201*, 1464-1469.
- (45) Ortiz de Montellano, P. R.; De Voss, J. J. *Nat. Prod. Rep.* **2002**, *19*, 477-493.
- (46) Kendrick, K. M.; Guzman, R. G.; Zorrilla, J.; Hinton, M. R.; Broad, K. D.; Mimmack, M.; Okura, S. *Nature* **1997**, *388*, 670-674.
- (47) Huang, P. L.; Huang, H. H.; Mashimo, H.; Bloch, K. D.; Moskowitz, M. A.; Bevan, J. A.; Fishman, M. C. *Nature* **1995**, *377*, 239-242.
- (48) Ko, G. Y.; Kelly, P. T. *J. Neurosci.* **1999**, *19*, 6784-6794.
- (49) Luth, H. J.; Holzer, M.; Gertz, H. J.; Arendt, T. *Brain Res.* **2000**, *852*, 45-55.
- (50) Mize, R. R.; Dawson, T. M.; Dawson, V. L.; Friedlander, M. J. *Nitric Oxide in Brain Development, Plasticity and Disease*; Elsevier, 1998.
- (51) Nathan, D. *J. Clin. Invest.* **1997**, *100*, 2417-2423.
- (52) Lancaster, J. *Nitric Oxide: Principles and Actions*; Academic Press: San Diego, CA, 1996.
- (53) Stuehr, D. J. *Biochim. Biophys. Acta* **1999**, *1411*, 217-230.
- (54) Bredt, D. S.; Hwang, P. M.; Glatt, C. E.; Lowenstein, C.; Reed, R. R.; Snyder, S. H. *Nature* **1991**, *351*, 714-718.
- (55) Janssens, S. P.; Simouchi, A.; Quertermous, T.; Bloch, D. B.; Bloch, K. D. *J. Biol. Chem.* **1992**, *267*, 22694.

- (56) Lamas, S.; Marsden, P. A.; Li, G. K.; Tempst, P.; Mickel, T. *Proc. Natl. Acad. Sci. U.S.A.* **1992**, *89*, 6348-6352.
- (57) Lowenstein, C. J.; Glatt, C. S.; Brecht, D. S.; Snyder, S. H. *Proc. Natl. Acad. Sci. U.S.A.* **1992**, *89*, 6711-6715.
- (58) Xie, Q. W.; Cho, H. J.; Calaycay, J.; Mumford, R. A.; Swiderek, K. M.; Lee, T. D.; Ding, A.; Troso, T.; Nathan, C. *Science* **1992**, *256*, 225-228.
- (59) Pant, K.; Bilwes, A. M.; Adak, S.; Stuehr, D. J.; Crane, B. R. *Biochemistry* **2002**, *41*, 11071-11079.
- (60) Dawson, V. L.; Dawson, T. M. *Prog. Brain Res.* **1998**, *118*, 215-229.
- (61) Dimmeler, S.; Zeiher, A. M. *Cell Death Differ.* **1999**, *6*, 964-968.
- (62) MacMicking, J. D.; North, R. J.; LaCourse, R.; Mudgett, J. S.; Shah, S. K.; Nathan, C. F. *Proc. Natl. Acad. Sci. U.S.A.* **1997**, *94*, 5243-5248.
- (63) Cho, H. J.; Xie, Q. W.; Calaycay, J.; Mumford, R. A.; Swiderek, K. M.; Lee, T. D.; Nathan, C. *J. Exp. Med.* **1992**, *176*, 599-604.
- (64) Alderton, W. K.; Cooper, C. E.; Knowles, R. G. *Biochem. J.* **2001**, *357*, 593-615.
- (65) Siddhanta, U.; Wu, C. Q.; Abu-Soud, H. M.; Zhang, J. L.; Ghosh, D. K.; Stuehr, D. J. *J. Biol. Chem.* **1996**, *271*, 7309-7312.
- (66) Crane, B. R.; Rosenfeld, R. J.; Arvai, A. S.; Ghosh, D. K.; Ghosh, S.; Tainer, J. A.; Stuehr, D. J.; Getzoff, E. D. *EMBO J.* **1999**, *18*, 6271-6281.

- (67) Rosen, G. M.; Tsai, P.; Pou, S. *Chem. Rev.* **2002**, *102*, 1191-1199.
- (68) Davydov, R.; Ledbetter-Rogers, A.; Martasek, P.; Larukhin, M.; Sono, M.; Dawson, J. H.; Masters, B. S. S.; Hoffman, B. M. *Biochemistry* **2002**, *41*, 10375-10381.
- (69) Wei, C. C.; Wang, Z. Q.; Wang, Q.; Meade, A. L.; Hemann, C.; Hille, R.; Stuehr, D. J. *J. Biol. Chem.* **2001**, *276*, 315-319.
- (70) Wilker, J. J.; Dmochowski, I. J.; Dawson, J. H.; Winkler, J. R.; Gray, H. B. *Angew. Chem. Int. Ed. Eng.* **1999**, *38*, 90-92.
- (71) Dmochowski, I. J.; Crane, B. R.; Wilker, J. J.; Winkler, J. R.; Gray, H. B. *Proc. Natl. Acad. Sci. USA* **1999**, *96*, 12987-12990.
- (72) Dmochowski, I. J.; Winkler, J. R.; Gray, H. B. *J. Inorg. Biochem.* **2000**, *81*, 221-228.
- (73) Dmochowski, I. J. In *Chemistry and Chemical Engineering*; California Institute of Technology: Pasadena, CA, 2000.
- (74) Dmochowski, I. J.; Dunn, A. R.; Wilker, J. J.; Crane, B. R.; Green, M. T.; Dawson, J. H.; Sligar, S. G.; Winkler, J. R.; Gray, H. B. *Methods Enzymol.* **2002**, *357*, 120-133.
- (75) Sligar, S. G.; Lipscomb, J. D.; Debrunner, P. G.; Gunsalus, I. C. *Biochem. Biophys. Res. Commun.* **1974**, *61*, 290-296.

- (76) Rosenfeld, R. J.; Hays, A.-M. A.; Musah, R. A.; Goodin, D. B. *Protein Sci.* **2002**, *11*, 1251-1259.
- (77) Hays, A.-M. A.; Gray, H. B.; Goodin, D. B. *Protein Sci.* **2003**, *12*, 278-287.
- (78) Hess, C. R. In *Chemistry and Chemical Engineering*; California Institute of Technology: Pasadena, 2002.

Chapter 2

Nanosecond Photoreduction of Cytochrome P450cam by Channel-Specific Ru- diimine Electron Tunneling Wires

Acknowledgements:

Data discussed in this chapter were collected in collaboration with Ivan Dmochowski.

ABSTRACT The synthesis and characterization of Ru-diimine complexes designed to bind to cytochrome P450cam (CYP101) is described. The sensitizer core has the structure $[\text{Ru}(\text{L}_2)\text{L}]^{2+}$, where L' is a perfluorinated biphenyl bridge (F₈bp) connecting 4,4'-dimethylbipyridine to an enzyme substrate (adamantane, F₈bp-Ad), a heme ligand (imidazole, F₈bp-Im), or F (F₉bp). The electron-transfer (ET) driving force ($-\Delta G^\circ$) is varied by replacing the ancillary 2,2'-bipyridine ligands with 4,4',5,5'-tetramethylbipyridine (tmRu). The four complexes all bind P450cam tightly: Ru-F₈bp-Ad (**1**, $K_d = 0.077 \mu\text{M}$); Ru-F₈bp-Im (**2**, $K_d = 3.7 \mu\text{M}$); tmRu-F₉bp (**3**, $K_d = 2.1 \mu\text{M}$); and tmRu-F₈bp-Im (**4**, $K_d = 0.48 \mu\text{M}$). Binding is predominantly driven by hydrophobic interactions between the Ru-diimine wires and the substrate access channel. With Ru-F₈bp wires, redox reactions can be triggered on the nanosecond timescale. Ru-wire **2**, which ligates the heme iron, shows a small amount of transient heme photoreduction (*ca.* 10%), whereas the transient photoreduction yield for **4** is 76%. Forward ET with **4** occurs in roughly 40 ns ($k_f = 2.8 \cdot 10^7 \text{ s}^{-1}$); and back ET ($\text{Fe}^{\text{II}} \rightarrow \text{Ru}^{\text{III}}$, $k_b \sim 1.7 \cdot 10^8 \text{ s}^{-1}$) is near the coupling-limited rate (k_{max}). Direct photoreduction was not observed for **1** or **3**. The large variation in ET rates among the Ru-diimine:P450 conjugates strongly supports a through-bond model of Ru:heme electronic coupling.

INTRODUCTION

Electron transfer (ET) is often the rate-determining step in biological catalysis. The reactions of the cytochromes P450 are an excellent case in point.¹ In the archetypal P450 from *Pseudomonas putida* (P450cam), the natural redox partner, putidaredoxin (Putd), reduces the enzyme far too slowly ($k_{\text{red}} \sim 50 \text{ s}^{-1}$) to allow catalytic intermediates to accumulate under biological conditions (Scheme 2.1).²

We are studying a variety of Ru-diimine sensitizers designed to replace the slow biological reduction with a rapid optical redox trigger.^{3,4} Each of the most promising sensitizers employs a perfluorobiphenyl group (F₈bp) that couples the Ru-diimine to a terminal functionality (Chart 2.1).

In these Ru-diimine:P450 conjugates, the Ru donor and the ferriheme acceptor are held in position mainly by noncovalent interactions. Thus, the synthetic flexibility of the sensitizer together with the structural framework provided by the enzyme make this an ideal system for exploring basic ET parameters in a biologically relevant milieu.

Scheme 2.1. The cytochrome P450cam catalytic cycle. Upon binding, the substrate displaces water, converting the heme from 6-coordinate, low spin (**1**) to 5-coordinate, high spin (**2**). Subsequent reduction by Putd produces the ferrous heme, which binds dioxygen (**3**). Reduction of **3** produces the ferrous, peroxide bound heme (**4**), which rapidly protonates (**5**).⁵ In the prevalent model, the peroxide then undergoes heterolysis to produce water and a ferryl $[\text{Fe}^{\text{IV}}=\text{O}]^{\bullet+}$ species (compound I, **6**), which oxidizes the substrate.⁶

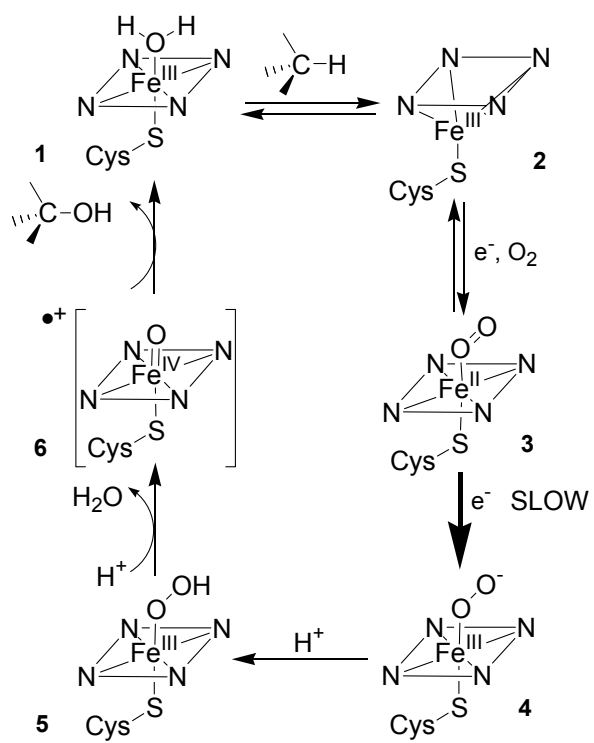
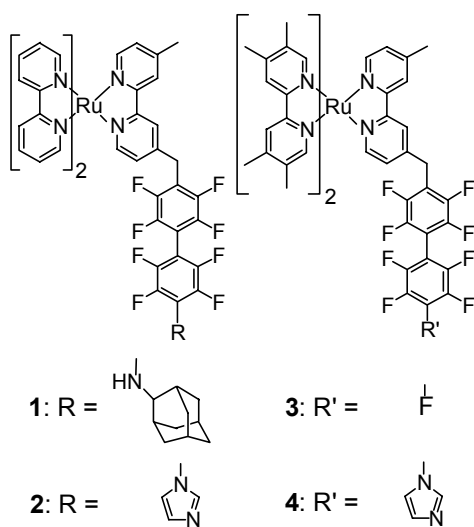


Chart 2.1. Ru-diimine wires: **1** Ru-F₈bp-Ad; **2** Ru-F₈bp-Im; **3** tmRu-F₉bp; **4** tmRu-F₈bp-Im.



MATERIALS AND METHODS

General. P450cam and the mutant Y29F were expressed in *E. coli* and purified using standard procedures.^{3,7} Site-directed mutagenesis was performed using Stratagene QuikChange mutagenesis kits. P450cam was stored in small aliquots and thawed immediately before use. Samples were prepared in 50 mM potassium phosphate buffer (pH 7.4) containing 100 mM KCl. P450 concentration was quantified using the heme Soret absorption at 416 nm ($\epsilon_{416}=115 \text{ mM}^{-1}\text{cm}^{-1}$). All experiments were performed on samples with a ratio $\text{Abs}_{418}/\text{Abs}_{280} \geq 1.55$ when camphor-free. Spectroscopic experiments used custom quartz cuvettes fitted with Kontes Teflon stopcocks. Oxygen was removed from the sample by completing at least 30 cycles of partial vacuum followed by an influx of argon.

Absorption spectra were taken on a HP-8452A spectrophotometer. Steady-state luminescence spectra were taken on an ISS K2 fluorometer. Emission quantum yields were calculated relative to a $\text{Ru}(\text{bpy})_3^{2+}$ standard, whose luminescence quantum yield was taken to be 0.042 in water.^{8,9,10}

Reduction of P450cam. P450cam (5.1 μM) was reduced with sodium dithionite under an atmosphere of carbon monoxide in the presence of 1.2 equivalents of tmRu-F₈bp-Im, producing the characteristic Soret peak at 446 nm. Carbon monoxide was then removed by gently bubbling argon through the sample for five minutes, resulting in both a change

in shape and a decrease in intensity of the Soret peak (446 nm). This species was assigned as the imidazole-ligated ferrous heme, in agreement with the previously determined spectrum of N-phenylimidazole-ligated ferrous P450cam.¹¹ Subsequent addition of carbon monoxide to the cuvette resulted in the restoration of the Soret band of CO-ligated P450cam.

As a control, the same procedure was performed with 50 μM camphor replacing tmRu-F₈bp-im. Five minutes of argon purging were sufficient to shift the Soret peak from 446 to 408 nm, indicative of the complete conversion of CO-bound to five-coordinate ferrous heme.

Transient Spectroscopy. Microsecond transient absorption and emission data were collected using instruments described previously.^{12,13} The instrument possesses a response time of 20 ns (FWHM) and the data is digitized at 200 megasamples s⁻¹. For nanosecond luminescence decay measurements, the sample was excited at 10 Hz with 70 ps, 355 nm pulses from a regeneratively amplified mode-locked Nd-YAG laser. Luminescence from the cuvette was filtered with a 650 nm long-pass filter, collected directly by a fiber optic (Fiberguide Industries), and detected with a Hamamatsu C5680 streak camera. The data were recorded using Hamamatsu High Performance Digital Temporal Analyzer 3.1.0 software and fit using Microcal Origin 5.0.

Binding constants. Luminescence decay profiles were fit to a biexponential function

(Eq. 1):

$$I(t) = c_1 e^{-k_1 t} + c_2 e^{-k_2 t} \quad (1)$$

using nonlinear least squares with iterative reconvolution to account for finite instrument response. The ratio of enzyme-bound to free ruthenium complex is c_1/c_2 , where k_1 and k_2 are the luminescence decay rate constants for the enzyme-bound and free ruthenium complexes.

This procedure has several advantages over steady-state UV-Vis titrations. The absorption due to the ruthenium complexes complicates the determination of a dissociation constant from the direct titration of P450cam with a Ru-wire. Previous results demonstrate that camphor and luminescent probe molecules may bind simultaneously to the enzyme, again complicating the derivation of dissociation constants from competition binding assays.¹⁴

Fitting errors for c_1 , c_2 , k_1 , and k_2 were determined by fixing one parameter while leaving the other three free to adopt whatever value minimized the sum of absolute values of the residual between the model and the data. Limits on a particular parameter were defined as the values that resulted in clear residuals. In practice, the fitting error on c_1 and c_2 was found to be about 10% of the total amplitude: $\text{err}(c_1) = 0.1(c_1 + c_2)$. Propagation of this error through the determination of K_d , assuming the worst-case

perfect correlation of c_1 and c_2 , shows that the fitting error is 20% when $c_1 = c_2$, but becomes substantial when one phase predominates. For instance, when c_1 and c_2 account for 20 and 80% of the amplitude the resulting K_d becomes uncertain to within a factor of 2.3.

ET rate constants. The raw transient absorption kinetics contain contributions from both heme/Ru redox processes and the bleach associated with the Ru-diimine excited state ($*Ru^{2+}$). The observed kinetics at 420 and 445 nm were corrected for the contribution of $*Ru^{2+}$ prior to fitting. The $*Ru^{2+}$ decay was recorded at 427 nm (the ferrous/ferric heme isosbestic). This trace was then scaled to account for the differences in $*Ru^{2+}/Ru^{2+}$ extinction coefficients at 420, 427 and 445 nm ($*Ru^{2+}/Ru^{2+} \Delta\epsilon_{445}/\Delta\epsilon_{427} = 1.06$, $\Delta\epsilon_{420}/\Delta\epsilon_{427} = 0.83$), and subtracted from the kinetics at 420 and 445 nm.

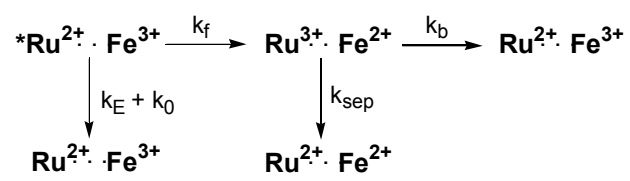
Transient absorption kinetics were interpreted according to the model shown in Scheme 2.2. The change in optical density (ΔOD) at time t is given by Eq. 2:

$$\Delta OD(t) = \frac{k_f \cdot [*Ru]_0 \cdot \Delta\epsilon}{k_b + k_{sep} - k_L} \left(\left(1 - \frac{k_{sep}}{k_L} \right) e^{-k_L t} - \left(1 - \frac{k_{sep}}{k_b + k_{sep}} \right) e^{-(k_b + k_{sep})t} + \frac{k_{sep}}{k_L} - \frac{k_{sep}}{k_b + k_{sep}} \right) \quad (2)$$

where $[*Ru^{2+}]_0$ (M^{-1}) is the concentration of excited ruthenium complex at time zero and $\Delta\epsilon$ is the change in molar extinction coefficients (Eq. 3):

$$\Delta\epsilon(\lambda) = \epsilon_{Fe^{II}} - \epsilon_{Fe^{III}} + \epsilon_{Ru^{III}} - \epsilon_{Ru^{II}} \quad (3)$$

Scheme 2.2. $*\text{Ru}^{2+}$ reduces the heme (k_f) or decays to the ground state through a combination of intrinsic decay (k_0) and energy transfer to the heme (k_E), which decays non-radiatively to the ground state. The charge-separated state ($\text{Ru}^{3+} \cdot \cdot \text{Fe}^{2+}$) undergoes back electron transfer (k_b) or decays to form a long-lived ferrous heme (k_{sep}).²¹



Sufficient laser power was used to assure that all photosensitizer molecules were excited; $[*Ru^{2+}]_0 = [Ru]_{tot}$. The values $\Delta\epsilon_{445} = 90 \text{ mM}^{-1}\text{cm}^{-1}$ and $\Delta\epsilon_{420} = -72 \text{ mM}^{-1}\text{cm}^{-1}$ were derived from the steady-state spectra of reduced and oxidized P450cam bound to tmRu-F₈bp-Im plus the known Ru^{II}/Ru^{III} $\Delta\epsilon$ values.^{15,16} The rate constant k_L (s^{-1}) is the observed decay rate of $*Ru^{2+}$ in the presence of P450 (Eq. 4):

$$k_L = k_0 + k_f + k_E \quad (4)$$

where the other rate constants are for the intrinsic decay (k_0), forward electron transfer (k_f), and Förster energy transfer to the heme (k_E).

Because the rates of forward and back ET are comparable to the response time of our instrument, the instrumental response function was deconvolved from the observed kinetics.¹⁷ The recorded ΔOD was converted into an intensity (Eq. 5):

$$I = I_0 \cdot 10^{-\Delta OD} \quad (5)$$

The response function was then deconvolved from the observed intensity I by iterative reconvolution using Eq. 5. The algorithm used was written in MatLab 5.3, and relies on the built-in simplex minimization algorithm.

Fitting errors for k_f , k_b and k_{sep} were determined by systematically adjusting one parameter while leaving the other two free to adopt whatever values minimized the sum of the absolute values of the residual between the model and the data. Limits on a particular parameter were defined as the values that resulted in clear residuals. Error in

the rates is best expressed as a multiplicative factor. The errors are estimated to be: $k_f(445 \text{ nm})$ 2.1; $k_f(420 \text{ nm})$ 1.8; $k_b(445 \text{ nm})$ 2.3; $k_b(420 \text{ nm})$ 2.0; $k_{\text{sep}}(445 \text{ nm})$ 1.1; $k_{\text{sep}}(420 \text{ nm})$ 1.5. These errors are in accord with those expected for a multiexponential fit to moderate quality data.¹⁷

Förster energy transfer. The rate constant k_E was calculated from standard theoretical expressions (Eqs. 6-8):¹⁸

$$k_E = k_0 \left(\frac{R_0}{r} \right)^6 \quad (6)$$

$$R_0^6 = 8.8 \cdot 10^{-5} (\kappa^2 n^{-4} \phi_0 J) \quad (7)$$

$$J = \frac{\int_0^\infty F_0(\lambda) E_A(\lambda) \lambda^4 d\lambda}{\int_0^\infty F_0(\lambda) d\lambda} \quad (8)$$

where J is the overlap between the luminescence spectrum of the donor and absorption spectrum of the acceptor (weighted by λ^4), ϕ_0 is the luminescence quantum yield in the absence of energy transfer, n is the index of refraction, and κ is an orientation factor dependent on the alignment of the donor and acceptor dipoles ($\kappa^2 = 2/3$ for random alignment).

Calculation of buried surface area. The solvent-exposed surface areas of Ru-F₈bp-Ad, P450cam, and the P450cam:Ru-F₈bp-Ad conjugate (pdb code 1k2o) were calculated with the Solvation module of InsightII using a 1.4 Å probe. Buried surface area was computed

by subtracting the surface area of the conjugate from that of Ru-F₈bp-Ad and P450cam alone. The difference in buried surface areas for the Δ and Λ stereoisomers of Ru-F₈bp-Ad is negligible.

RESULTS

Synthesis. Sequential nucleophilic substitution of decafluorobiphenyl proved to be an especially efficient route to the desired conjugated compounds (Scheme 2.3). Absorption and emission maxima at 456 and 620 nm (**1** and **2**) and 444 and 654 nm (**3** and **4**) are consistent with the previously reported spectra of [Ru(bpy)₂(Me₂bpy)]²⁺ and [Ru(tmbpy)₂(bpy)]²⁺.¹⁹

Binding. All of the Ru-diimine wires (**1-4**) bind to P450. Binding of Ru-F₈bp-Ad induces a shift in the Soret absorption maximum from 416 to 414 nm, consistent with partial displacement of water from the heme iron. Similarly, coordination of both Ru-F₈bp-Im and tmRu-F₈bp-Im shifts the Soret peak to 420 nm (Figure 2.1), consistent with the value of 421 nm reported for the ferric P450cam:N-phenylimidazole complex.²⁰ The measured extinction coefficient at 446 nm in the spectrum of the tmRu-F₈bp-Im:Fe^{II}-P450cam conjugate is 117 mM⁻¹cm⁻¹, in agreement with the value of 116 mM⁻¹cm⁻¹ reported for the N-phenylimidazole complex.¹¹ All of the absorption spectra are consistent with predominantly low-spin hemes in the Ru-wire:P450cam conjugates.

Scheme 2.3. Synthesis of Ru-diimine wires: deprotonation of 4,4'-dimethyl-2,2'-bipyridine with lithium diisopropyl amine (LDA) followed by nucleophilic attack on decafluorobiphenyl results in the ET bridge **7**.

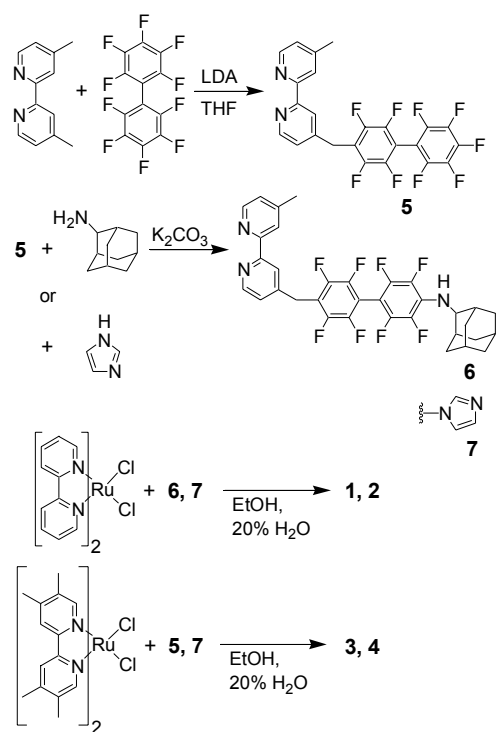
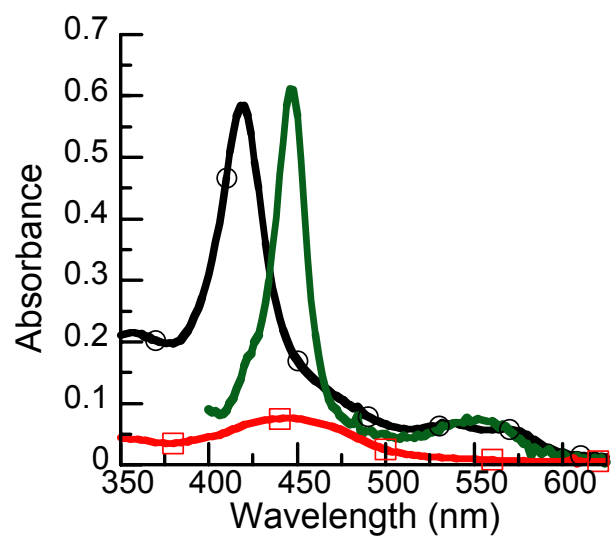


Figure 2.1. UV-vis absorption spectra of ferric P450cam (black, open circles), 5.2 μM tmRu-F₈bp-im (red, open squares), and ferrous P450cam ligated by tmRu-F₈bp-im (green).



All of the Ru-wires show biphasic luminescence decays in the presence of P450cam. The fast phase results from partial quenching due to energy transfer to the heme, and in the case of Ru-F₈bp-Im and tmRu-F₈bp-Im, electron transfer (Scheme 2.2, following sections). Typical biphasic luminescence decays for a Ru-wire in the presence of P450 are shown in Figure 2.2. The ratio of the amplitudes of the fast (bound) and slow (free Ru-wire) phases was used to calculate binding constants (Table 2.1).

Electron Transfer. Upon 470 nm excitation, both tmRu-F₈bp-im and Ru-F₈bp-im reduce P450cam. The bleach at 420 nm and increase in optical density at 445 nm confirm the conversion of $({}^{\text{Im}}\text{N})({}^{\text{CysS}})\{\text{PorN}_4\text{Fe}^{\text{III}}\}$ to $({}^{\text{Im}}\text{N})({}^{\text{CysS}})\{\text{PorN}_4\text{Fe}^{\text{II}}\}$ (Figure 2.3). Neither *Ru-F₈bp-Ad (*1) nor *tmRu-F₉bp (*3) reduces P450cam, as judged by the lack of a transient absorption signal.

Photoexcitation of equimolar tmRu-F₈bp-im and P450cam shows complex early kinetics (Figure 2.4, Scheme 2.2). The sharp rise and fall at the beginning of the trace recorded at 445 nm are attributed to fast forward (k_f) and back (k_b) ET. The rates of accumulation and decay of Fe^{II} are comparable to the rise time of the instrument. Deconvolution was necessary to eliminate the instrument response contribution from the observed kinetics. Optimization of the parameters k_f , k_b , and k_{sep} at 420 and 445 nm yielded the following rate constants: $k_f = 2.8 \cdot 10^7$; $k_b = 1.7 \cdot 10^8$; $k_{\text{sep}} = 9.0 \cdot 10^6 \text{ s}^{-1}$.²¹

Figure 2.2. Luminescence decay. (A) 10 μM 1:1 tmRu-F₈bp-im:P450cam luminescence decay (tmRu-F₈bp-im, black; tmRu-F₈bp-im + 1 eq. P450cam, red, open circles). (B) Nanosecond timescale luminescence decay of 1:1 tmRu-F₈bp-im:P450cam (4.5 μM) (instrument response *ca.* 70 ps, see Experimental). The initial rapid ($k > 1 \cdot 10^9 \text{ s}^{-1}$) decay is intrinsic to P450cam and likely represents a trace impurity. The slower decay on this timescale corresponds to the rapid decay in Figure 2.2a ($k_L = 3.7 \cdot 10^8 \text{ s}^{-1}$). Green, P450cam; black, P450cam + tmRu-F₈bp-im; red, monoexponential fit.

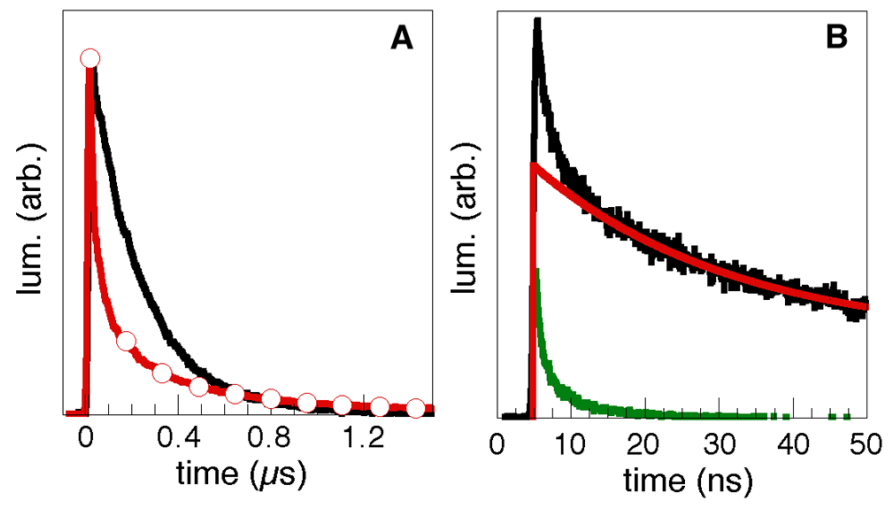


Table 2.1. Dissociation Constants.

Ru-wire	μM^a
Ru-F ₈ bp-Ad	0.077 ± 0.011
Ru-F ₈ bp-Im	3.7 ± 0.5
tmRu-F ₈ bp-Im	0.48 ± 0.18
tmRu-F ₉ bp	2.1 ± 1.3

a Uncertainties are standard deviations derived from independent analysis of at least 3 measurements.

Figure 2.3. Transient absorption spectrum measured 20 μs after 470 nm excitation of equimolar tmRu-F₈bp-im and P450cam (9.6 μM). Observed changes in optical density are chiefly due to the conversion of ferric to ferrous heme, with comparatively minor contributions from Ru^{II} to Ru^{III} oxidation.

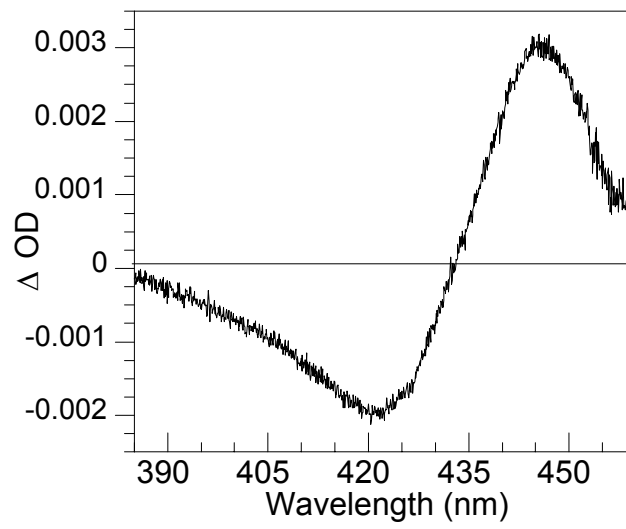
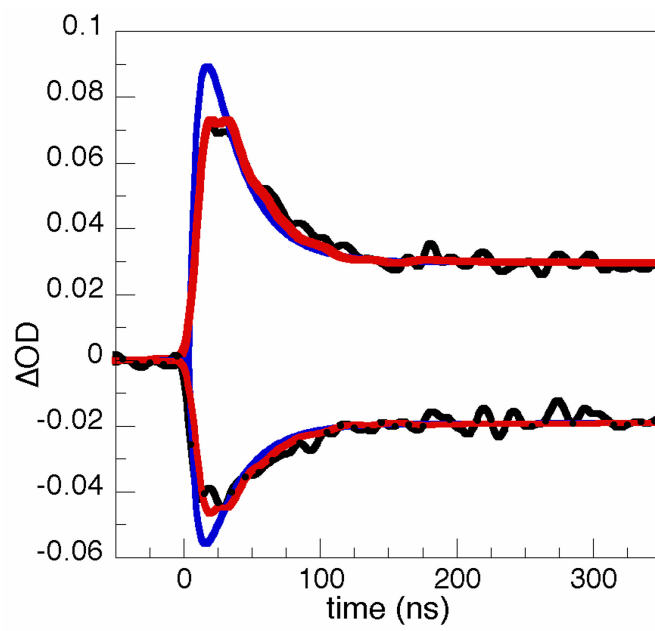


Figure 2.4. Transient absorption at 445 (top) and 420 nm (bottom) for 10 μ M 1:1 tmRu-F₈bp-im:P450cam (black, data; blue, fit; red, convolved fit). The kinetics were corrected for both free and bound *Ru²⁺ by measuring the transient absorption of *Ru²⁺ at a P450cam Fe^{II}/Fe^{III}, Ru^{II}/Ru^{III} isosbestic (427 nm). This spectrum was then scaled and subtracted from the kinetics recorded at 420 and 445 nm (Experimental). The data were fit to the kinetics model in Scheme 2.2 using iterative reconvolution to account for instrument response. The fit yielded the following rate constants: $k_f = 2.9 \cdot 10^7$, $k_b = 1.6 \cdot 10^8$, $k_{sep} = 8.6 \cdot 10^6 \text{ s}^{-1}$ (445 nm); and $k_f = 2.6 \cdot 10^7$, $k_b = 1.9 \cdot 10^8$, $k_{sep} = 9.3 \cdot 10^6 \text{ s}^{-1}$ (420 nm). The same procedure could not be applied to the transient absorption spectra of Ru-F₈bp-Im because the signal due to *Ru²⁺ is much larger than the signal due to the heme.



In the absence of competing electron transfer (Ru-F₈bp-Ad and tmRu-F₉bp), the Ru-Fe distance can be calculated using Förster theory from k_E , the ruthenium emission spectrum, and the heme absorption spectrum (Table 2.2). The Ru-Fe distance (22.1 Å) calculated for Ru-F₈bp-Ad is in excellent agreement with the value from the crystal structure. The distance of 17 Å calculated for tmRu-F₉bp agrees well with structural modeling of the tmRu-F₉bp:P450cam conjugate, and corresponds to a ~2 Å gap between the end of the perfluorinated biphenyl bridge and the heme.

Using Eq. 4, we calculate that k_E for tmRu-F₈bp-Im is $4.4 \cdot 10^6 \text{ s}^{-1}$ (Table 2.2). This rate of energy transfer corresponds to a Ru-Fe distance of 18.1 Å, a reasonable distance given the geometric constraints of the fluorobiphenyl bridge. A Ru-Fe distance of 18.1 Å can in turn be used to calculate a k_E of $6.6 \cdot 10^6 \text{ s}^{-1}$ for Ru-F₈bp-Im, corresponding to $k_f = 4.4 \cdot 10^6 \text{ s}^{-1}$, which is 6 times slower than photoinduced reduction of ferric P450cam by tmRu-F₈bp-Im. With $\phi = (k_f/k_L)$, we find total ferrous heme yields of 76% for tmRu-F₈bp-im and roughly 30% for Ru-F₈bp-im.

DISCUSSION

The observed binding constants suggest that the interaction between the ruthenium complex and the enzyme is primarily hydrophobic in nature. Ru-F₈bp-Ad, which has the largest hydrophobic surface area, binds best, and tmRu-F₈bp-im binds better than its nonmethylated analog Ru-F₈bp-im. Previous work suggests that the binding energy

Table 2.2. Derivation of k_f and Ru-Fe distances from luminescence decay measurements. Variation in R_0 stems from variation in the heme Q bands and the emission spectrum of the complex.

Compound	$k_L \cdot 10^{-6} \text{ (s}^{-1}\text{)}$	$k_0 \cdot 10^{-6} \text{ (s}^{-1}\text{)}$	$k_E \cdot 10^{-6} \text{ (s}^{-1}\text{)}$	$k_f \cdot 10^{-6} \text{ (s}^{-1}\text{)}$	Ru-Fe (Å)	$R_0 \text{ (Å)}^a$
tmRu-F ₈ bp-im	37	4.6	4.4 ^b	28 ^c	18.1 ^a	18.0
Ru-F ₈ bp-im	13	2.0	6.6 ^a	4.4	18.1 ^d	22.1
Ru-F ₈ bp-Ad	5.5	2.0	3.5 ^b	-	22.1 ^a	24.3
					c.f. 21.8 ^e	
tmRu-F ₉ bp	13	4.6	8.4 ^b	-	17.0 ^a	18.8

a Calculated from Förster theory (Eqs. 6-8).

b $k_E = k_L - k_0 - k_f$.

c From transient absorption kinetics.

d In accord with the calculated Ru-Fe distance for tmRu-F₈bp-Im.

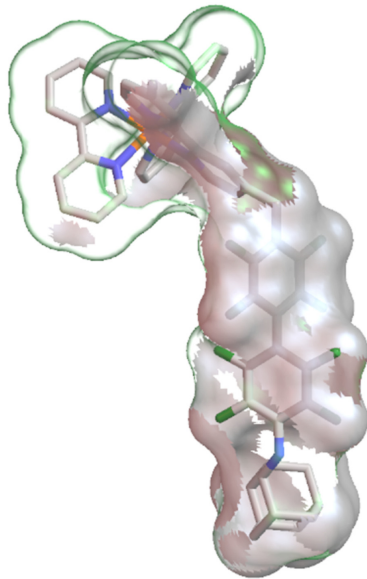
e From the crystal structure of Ru-F₈bp-Ad:P450cam (ref. 23).

derived from burying hydrophobic surfaces is around $15 \text{ cal } \text{Å}^{-2}$ for protein-protein interactions.²² The crystal structure of Ru-F₈bp-Ad bound to P450cam shows extensive contacts between the Ru-wire and the hydrophobic substrate access channel,²³ resulting in $1.2 \cdot 10^3 \text{ Å}^2$ of buried surface area (Figure 2.5), corresponding to $8.2 \text{ cal } \text{Å}^{-2}$. A similar calculation based on the crystal structure of Ru-C₉-Ad bound to P450cam (Figure 2.6) yields similar binding energies (Δ isomer: $9.13 \text{ kcal mol}^{-1}$, $8.4 \text{ cal } \text{Å}^{-2}$; Λ isomer: $9.69 \text{ kcal mol}^{-1}$, $9.3 \text{ cal } \text{Å}^{-2}$).¹² The gain in binding for hydrophobic burial is lower for our complexes than is observed at protein interfaces. In part this result must reflect the energetic cost of "opening" the enzyme.²³

The imidazole-functionalized complexes weakly ligate the ferric heme, as tmRu-F₈bp-im binds with only $0.87 \text{ kcal mol}^{-1}$ greater affinity than tmRu-F₉bp. The small energetic contribution of coordination may result from steric effects or poorer σ -donating ability stemming from the electron-withdrawing perfluorobiphenyl unit.

These results, and previous work,¹⁴ suggest that designing a small molecule to bind in a given enzyme active site can be relatively straightforward. Hydrophobic interactions are non-directional, predictable, and hence easily engineered: 1000 Å^2 of buried surface area should result in a low-micromolar dissociation constant. Of course, this simple strategy does not include considerations such as target specificity or water solubility, two important qualities in drug design.

Figure 2.5. The Ru-F₈bp-Ad wire is partially buried upon binding to P450cam. The buried surface (gray, 56% of the total surface area) was computed with the program GRASP using a 1.4 Å radius probe.

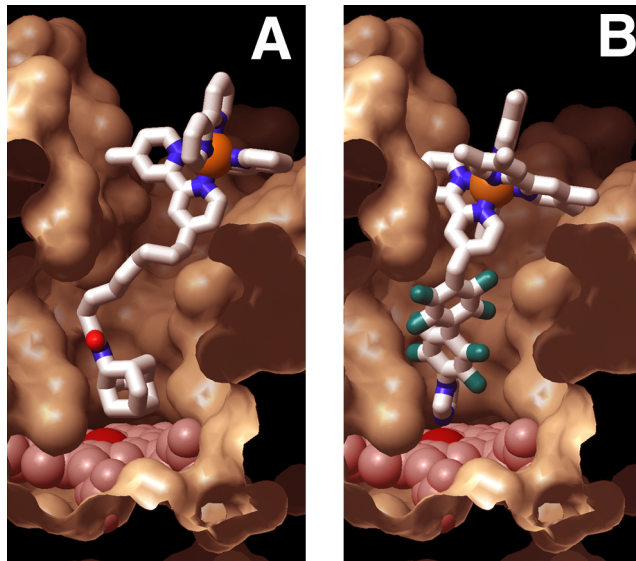


ET kinetics. According to semiclassical theory, coupling-limited electron tunneling (k_{\max}) will occur when the driving force ($-\Delta G^\circ$) equals the reorganization energy (λ).^{24,25} Back electron transfer in the P450cam:tmRu-F₈bp-Im conjugate ($-\Delta G^\circ \sim 1.5$ eV) should be in the inverted region for λ in the range 0.7–0.9 eV; the reaction should be 10 ($\lambda = 0.9$ eV) to 5,000 ($\lambda = 0.7$ eV) times slower than forward electron transfer.²⁶ The inverted effect has been observed in several biological²⁷ and synthetic ET systems.²⁸ We find, however, that back ET is 10 times faster than the forward reaction. One possible explanation is that electron transfer initially produces an electronically excited product;^{29,30} another is phonon-modified inelastic tunneling, which can be activationless in the conventional inverted region.³¹

The transient absorption data show that tmRu-F₈bp-Im injects electrons into the ferriheme of P450cam more efficiently than Ru-F₈bp-Im. The methyl groups in tmRu-F₈bp-Im increase the driving force for forward electron transfer by 0.13 eV (Table 2.3). Semiclassical theory predicts a 4-fold increase in the rate of forward electron transfer, in qualitative agreement with the ET rates calculated from transient absorbance and luminescence decay rates (Table 2.2).

In any case, it is likely that back electron transfer occurs at close to the coupling limited rate (k_{\max}). With this assumption, we can estimate the reorganization energy (λ_{tot})

Figure 2.6. (A) Cutaway view of the 1.55 Å resolution crystal structure of $[\text{Ru-C}_9\text{-Ad}]^{2+}$ bound to P450cam.²⁰ Photochemically generated $[\text{Ru-C}_9\text{-Ad}]^+$ reduces ferric P450cam with a time constant of about 50 μs ($-\Delta G^\circ \sim 1.0$ eV).⁴ (B) tmRu-F₈bp-Im modeled into the active site of P450cam. The perfluorobiphenyl bridge improves the electronic coupling between $^*\text{Ru}^{2+}(\text{L}_2)\text{L}'$ and the heme, resulting in direct photoreduction with a time constant of 36 ns even at lower driving force ($-\Delta G^\circ \sim 0.45$ eV).



for the reaction:³²

$$k_{ET} = k_{\max} \exp\left(\frac{-(\Delta G^\circ + \lambda_{\text{tot}})^2}{4\lambda_{\text{tot}}k_B T}\right)$$

Using $k_{\max}=1.7\cdot 10^8 \text{ s}^{-1}$ and $\Delta G^\circ_f = -0.45 \text{ eV}$ (Table 2.3), we find that $\lambda_{\text{tot}} \sim 0.85 \text{ eV}$,³³ a value comparable to the λ 's observed in $\text{Ru}(\text{bpy})_3^{2+}$ -modified cytochrome *c* (0.74 eV)^{30a} and cytochrome *b*₅ (0.94 eV).^{27a} Given a $\text{Ru}(\text{bpy})_3^{2+}$ reorganization energy of 0.6 eV,³⁴ we estimate that $\lambda_{\text{P450}} \sim 1.1 \text{ eV}$, a value that is larger than the reorganization energy of cytochrome *c* ($\lambda = 0.7 \text{ eV}$),^{25,26,35} but below the estimated reorganization energy of a water-exposed heme ($\lambda \approx 1.2 \text{ eV}$).²⁶ Our estimate of λ_{P450} is in accord with the proposal that a reorganization barrier prevents P450cam reduction in the absence of substrate.³⁶

Structural variations in the Ru-wires allowed us to test the role of the intervening medium on the rate of electron transfer. Taking into account the differences in Ru-heme distances and driving forces, a coupling model with a uniform distance decay³⁷ of 1.1 \AA^{-1} and $\lambda = 0.8 \text{ eV}$ ^{27a, 30} predicts only 12-fold faster ET for tmRu-F₈bp-Im compared to Ru-C₉-Ad, instead of the 1400-fold rate difference that is observed (Figure 2.6). Similarly, tmRu-F₈bp-Im efficiently reduces P450cam while tmRu-F₉bp does not, despite the similarity in donor-acceptor distances and driving forces. The saturated bonds in Ru-C₉-Ad and the through-space jump in tmRu-F₉bp likely weaken electronic couplings compared to those associated with the imidazole-terminated Ru-wires, and hence greatly

Table 2.3. Reduction potentials.

Compound	Potential (V, NHE)
P450cam ($\text{Fe}^{3+/2+}$)	$\sim -0.3^a$
$[\text{Ru}(\text{bpy})_3]^{3+/2+*}$	-0.62^b
$[\text{Ru}(\text{tmbpy})_3]^{3+/2+*}$	-0.75^c
$[\text{Ru}(\text{bpy})_3]^{3+/2+}$	1.26^b
$[\text{Ru}(\text{tmbpy})_2(\text{dmbpy})]^{3+/2+}$	1.07^d

a low spin (ref. 38).

b Ref. 8.

c Ref. 39.

d In MeCN vs. SSCE (ref. 19).

slow ET.⁴⁰ Our results thus strongly support a through-bond model for coupling the Ru and heme centers.⁴¹

The biological reduction of P450cam by Putd (50 s^{-1}) is slow for two reasons: the driving force is low and the coupling to the deeply buried heme is weak. The coupling to the ferriheme was enhanced in enzyme conjugates containing the first generation of ruthenium sensitizer-linked substrates, which featured a direct ET pathway through a saturated alkyl chain. As a result, ET occurs on a submillisecond timescale ($2 \cdot 10^4 \text{ s}^{-1}$).⁴ Both theory and experiment indicate that incorporating aromatic groups into the linker will further enhance the electronic coupling.⁴² By employing a more direct, largely conjugated path, tmRu-F₈bp-Im is able to photoreduce P450cam in nanoseconds ($2.8 \cdot 10^7 \text{ s}^{-1}$), 10^3 times faster than the Ru-wire with alkyl chain linker, and $5 \cdot 10^5$ times faster than putidaredoxin.

CONCLUDING REMARKS

Photoreduction of the enzyme by the channel-specific Ru-imidazole wires occurs on the nanosecond timescale, fully 5 orders of magnitude faster than reduction by the natural redox partner putidaredoxin. Fast electron injection was only observed in the imidazole-terminated Ru-wires. However, calculations based on simple electronic

coupling models suggest that improved conjugation will overcome the loss of a direct bond to the heme.⁴⁰

Hydroxylation catalyzed by P450cam is only one example of numerous biological processes, including photosynthesis and respiration, that involve oxidation and reduction steps. Current methods for studying enzyme reactions, for instance, stopped-flow mixing and photocaged substrates, have time resolutions limited by diffusion. ET is intramolecular in Ru-substrate:enzyme conjugates, dramatically improving the accessible time resolution.

One goal of our research is to generate and study cytochrome P450 reactive intermediates. However, the pursuit of this goal has led to an improved understanding of how to mesh natural and synthetic photochemical systems. The desire to combine biological and man-made photochemistry stems from the need to understand two seminal chemical problems: how to catalyze endergonic reactions, and how to control multiple proton and electron transfers. Nature has found solutions to both of these problems, the most obvious example being photosynthesis. In order to understand biological systems, it is necessary first to dissect them. The lessons illustrated in this study—the usefulness of the hydrophobic effect in designing molecular interactions, the importance of a well-coupled ET pathway, and the suppression of the inverted effect—should be generally applicable to chemical systems at the interface of biological and inorganic chemistry.

ACKNOWLEDGEMENT

This work was supported by the Fannie and John Hertz Foundation (ARD), the National Institutes of Health predoctoral program (IJD), the National Science Foundation, and the National Institutes of Health.

REFERENCES AND NOTES

1. Ortiz de Montellano, P. R. *Cytochrome P450: Structure, Mechanism and Biochemistry, 2nd edn.*; Plenum Press: New York, NY, 1995.
2. Fisher, M. T.; Sligar, S. G. *J. Am. Chem. Soc.* **1985** *107*, 5018-5019.
3. Dmochowski, I. J.; Crane, B. R.; Wilker, J. J.; Winkler, J. R.; Gray, H. B. *Proc. Natl. Acad. Sci. U.S.A.* **1999**, *96*, 12987-12990.
4. Wilker, J. J.; Dmochowski, I. J.; Dawson, J. H.; Winkler, J. R.; Gray, H. B. *Angew. Chem. Int. Ed. Engl.* **1999**, *38*, 90-92.
- 5 (a) Davydov, R.; Makris, T. M.; Kofman, V.; Werst, D. E.; Sligar, S. G.; Hoffman, B. M. *J. Am. Chem. Soc.* **2001**, *123*, 1403-1415. (b) Schlichting, I.; Berendzen, J.; Chu, K.; Stock, A. M.; Maves, S. A.; Benson, D. E.; Sweet, R. M.; Ringe, D.; Petsko, G. A.; Sligar, S. G. *Science* **2000**, *287*, 1615-1622.
6. Groves, J. T.; McClusky, G. A.; White, R. E.; Coon, M. J. *Biochem. Biophys. Res. Commun.* **1978**, *81*, 154-160.
7. Dmochowski, I. J. *Probing cytochrome P450 with sensitizer-linked substrates*; California Institute of Technology: Pasadena, CA, 2000.

8. Roundhill, D. M. *Photochemistry and Photophysics of Metal Complexes*; Plenum Press: New York, 1994.
9. van Houten, J.; Watts, R. J. *J. Am. Chem. Soc.* **1976**, *98*, 4853-4858.
10. Cook, M. J.; Lewis, A. P.; McAuliffe, G. S. G.; Skarda, V.; Thomson, A. J.; Gasper, J. L.; Robbins, D. J. *J. Chem. Soc., Perkin Trans.* **1984**, *2*, 1293-1301.
11. Dawson, J. H.; Andersson, L. A.; Sono, M. *J. Biol. Chem.* **1983**, *258*, 13637-13645.
12. Dmochowski, I. J.; Winkler, J. R.; Gray, H. B. *J. Inorg. Biochem.* **2000**, *81*, 221-228.
13. Low, D. W.; Winkler, J. R.; Gray, H. B. *J. Am. Chem. Soc.* **1996**, *118*, 117-120.
14. Dunn, A. R.; Hays, A.-M. A.; Goodin, D. B.; Stout, C. D.; Chiu, R.; Winkler, J. R.; Gray, H. B. *J. Am. Chem. Soc.* **2002**, *124*, 10254-10255.
15. Kotkar, D.; Joshi, V.; Ghosh, P. K. *J. Chem. Soc., Chem. Commun.* **1987**, *1*, 4-6.
16. Miller, R. R.; Brandt, W. W.; Puke, M. *J. Am. Chem. Soc.* **1955**, *77*, 3178-3180.

17. Demas, J. N. *Excited State Lifetime Measurements*; Academic Press: New York, 1983.
18. Wu, P.; Brand, L. *Anal. Biochem.* **1994**, *218*, 1-13.
19. Opperman, K. A.; Mecklenburg, S. L.; Meyer, T. J. *Inorg. Chem.* **1994**, *33*, 5295-5301.
20. Dawson, J. H.; Andersson, L. A.; Sono, M. *J. Biol. Chem.* **1982**, *257*, 3606-3617.
21. Although most of the photoproducted ferrous heme decays in 50 ns, a small percentage remains. The Soret maximum remains at 445 nm on all the timescales we can measure, suggesting that dissociation does not explain the long-lived charge-separated state. The mutations Y29F and Y96A do not affect the observed kinetics, indicating that the transiently generated $\text{Ru}(\text{bpy})_3^{3+}$ does not oxidize these nearby residues. Ru-diimine complexes have been previously shown to be capable of oxidizing tyrosine residues [(a) Sjodin, M.; Styring, S.; Åkermark, B.; Sun, L. C.; Hammarström, L. *J. Am. Chem. Soc.* **2000**, *122*, 3932-3936. (b) Magnuson, A.; Berglund, H.; Korall, P.; Hammarström, L.; Åkermark, B.; Styring, S.; Sun, L. C. *J. Am. Chem. Soc.* **1997**, *119*, 10720-10725.]. Several studies have shown that $[\text{Ru}(\text{bpy})_3]^{3+}$ decays through multiple pathways in aqueous solution [(a) Brune, S. N.; Bobbitt, D. R. *Talanta* **1991**, *38*, 419-424. (b) Ledney,

M.; Dutta, P. K. *J. Am. Chem. Soc.* **1995**, *117*, 7687-7695. (c) Ghosh, P. K.; Brunschwig, B. S.; Chou, M.; Creutz, C.; Sutin, N. *J. Am. Chem. Soc.* **1984**, *106*, 4772-4783. (d) Arce-Sagues, J. A.; Gillard, R. D.; Lancashire, R. J.; Williams, P. A. *J. Chem. Soc., Dalton Trans.* **1979**, *1*, 193-198. (e) Creutz, C.; Sutin, N., *Proc. Natl. Acad. Sci. U.S.A.* **1975**, *72*, 2858-2862.]. The yield of reduced P450 at 5 μ s is about 1.7% for tmRu-F8bp-im and 0.5% for Ru-F8bp-im, as judged by transient absorption at 445 nm. Thus, the processes leading to the long-lived ferrous heme constitute a minor side reaction compared to the initial forward and back electron transfer.

22. Eisenberg, D.; McLachlan, A. D. *Nature* **1986**, *319*, 199-203.

23. Dunn, A. R.; Dmochowski, I. J.; Bilwes, A. M.; Gray, H. B.; Crane, B. R. *Proc. Natl. Acad. Sci. USA* **2001**, *98*, 12420-12425.

24. Marcus, R. A. *J. Chem. Phys.* **1956**, *24*, 966-989.

25. Marcus, R. A.; Sutin, N. *Biochim. Biophys. Acta* **1985**, *811*, 265-322.

26. We assume that $\lambda_{\text{Ru}} = 0.57$ eV and λ_{heme} falls between 0.7 and 1.2 eV [Winkler, J. R.; Wittung-Stafshede, P.; Leckner, J.; Malmstrom, B. G.; Gray, H. B. *Proc. Natl. Acad. Sci. U.S.A.* **1997**, *94*, 4246-4249].

27. (a) Scott, J. R.; Willie, A.; McLean, M.; Stayton, P. S.; Sligar, S. G.; Durham, B.; Millett, F., *J. Am. Chem. Soc.* **1993**, *115*, 6820-6824. (b) Turro, C.; Zaleski, J. M.; Karabatsos, Y. M.; Nocera, D. G. *J. Am. Chem. Soc.* **1996**, *118*, 6060-6067.
28. (a) Gould, I. R.; Moser, J. E.; Armitage, B.; Farid, S.; Goodman, J. L.; Herman, M. S. *J. Am. Chem. Soc.* **1989**, *111*, 1917-1919. (b) Wasielewski, M. R.; Niemczyk, M. P.; Svec, W. A.; Pewitt, E. B. *J. Am. Chem. Soc.* **1985**, *107*, 1080-1082. (c) Ohno, T.; Yoshimura, A.; Mataga, N. *J. Phys. Chem.* **1986**, *90*, 3295-3297. (d) Chen, P.; Duesing, R.; Tapolsky, G.; Meyer, T. J. *J. Am. Chem. Soc.* **1989**, *111*, 8305-8306. (e) Closs, G. L.; Miller, J. R. *Science* **1988**, *240*, 440-447. (g) Fox, L. S.; Kozik, M.; Winkler, J. R.; Gray, H. B. *Science* **1990**, *247*, 1069-1071.
29. Beitz, J. V.; Miller, J. R. *J. Chem. Phys.* **1979**, *71*, 4579-4595.
30. (a) Mines, G. A.; Bjerrum, M. J.; Hill, M. G.; Casimiro, D. R.; Chang, I.-J.; Winkler, J. R.; Gray, H. B. *J. Am. Chem. Soc.* **1996**, *118*, 1961-1965. (b) Makinen, M. W.; Churg, A. K. Structural and analytical aspects of the electronic spectra of heme proteins. In *Iron Porphyrins, vol. 1*; Lever, A. B. P. and Gray, H. B., Ed.; Addison-Wesley: Reading, 1983, pp. 141-236.

31. Daizadeh, I.; Medvedev, E. S.; Stuchebrukhov, A. A. *Proc. Natl. Acad. Sci. U.S.A.* **1997**, *94*, 3703-3708.
32. Assuming that the electronic coupling between $\text{Ru(L)}_2\text{L}'$ and the heme is the same for the forward and back electron transfer.
33. The sources of error in the calculation of λ are ΔG and the ratio k_f/k_{max} . Formal error analysis using the values $\Delta G = -0.45 \pm 0.05$ V and $k_f/k_{\text{max}} = 0.16 \pm 0.1$ gives $\lambda = 0.85 \pm 0.11$ eV.
34. Brown, G. M.; Sutin, N. *J. Am. Chem. Soc.* **1979**, *101*, 883-892.
35. Andrew, S. M.; Thomasson, K. A.; Northrup, S. H. *J. Am. Chem. Soc.* **1993**, *115*, 5516-5521.
36. Honeychurch, M. J.; Hill, H. A. O.; Wong, L.-L. *FEBS Lett.* **1999**, *451*, 351-353.
37. Langen, R.; Colon, J. L.; Casimiro, D. R.; Karpishin, T. B.; Winkler, J. R.; Gray, H. B. *J. Biol. Inorg. Chem.* **1996**, *1*, 221-225.
38. (a) Gunsalus, I. C.; Meeks, J. R.; Lipscomb, J. D. *Ann. N.Y. Acad. Sci.* **1973**, *212*, 107-121. (b) Sligar, S. G.; Gunsalus, I. C. *Proc. Natl. Acad. Sci. U.S.A.* **1976**, *73*, 1078-1082.

39. Elliott, C. M.; Freitag, R. A.; Blaney, D. D. *J. Am. Chem. Soc.* **1985**, *107*, 4647-4655.
40. Beratan, D. N.; Skourtis, S. S. *Curr. Opin. Chem. Biol.* **1998**, *2*, 235-243.
41. Winkler, J. R. *Curr. Opin. Chem. Biol.* **2000**, *4*, 192-198.
42. (a) Smalley, J. F.; Feldberg, S. W.; Chidsey, C. E. D.; Linford, M. R.; Newton, M. D.; Liu, Y.-P. *J. Phys. Chem.* **1995**, *99*, 13141-13149. (b) Warman, J. M.; Smit, K. J.; de Haas, M. P.; Jonker, S. A.; Paddon-Row, M. N.; Oliver, A. M.; Kroon, J.; Oevering, H.; Verhoeven, J. W. *J. Phys. Chem.* **1991**, *95*, 1979-1987. (c) Langen, R.; Chang, I.-J.; Germanas, J. P.; Richards, J. H.; Winkler, J. R.; Gray, H. B. *Science* **1995**, *268*, 1733-1735. (d) Creager, S.; Yu, C. J.; Bamdad, C.; O'Connor, S.; MacLean, T.; Lam, E.; Chong, Y.; Olsen, G. T.; Luo, J. Y.; Gozin, M.; Kayyem, J. F. *J. Am. Chem. Soc.* **1999**, *121*, 1059-1064. (e) Sikes, H. D.; Smalley, J. F.; Dudek, S. P.; Cook, A. R.; Newton, M. D.; Chidsey, C. E. D.; Feldberg, S. W. *Science* **2001**, *291*, 1519-1523. (f) Pollard, W. T.; Felts, A. K.; Friesner, R. A. *Adv. Chem. Phys.* **1996**, *93*, 77-134. (g) Davis, W. B.; Wasielewski, M. R.; Ratner, M. A.; Mujica, V.; Nitzan, A. *J. Phys. Chem. A* **1997**, *101*, 6158-6164. (h) McConnell, H. M. *J. Chem. Phys.* **1961**, *35*, 508-515.

Chapter 3

Probing the open state of cytochrome P450cam with ruthenium-linker substrates[†]

[†]Adapted from: Dunn, A. R.; Dmochowski, I. J.; Bilwes, A. M.; Gray, H. B.; Crane, B. R. *Proc. Natl. Acad. Sci. U.S.A.* **2001**, *98*, 12420-12425.

Acknowledgements:

The crystal structure of the Ru-C₉-Ad:P450cam conjugate discussed in this chapter was determined by Brian Crane and Ivan Dmochowski. The crystal structure of the Ru-F₈bp-Ad:P450cam conjugate was determined in collaboration with Brian Crane and Alexandrine Bilwes, who also provided invaluable help with protein expression and purification. The author thanks SSRL for access to data collection facilities and the staff of beamlines 9-1 and 9-2 for their assistance with data collection. The author also thanks Prof. Doug Rees for access to the computational facilities used in solving these crystal structures.

ABSTRACT

Cytochromes P450 play key roles in drug metabolism and disease by oxidizing a wide variety of natural and xenobiotic compounds. High resolution crystal structures of P450cam bound to ruthenium sensitizer-linked substrates reveal an open conformation of the enzyme that allows substrates to access the active center via a 22 Å deep channel. Interactions of alkyl and fluorinated biphenyl linkers with the channel demonstrate the importance of exploiting protein dynamics for specific inhibitor design. Large changes in peripheral enzyme structure (F and G helices) couple to conformational changes in active center residues (I helix) implicated in proton pumping and dioxygen activation. Common conformational states among P450cam and homologous enzymes indicate that static and dynamic variability in the F/G helix region allows the 54 human P450s to oxidize thousands of substrates.

INTRODUCTION

Cytochromes P450 catalyze the transformations of many diverse substrates.¹ Most notably, P450s hydroxylate aliphatic carbon by generating a reactive heme-oxygen species: $R-H + O_2 + 2H^+ + 2e^- \rightarrow R-OH + H_2O$. Found in all phyla, P450s have the same protein fold and cysteine-ligated heme, despite low sequence similarity between some members (structurally similar P450cam and P450BM-3 have only 17% sequence identity).² Humans have at least 54 different P450 isozymes.³ They play key roles in steroid biosynthesis and arachidonic acid metabolism, as well as in the transformations of xenobiotics in detoxification and carcinogenesis.⁴ Particularly striking is the finding that P450 3A4 metabolizes up to half of all drugs in use.⁵ Despite broad substrate diversity, all P450s have significant structural constraints on their activity: P450s must control water access to the active center to avoid the conversion of activated dioxygen to superoxide or peroxide. Thus, the binding sites of P450 isozymes must be structurally diverse, yet conserve a mechanism of catalysis and solvent exclusion. An unanswered question is how thousands of substrates are metabolized by one enzyme family whose chemistry requires significant structural constraint.

As part of our investigation of cytochrome P450cam using sensitizer linked substrates (SLS),⁶ we sought to determine the structures of P450cam bound to several different Ru-diimine photosensitizers. This chapter describes the structures of two such

Ru-substrate:P450cam conjugates. As predicted, the substrate moieties bind at the active center, and the Ru-sensitizers bind near the protein surface. Importantly, the enzyme changes conformation to accommodate the linkers. The open conformation we observe mimics structures of other P450 enzymes and reveals a likely path for substrates to access the active center. Notably, this rearrangement is coupled to conformational changes of catalytically important residues.

MATERIALS AND METHODS

Crystallization and data collection: Purification and crystallization of P450cam:Ru-C₉-Ad have been described previously.^{6a} P450cam:Ru-F₈bp-Ad seed crystals in the space group P1 (cell dimensions 63.8 × 67.1 × 72.5 Å³, two molecules per asymmetric unit; Matthews coefficient (V_M) = 2.56; solvent content = 51.9%) nucleated from C334A P450cam separated from camphor and complexed with stoichiometric Ru-F₈bp-Ad. Hanging drops contained an equal volume mixture of reservoir and 396 μM P450:Ru-F₈bp-Ad in 20 mM Hepes, 100 mM KCl, 1mM DTT pH 7.5. The reservoir (pH 6.5) contained 0.1 M sodium cacodylate, 200 mM KCl 8-15% (wt/vol) molecular weight 8,000 polyethylene glycol (PEG). Crystal nucleation was induced by setting the crystallization trays on ice for 30 min. The resulting temperature gradient causes partial dehydration of the hanging drops. The trays were then removed from the ice and stored at 4 °C; seed crystal growth occurred overnight. Diffraction quality crystals were grown

over 24 hours by moving seed crystals into sitting drops with reservoir PEG concentrations of 8-11%.

Two data sets were collected at the Stanford Synchrotron Research Laboratory (SSRL). Data set 1 (1.80 Å resolution) was collected at 100 K on beamline 9-2 ($\lambda=1.03$ Å) at SSRL and processed with DENZO and SCALEPACK.⁷ Data set 2 (1.65 Å resolution) was collected at 100 K on beamline 9-1 ($\lambda=0.72$ Å) and similarly processed.

Structure determination of P450:Ru-F₈bp-Ad: An initial molecular replacement solution (correlation coefficient = 46.1 and $R_{\text{cryst}} = \frac{\sum ||F_{\text{obs}}| - |F_{\text{calc}}||}{\sum |F_{\text{obs}}|} = 44.7\%$) for diffraction data set 1 (20.0 to 3.5 Å resolution) was found with AMORE⁸ by using two probe molecules, each derived from the structure of camphor bound P450cam (PDB code: 2cpp). The initial model derived from molecular replacement on data set 1 was replaced with the protein coordinates from Ru-C₉-Ad bound P450cam (PDB code: 1qmq) by least squares fitting and was further improved by simulated annealing. Ru-F₈bp-Ad was positioned into the remaining difference density. Refinement was completed by iterative rounds of torsion-angle molecular dynamics and positional refinement with CNS⁹ and XFIT¹⁰ amidst model rebuilding, water molecule placement, and resolution extension to 1.65 Å. Overall anisotropic thermal factor correction, bulk solvent correction, individual thermal factor refinement, and grouped occupancy refinement of Ru-F₈bp-Ad produced the final model (7688 scatterers in the asymmetric unit, 2

P450:Ru-F₈bp-Ad molecules, each containing a superposition of Ru-F₈bp-Ad Δ and Λ stereoisomers; 18 residues in multiple conformations; 5 cacodylate molecules bound to cysteines 58A, 85A, 58B, 85B and 136B; 693 water molecules). Noncrystallographic symmetry restraints were not applied between the two molecules per asymmetric unit. The final model has excellent stereochemistry (Table 3.1) with 90.5% of all residues in the most favored regions of ϕ/ψ space as defined by PROCHECK.¹¹ The residue Glu94 falls outside the accepted regions of ϕ/ψ space due to steric interactions with the cacodylate bound to Cys85. Figures were generated with Bobscrip,¹² MOLSCRIPT,¹³ Raster3D¹⁴ and InsightII. Molecular surfaces were calculated with MSMS¹⁵ and rendered with AVS (Advanced Visualization Systems, Inc.).

RESULTS AND DISCUSSION

Ru-substrate binding reveals a substrate access channel in P450cam

The P450cam complexes with Ru-C₉-Ad and Ru-F₈bp-Ad have strikingly similar protein conformations ($C\alpha$ r.m.s.d. = 0.7 Å) and SLS binding modes, despite having crystallized in different space groups. Ru-C₉-Ad and Ru-F₈bp-Ad share the same [Ru^{II}(bpy)₃]²⁺ and adamantyl functionalities, but are linked with a nine carbon alkyl chain in Ru-C₉-Ad and a 4,4'-substituted octafluorobiphenyl in Ru-F₈bp-Ad.

Table 3.1: X-ray data collection and refinement

	data set 1	data set 2
Unit cell	64.0 67.3 72.5 Å 71.3 65.8 62.4°	63.8 67.1 72.5 Å 71.2 65.2 62.3°
Space group	P1	P1
Resolution (Å)	1.80 (1.86-1.80) *	1.65 (1.71-1.65) *
R _{sym} †	3.7 (25.6) *	3.8 (29.2) *
Completeness	96.8 (95.4) *	97.8 (97.0) *
Wilson B (Å ²)		19.0
I/s(I) ‡	21.9 (3.80) *	16.43 (1.99) *
# molecules/unit cell		2
R _{fac} §		21.0 (29.2) *
R _{free} ¶		22.6 (28.7) *
r.m.s.d. bonds, angles		0.007 Å, 1.2°
Protein atoms, 		6569, 23.16 Å ²
Waters, 		693, 34.3 Å ²
Ru-F ₈ bp-Ad atoms, 		280, 25.7 Å ²
Residues not modeled		A1-A9, B1-B9
Additional ligands		5 cacodylate

* Highest resolution range for compiling statistics.

† $R_{\text{sym}} = \sum \sum_j |I_j - \langle I \rangle| / \sum \sum_j I_j$, I_j = intensity of observation j .

‡ Intensity signal to noise.

§ $R = \sum ||F_{\text{obs}}| - |F_{\text{calc}}|| / \sum |F_{\text{obs}}|$ for all reflections (no σ cutoff).

¶ Free R calculated against 7.4% of reflections removed at random.

|| Root-mean-square deviations (r.m.s.d.) from ideal bond and angle restraints.

The ruthenium complexes bind P450cam in a channel that likely gives natural substrates access to the buried active center (Figure 3.1). Movement of the F (residues 173-185) and G (192-214) helices against the perpendicular I helix (234-267) retracts the F/G loop (185-192) from the β -sheet domain and thereby opens an access channel to the heme that is 22 Å deep and 11 Å across (Figure 3.2). In effect, the F and G helices translate relative to the protein core in a “shear” mechanism,¹⁶ whereas the core itself undergoes smaller motions to maintain hydrophobic interactions.

On opening of the access channel, the interactions of the F and G helices with the protein core manifest in two ways: 1) the making and breaking of salt-bridges to stabilize helix juxtaposition; and 2) slight distortion of the core backbone to conserve hydrophobic packing. Rearrangements of inter-residue salt bridges and hydrogen bonding interactions among the F helix, F/G loop, and the I helix facilitate sliding of the F helix relative to the I helix. These rearrangements (Figure 3.3) either exploit the conformational flexibility of long side chains to maintain hydrogen bonding interactions (e.g., Glu171 to Arg161, Arg186 to Asp251) or involve the breaking and making of hydrogen bonds (e.g., Lys178 to Asp251 and Leu250 exchanged for Lys178 to Glu156).

The tendency to maintain hydrophobic packing interactions between the G helix and both the I helix and the B' loop (residues 89-101) causes main-chain conformational distortions within the protein core in response to the new F/G helix positions.

Figure 3.1. Comparison of P450cam bound to Ru-C₉-Ad (*A*) and adamantane (*B*).¹⁷ On binding the Ru-substrate (Λ -stereoisomer in blue, Δ -stereoisomer in green) the F and G helices (red ribbons) retract from the P450cam β -sheet domain (gray ribbons). The adamantyl moiety binds in the same position above the heme (yellow) as free adamantane. (*C*) Movement of the F, G, H, and I helices (rotated *ca.* 180° from *A* and *B*). For comparison, P450cam bound to camphor is shown in gray. Residues on the F/G loop move as much as 7.5 Å as the F and G helices slide approximately one helical turn (4.5 Å) across the I helix. The H helix (218-225) and the N-terminus of the I helix (234-267) shift with the G helix to conserve interhelical contacts.

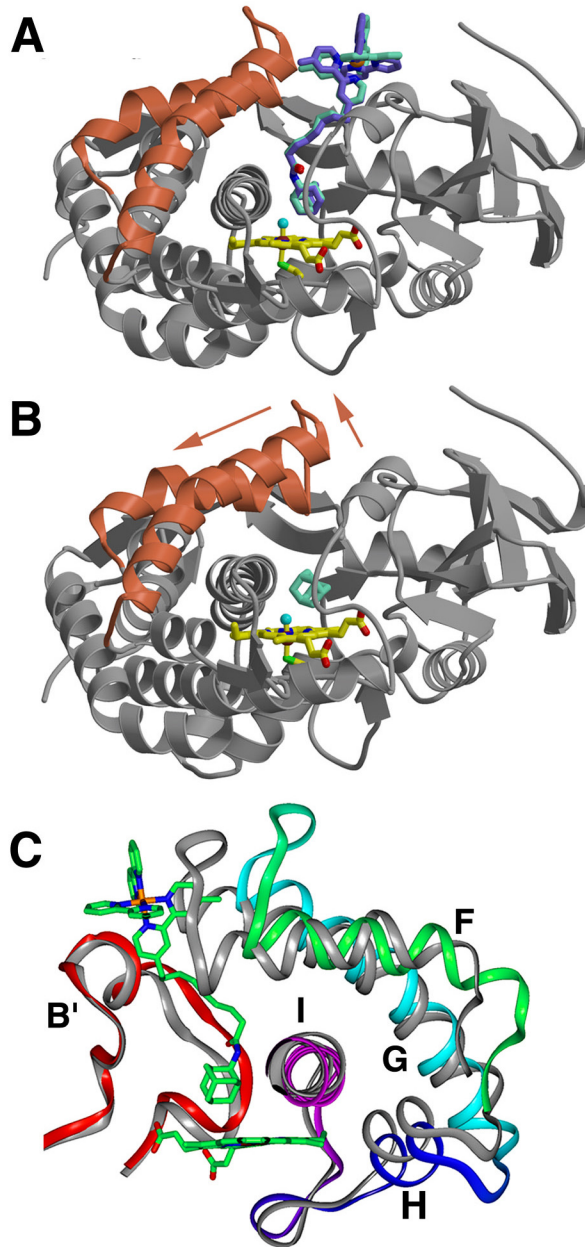


Figure 3.2. Shape complementarity and hydrophobic interactions between Ru-F₈bp-Ad and P450cam. The water molecules (red) hydrate newly exposed surface area in the P450cam:Ru-F₈bp-Ad structure.

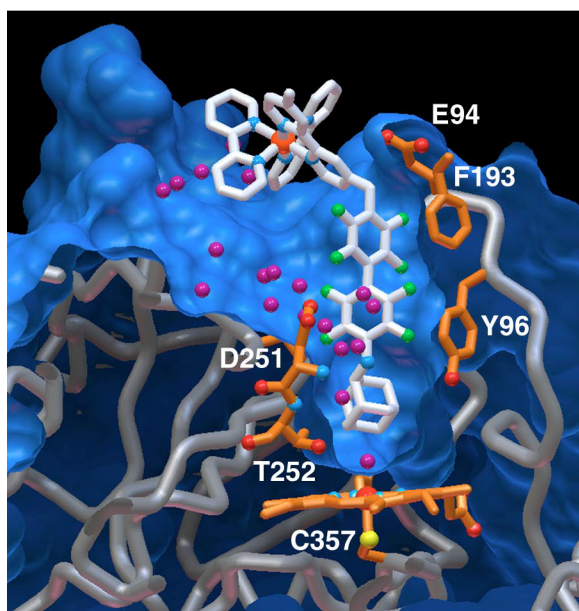
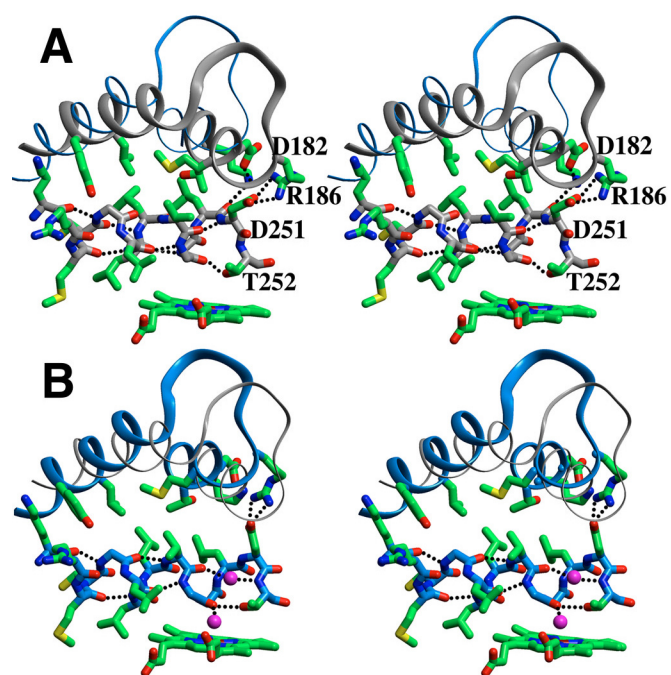


Figure 3.3. Side chain interactions in closed (*A*) and open (*B*) P450cam. The charged residues Lys178 (F helix), Asp182 (F helix) Thr185 (F/G loop), and Arg186 (F/G loop) alter their interactions with Asp251, a key residue on the I helix implicated in delivering protons to activate heme-bound dioxygen. Alternate conformations of Arg186 and Asp251 are present in the Ru-C₉-Ad complex, indicating conformational mobility. The N-terminal I helix segment translates and rotates to maintain a hydrophobic core of interdigitated branched hydrophobic residues (Leu246, Leu250, and Val247) with the F (Leu177, Thr181, and Met184) and G (Leu200, Tyr201, Leu204, and Ile208) helices.

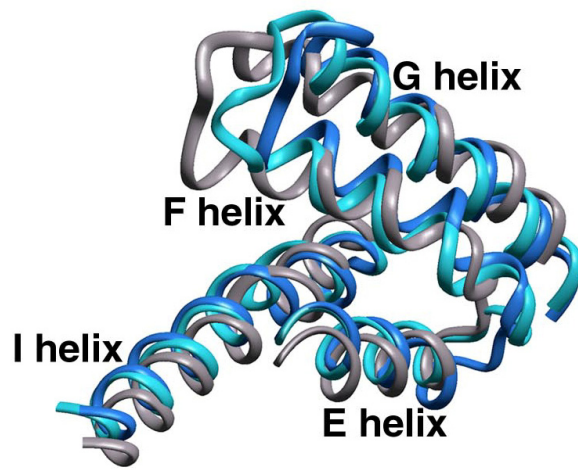


For example, the B' loop moves to maintain packing of F87, Y96, and F98 with F193 and Y201 on the G helix. Similarly, the numerous contacts among the hydrophobic side chains of the F, G, and I helices cause the N-terminal half of the I helix to rotate in response to the translation of the F and G helices in the open structure. As discussed below, this change in I-helix main-chain conformation and hydrogen bonding in turn affects the conformation of the active site.

The position of the F and G helices in other P450s closely matches the conformations found in our open structures of P450cam. Substrate-free P450BM-3 crystallizes in an open form and P450NOR has a large, permanent access channel analogous to that observed in the Ru-substrate:P450cam structures (Figure 3.4).¹⁸ The structural similarity of the open P450cam structure with P450BM-3 and P450NOR suggests that the open conformation is important for substrate binding. The Ru-substrates stabilize a conformation that may exist only transiently for P450cam, but which is clearly stable for other cytochromes P450. Thus, the P450 fold apparently allows an opening motion of the F and G helices with the relative stability of open and closed forms weighted differently among P450s.

The conformation of the F/G loop is similar in the open and closed structures of P450cam. However, mobility of the F/G loop is suggested by disorder in the crystal structures of P450terp and P450 2C5.¹⁹ Furthermore, the F/G loop of CYP 119

Figure 3.4. The F, G, and I helices of P450cam in its closed (gray) and open (blue) states compared to those of P450NOR (light blue).



undergoes rearrangement on binding bulky substrates.²⁰ Thus, F/G loop flexibility may also play an important role in P450 substrate binding.

Solution studies support a transient open state of P450cam. Photoacoustic calorimetry indicates that a short-lived (~130 ns) intermediate of larger volume forms during the photolysis of heme-bound carbon monoxide and expulsion of camphor.²¹ Our structures confirm an earlier prediction based on photoacoustic spectroscopy that the residues Arg186, Asp251, Lys178, and Asp182 undergo rearrangement during substrate binding.²² Furthermore, tryptophan fluorescence quenching measurements show that substrate-free P450cam is conformationally more labile than the camphor-bound enzyme.²³

Indirect evidence also suggests an open/closed equilibrium in other P450s. Cooperative substrate hydroxylation, consistent with a flexible binding site, has been observed in P450 3A4, the most abundant hepatic P450.²⁴ Eukaryotic P450s, for instance P450_{sc}, are known to exist in multiple conformational states.²⁵ Drug resistance mutations in the fungal P450 CYP51 occur in the G and H helices, far from the active site.²⁶ Finally, computer simulations support F/G helix fluctuations in both P450cam and P450BM-3.²⁷

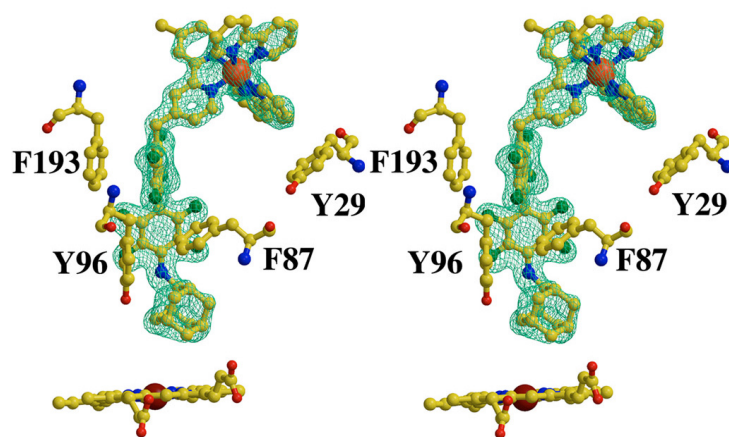
Interactions of Ru-substrates with P450cam

Two current problems in drug design are as follows: 1) how to avoid the deactivation of drugs by hepatic P450s; and 2) how to selectively inhibit specific pathogenic P450s.²⁸ Our Ru-substrate complexes bind with submicromolar dissociation constants, but are structurally very different from camphor. Thus, the interactions of the Ru-substrates with P450cam provide insight into why some P450s are promiscuous binders and suggest how to design specific P450 isozyme inhibitors.

Our structures provide examples of rarely characterized interactions among proteins, metal complexes, and fluorinated aromatics. Both Ru-substrates bind P450cam in a similar fashion. Notably, the ruthenium atom and adamantyl centroids are only 1.64 and 1.07 Å apart in the superimposed structures. In part this is due to design: Ru-F₈bp-Ad was synthesized after the crystal structure of Ru-C₉-Ad was known. However, preferred interactions between the protein and Ru:substrates lead to similar structures.

Ru-F₈bp-Ad interactions: Although direct contacts between [Ru^{II}(bpy)₃]²⁺ and the protein are limited, both the Δ and Λ isomers of the complex could be discerned due to the rigidity of Ru-F₈bp-Ad (Figure 3.35). There are very few crystal structures of fluorinated aromatics bound to proteins. Phenyl and perfluorophenyl functionalized molecules are known to stack in the solid state due to favorable π - π interactions between the electron-rich phenyl groups and electron-poor perfluorophenyl groups.²⁹ These

Figure 3.5. Simulated-annealing omit map ($F_{\text{obs}}-F_{\text{calc}}$) calculated with Ru-F₈bp-Ad removed from F_{calc} . Electron density is shown at 1.65 Å resolution and contoured at 2.5 σ . For clarity only one isomer is shown. The bipyridyl ring contacts Tyr29. Phe193 contacts one fluorinated ring with 3.4 Å between rings, consistent with the 3.4 Å face-to-face distance observed in the benzene-hexafluorobenzene crystal structure.³⁰ Phe87 contacts the perfluorobiphenyl unit in an edge-on fashion, with the ϵ carbon 3.5 Å from the face of the biphenyl unit. Tyr96 packs against the biphenyl unit in an edge-on fashion, with fluorine-carbon contacts ranging from 3.2 to 3.9 Å.



attractive interactions, which have been estimated to be worth about 15 kJ/mol in vacuum, make the hydrophobic perfluorophenyl group a potentially useful functionality for drug design.³¹

The P450cam:Ru-F₈bp-Ad complex shows both parallel and perpendicular stacking between the octafluorobiphenyl unit and aromatic residues (Figure 3.2, 3.5). The crystal structure of a matrix metalloproteinase inhibitor also shows a parallel stacking interaction (3.7 Å separation) between a pentafluorophenyl group and a tyrosine, which contributes to the binding affinity of the inhibitor relative to the phenyl analog.^{31d} In contrast, the crystal structure of a carbonic anhydrase inhibitor shows perpendicular stacking between a phenylalanine and a pentafluorophenyl group.³² Our results further demonstrate that the interaction between an aromatic electron donor and a fluorinated ring can be parallel or perpendicular and is influenced both by the intrinsic attraction and the structural constraints imposed by the tertiary structure.

Ru-C₉-Ad interactions: Due to the flexibility of the alkyl chain, the bipyridyl ligands of Ru-C₉-Ad were difficult to discern in the electron density. Anomalous scattering measurements revealed two distinct positions for the ruthenium atom separated by ~1 Å in the access channel. The best fit to the electron density included both Δ and Λ isomers and interactions with Tyr29 and Pro187, as in the Ru-F₈bp-Ad structure (Figure 3.1, 3.2). In addition, a bipyridine contacts Ala92, and an acetate molecule (present in the

crystallization solution) sandwiches between the $[\text{Ru}^{\text{II}}(\text{bpy})_3]^{2+}$ unit and Phe193. The hydrocarbon tether linking the ruthenium complex to the adamantyl unit winds across the side chains of Ile395, Phe193, Phe87 and Tyr96—the same residues that contact the fluorinated biphenyl unit in Ru-F₈bp-Ad.

Tyr96 is hydrogen bonded to the carbonyl of the Ru-C₉-Ad amide bond as it is to the camphor ketone group in the substrate complex.³³ The adamantyl unit binds in the same pocket as in the Ru-F₈bp-Ad structure but enjoys more extensive hydrophobic interactions with Leu244, Thr101, Ile395, Val295, Thr252 and the Gly248 C α . The strain induced by the short separation (3.00 Å) of the adamantyl unit and heme-bound water perhaps explains the partial low- to high-spin heme shift that occurs upon binding (data not shown).

The $[\text{Ru}^{\text{II}}(\text{bpy})_3]^{2+}$ moiety does not force the substrate access channel open as it is pulled in by the adamantyl group. If the interaction with the ruthenium complex was unfavorable the enzyme could push the complex into solution and close around the alkyl chain. Instead, Förster energy transfer experiments indicate that the ruthenium resides the same distance from the heme even when the linker is much longer than the access channel.^{6a} Even in the Ru-C₉-Ad structure the alkyl chain is not fully extended. Thus, favorable binding interactions between Ru-substrate and the enzyme likely stabilize an open conformation that already exists transiently under normal conditions. Our structures

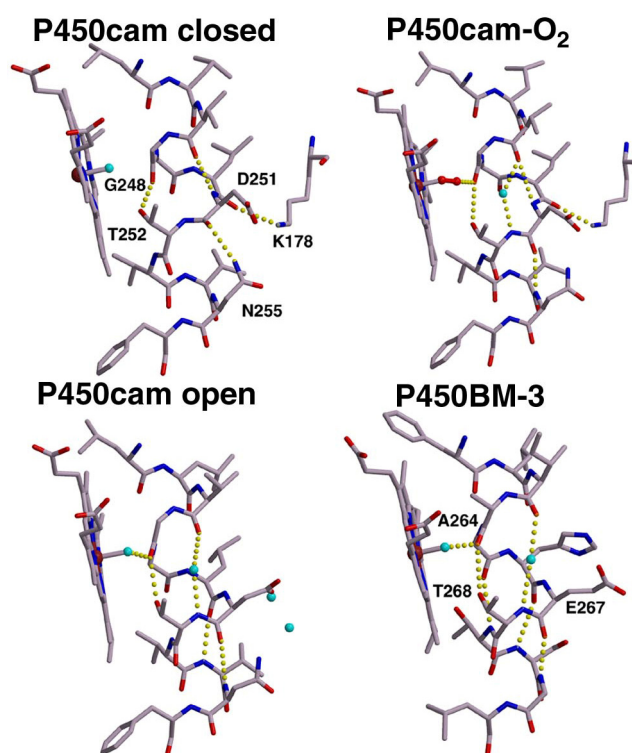
suggest that improved P450 inhibitors might be produced by taking advantage of the enzyme's intrinsic flexibility.

F/G loop movement affects the P450cam active site

The F/G loop movement in P450cam is coupled to changes in functionally important residues in the active center. I helix residues 248-252 participate in dioxygen activation.¹ In particular, Thr252, Asp251, and the Gly248 peptide carbonyl play crucial roles in the conversion of heme-bound dioxygen to high-valent iron-oxo or peroxo species. The open structure reveals that I helix residues also couple the coordination environment of the heme iron to enzyme tertiary structure peripheral to the active center.

In closed P450cam, the I helix segment adjacent to the heme iron bulges so that the peptide carbonyl groups of residues 248-251 do not form hydrogen bonds to C-terminal peptide nitrogens within the helix. A hydrogen bond between the Thr252 hydroxyl and Gly248 carbonyl stabilizes this bulge. In open P450cam, the bulge shifts toward the N-terminal end of the I helix. To effect this change the peptide bonds between residues 250-251 and 251-252 rotate 90° relative to the closed structure and anneal back into the helix (Figure 3.6), while the carbonyls of Leu245 and Leu246 are no longer hydrogen bonded within the helix but instead are bonded to a buried water molecule (Figure 3.6, 3.7). This shift in the I helix bulge arises from a 1.5 Å translation of the N-terminal half of this helix that preserves hydrophobic contacts with the retracted

Figure 3.6. The active sites of P450BM-3 and P450cam (closed, dioxygen bound, and open conformations). Regularization of the I helix between Leu250 and Asn255 compensates for the loss of main chain hydrogen bonds between Leu245 and Leu250 in the open P450cam structure. Interactions with the F and G helices break the hydrogen bond between the Asn255 side-chain amide and the Asp251 carbonyl, allowing the 251-252 peptide to flip down and hydrogen bond to the Asn255 peptide amide. As in dioxygen-bound ferrous P450cam, this peptide flip is accompanied by the introduction of a helix-bridging water molecule.³⁴ Movement of the F and G helices also breaks the hydrogen bond between Lys178 and the peptide carbonyl of Leu250, allowing the 250-251 peptide bond to flip 90 degrees and anneal into the helix.

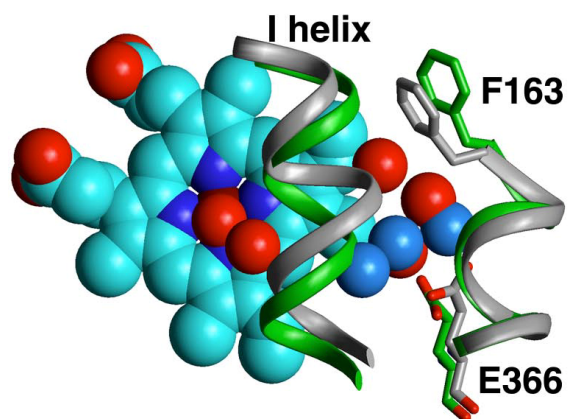


conformation of the F and G helices (Figure 3.3, 3.7).

The altered interactions of the F and G helices with the I helix in open P450cam regularizes the I helix to conformations similar to those found in other P450 structures. In P450BM-3 and P450NOR, the I helix residues equivalent to P450cam 249-251 all have standard helical conformations. This is one more helical residue (249) than open P450cam, two more residues than O₂-bound ferric P450cam (249 and 250), and three more residues than closed P450cam, where residues 249, 250, and 251 all form hydrogen bonds outside the I helix. Taken together, these structures show that the I helix backbone adopts different conformations depending on the ligand bound. Importantly, the I helix backbone conformation controls the water structure surrounding the heme iron (Figure 3.6).

The I helix communicates changes in the F and G helices to the coordination environment above the heme. As a result of the I helix conformational changes in the open structure, the Gly248 carbonyl is even closer to the heme iron (4.8 Å) than in either the O₂ complex (5.5 Å) or the low-spin closed conformation (6.4 Å). The resulting short hydrogen bond (2.6 Å) from the Gly248 carbonyl to the iron-ligating water molecule stabilizes water-bound, low-spin, low-potential heme in the open form of the enzyme. Tilting the equilibrium towards water-ligated, ferric heme may help prevent heme reduction and the subsequent production of superoxide, peroxide, and other toxic forms

Figure 3.7. Buried water molecules facilitate the I helix rearrangement between open (green ribbon and red waters) and closed states (gray ribbon and blue waters). Note the shift of the I helix bulge and concurrent rearrangement of the buried waters. Glu366, a highly conserved residue among P450s, anchors the water molecules.



of reduced dioxygen.

Solvation changes important for substrate binding and catalysis

Twenty-four additional ordered water molecules hydrate newly exposed surfaces in the Ru-bound structures of P450cam (Figure 3.2). This number agrees well with earlier results that suggested the involvement of 28 water molecules in the catalytic cycle of the enzyme.³⁵ Due to the motion of the F and G helices, 9 new ordered water molecules form hydrogen bonds to Asp251, Arg186, Asp182, and Lys178 between the F and I helices. In addition, the F helix residues Thr185 and Thr181 rotate in the open structure so that their hydroxyls can form hydrogen bonds to water. Although Asp251 has been implicated in proton delivery to the active center, this residue is sequestered in the closed structure. Hydration of Asp251 in the open structure suggests that the altered hydrogen bond patterns of this conformation are not only important for substrate binding but also in facilitating proton and/or water molecule exchange during catalysis.

Buried water molecules mediate conformational flexibility in proteins through their mobility and ability to switch hydrogen-bonding partners.³⁶ Three conserved water molecules that have analogs in P450terp, P450eryF, and P450NOR stabilize the disrupted I helix i to $i+4$ hydrogen bonds in both the open and closed conformations (Figure 3.7).^{19a,37} The role of water molecules in facilitating the open/closed transition of

P450cam is similar to that found in the facilitation of large scale conformational fluctuations of acetylcholinesterase.³⁸

Structural flexibility makes cytochrome P450 a versatile catalyst

The motions of the F and G helices we observe in the comparison of the open and closed P450cam structures, along with similar differences in structure between substrate-bound and free P450BM-3,³⁹ suggest an explanation for the extraordinary substrate diversity associated with human P450s. If P450cam, an enzyme specialized for a single, small substrate, undergoes such large motions upon substrate binding, many of the human liver isozymes may as well. In effect, the F and G helices act as a clamp, both to fix the substrate over the heme and to exclude excess water from the active site. Remarkably, P450cam hydroxylates Ru-substrates when suitable electron donors are provided.⁴⁰ This observation further underlines the extraordinary ability of P450s to handle widely varying substrates.

Cytochromes P450 provide yet another demonstration of the importance of energetically low-lying conformational states in protein function. As in P450cam, these alternate conformations may be difficult to detect if they form and decay on a submicrosecond time scale. Our structures show that regions distant from the active center are critical for substrate binding and catalysis in cytochromes P450. Thus,

although local structure tunes the reactivity of a metallo-cofactor, the entire polypeptide generates the dynamic properties necessary for enzymatic activity.

ACKNOWLEDGEMENT: This work was supported by the Fannie and John Hertz Foundation (A.R.D.), the Helen Hay Whitney Foundation (B.R.C.), the National Institutes of Health predoctoral program (I.J.D.), the National Science Foundation, and the National Institutes of Health.

REFERENCES

1. *Cytochrome P450: Structure, Mechanism and Biochemistry 2nd Edn.* ed. Ortiz de Montellano, P. R. Plenum Press: New York, NY 1995.
2. Nelson, D. R. *Arch. Biochem. Biophys.* **1999**, *369*, 1-10.
3. Nelson, D. R. Cytochrome P450 home page (15 March 2001)
<http://drnelson.utmem.edu/CytochromeP450.html>.
4. Guengerich, F. P. in *Cytochrome P450: Structure, Mechanism and Biochemistry*, ed. Ortiz de Montellano, P. R. Plenum Press: New York, NY 1995, pp. 473-536.
5. Guengerich, F. P. *Annu. Rev. Pharmacol. Toxicol.* **1999** *39*, 1-17.
6. (a) Dmochowski, I. J.; Crane, B. R.; Wilker, J. J.; Winkler, J. R.; Gray, H. B. *Proc. Nat. Acad. Sci. USA* **1999**, *96*, 12987-12990. (b) Wilker, J. J.; Dmochowski, I. J.; Dawson, J. H.; Winkler, J. R.; Gray, H. B. *Angew. Chem., Int. Ed. Engl.* **1999**, *38*, 90-92.
7. Otwinowski, Z.; Minor, W. *Methods Enzymol.* **1997**, *276*, 307-326.
8. Navaza, J. *Acta Crystallogr., Sect. A* **1994**, *50*, 157-163.
9. Brunger, A. T.; Adams, P. D.; Clore, G. M.; DeLano, W. L.; Gros, P.; Grosse-Kunstleve, R. W.; Jiang, J. S.; Kuszewski, J.; Nilges, M.; Pannu, N. S., *et al.* *Acta Crystallogr., Sect. D* **1998**, *54*, 905-921.
10. McRee, D. E. *J. Mol. Graphics* **1992**, *10*, 44-46.

11. Laskowski, R. A.; MacArthur, M. W.; Moss, D. S.; Thornton, J. M. *J. Appl. Crystallogr.* **1993**, *26*, 283-291.
12. Esnouf, R. M. *J. Mol. Graphics* **1997**, *15*, 133-138.
13. Kraulis, P. J. *J. Appl. Crystallogr.* **1991**, *24*, 946-950.
14. Merritt, E. A.; Bacon, D. J. *Methods Enzymol.* **1997**, *277*, 505-524.
15. Sonner, M. F.; Olson, A. J.; Sphener, J. C. *Biopolymers* **1996**, *38*, 305-320.
16. Gerstein, M.; Lesk, A. M.; Chothia, C. *Biochemistry* **1994**, *33*, 6740-6749.
17. Raag, R.; Poulos, T. L. *Biochemistry* **1991**, *30*, 2674-2684.
18. (a) Ravichandran, K. G.; Boddupalli, S. S.; Hasemann, C. A.; Peterson, J. P.; Deisenhofer, J. *Science* **1993**, *261*, 731-736. (b) Li, H.; Poulos, T. L. *Nature Struct. Biol.* **1997**, *4*, 140-146. (c) Park, S. Y.; Shimizu, H.; Adachi, S.; Nakagawa, A.; Tanaka, I.; Nakahara, K.; Shoun, H.; Obayashi, E.; Nakamura, H.; Iizuka, T. *et al. Nature Struct. Biol.* **1997**, *4*, 827-832.
19. (a) Hasemann, C. A.; Ravichandran, K. G.; Peterson, J. A.; Deisenhofer, J. *J. Mol. Biol.* **1994**, *236*, 1169-1185. (b) Williams, P. A.; Cosme, J.; Sridhar, V.; Johnson, E. F.; McRee, D. E. *Mol. Cell.* **2000**, *5*, 121-131.
20. Yano, J. K.; Koo, L. S.; Schuller, D. J.; Li, H.; Ortiz de Montellano, P. R.; Poulos, T. L. *J. Biol. Chem.* **2000**, *275*, 31086-31092.

21. DiPrimo, C.; Hoa, G. H. B.; Deprez, E.; Douzou, P.; Sligar, S. G. *Biochemistry* **1993**, *32*, 3671-3676.
22. Diprimo, C.; Deprez, E.; Sligar, S. G.; Hoa, G. H. B. *Biochemistry* **1997**, *36*, 112-118.
23. Prasad, S.; Mazumdar, S.; Mitra, S. *FEBS Lett.* **2000**, *477*, 157-160.
24. Ueng, Y.-F.; Kuwabara, T.; Chun, Y.-J.; Guengerich, F. P. *Biochemistry* **1997**, *36*, 370-381.
25. Lepesheva, G. I.; Strushkevich, N. V.; Usanov, S. A. *Biochim. Biophys. Acta* **1999**, *1434*, 31-43.
26. Podust, L. M.; Poulos, T. L.; Waterman, M. R. *Proc. Natl. Acad. Sci. USA* **2001**, *98*, 3068-3073.
27. (a) Paulsen, M. D.; Ornstein, R. L. *Proteins* **1995**, *21*, 237-243. (b) Li, H.; Poulos, T. L. *Acta Crystallogr., Sect D* **1995**, *51*, 21-32. (c) Ludemann, S. K.; Lounnas, V.; Wade, R. C. *J. Mol. Biol.* **2000**, *303*, 797-811.
28. Rendic, S.; Dicarlo, F. J. *Drug Metab. Rev.* **1997**, *29*, 413-580.
29. Patrick, C. R.; Prosser, G. S. *Nature* **1960**, *187*, 1021.
30. Williams, J. H.; Cockcroft, J. K.; Fitch, A. N. *Angew. Chem., Int. Ed. Eng.* **1992**, *31*, 1655.

31. (a) Sakai, T.; Miki, Y.; Tsuboi, M.; Takeuchi, H.; Ema, T.; Uneyama, K.; Utaka, M. *J. Org. Chem.* **2000**, *65*, 2740-2747. (b) Luhmer, M.; Bartik, K.; Dejaegere, A.; Bovy, P.; Reisse, J. *Bull. Soc. Chim. Fr.* **1994**, *131*, 603-606. (c) Bovy, P. R.; Getman, D. P.; Matsoukas, J. M.; Moore, G. J. *Biochim. Biophys. Acta* **1991**, *1079*, 23-28. (d) Jacobsen, E. J.; Mitchell, M. A.; Hemdges, S. K.; Belonga, K. L.; Skaletzky, L. L.; Stelzer, L. S.; Lindberg, T. J.; Fritzen, E. L.; Schoztarez, H. J.; O'Sullivan, T. J. *et al. J. Med. Chem.* **1999**, *42*, 1525-1536. (e) West, A. P.; Mecozzi, S.; Dougherty, D. A. *J. Phys. Org. Chem.* **1997**, *10*, 347-350.
32. Kim, C.-Y.; Chang, J. S.; Doyon, J. B.; Baird, T. T. J.; Fierke, C. A.; Jain, A.; Christianson, D. W. *J. Am. Chem. Soc.* **2000**, *122*, 12125-12134.
33. Poulos, T. L.; Finzel, B. C.; Gunsalus, I. C.; Wagner, G. C.; Kraut, J. *J. Biol. Chem.* **1985**, *260*, 16122-16130.
34. Schlichting, I.; Berendzen, J.; Chu, K.; Stock, A. M.; Maves, S. A.; Benson, D. E.; Sweet, R. M.; Ringe, D.; Petsko, G. A.; Sligar, S. G. *Science* **2000**, *287*, 1615-1622.
35. Diprimo, C.; Sligar, S. G.; Hoa, G. H. B.; Douzou, P. *FEBS Lett.* **1992**, *312*, 252-254.
36. Fischer, S.; Verma, C. S. *Proc. Natl. Acad. Sci. USA* **1999**, *96*, 9613-9615.

37. (a) Cupp-Vickery, J. R.; Poulos, T. L. *Nature Struct. Biol.* **1995**, *2*, 144-153. (b) Shimizu, H.; Obayashi, E.; Gomi, Y.; Arakawa, H.; Park, S.-Y.; Nakamura, H.; Adachi, S.-I.; Shoun, H.; Shiro, Y. *J. Biol. Chem.* **2000**, *275*, 4816-4826.
38. Koellner, G.; Kryger, G.; Millard, C. B.; Siman, I.; Sussman, J. L.; Steiner, T. *J. Mol. Biol.* **2000**, *296*, 713-726.
39. Li, H.; Poulos, T. L. *Biochim. Biophys. Acta* **1999**, *1441*, 141-149.
40. Dmochowski, I. J.; Dunn, A. R.; Wilker, J. J.; Crane, B. R.; Green, M. T.; Dawson, J. H.; Sligar, S. G.; Winkler, J. R.; Gray, H. B. *Methods Enzymol.* **2002**, *357*, 120-133.

Chapter 4

Fluorescent probes for cytochrome P450 structural characterization and inhibitor screening[†]

[†]Adapted from: Dunn, A. R.; Hays, A.-M. A.; Goodin, D. B; Stout, C. D.; Chiu, R.; Winkler, J. R.; Gray, H. B. *J. Am. Chem. Soc.*, **2002**, *124*, 10254-10255.

Acknowledgements:

The synthesis and spectroscopy discussed in this paper were performed in collaboration with Richard Chiu. The crystal structures of P450cam:danysl probe conjugates were determined by Anna-Maria Hays, David Goodin, and C. David Stout.

ABSTRACT

We have synthesized two dansyl-based luminescent probes (D-4-Ad and D-8-Ad) that target cytochrome P450cam. D-4-Ad luminescence is quenched by Förster energy transfer upon binding ($K_d = 0.83 \mu\text{M}$), but is restored when the probe is displaced from the active site by camphor. In contrast, D-8-Ad ($K_d \sim 0.02 \mu\text{M}$) is not displaced from the enzyme even in the presence of a large excess of camphor. The 2.2 Å resolution crystal structure of the D-8-Ad:P450cam complex reveals extensive hydrophobic contacts between the probe and the enzyme, which result from the conformational flexibility of the B', F and G helices. Probes with properties similar to those of D-4-Ad potentially could be useful for screening P450 inhibitors.

INTRODUCTION

Substrate-specific cytochromes P450 play major roles in steroid and eicosanoid biosynthesis, and thus constitute important drug design targets.¹ In contrast, P450 isozymes expressed in the liver take part in the metabolism of nearly all drugs.² Adverse drug reactions, for instance to Prozac,³ result from individual variations in hepatic P450s.⁴ It is thus important to predict which P450s interact with a potential drug candidate, and to understand the nature of these interactions.

We have developed fluorescent probe molecules for P450cam that consist of an α,ω -diaminoalkane chain connecting a dansyl fluorophore to the P450cam substrate adamantane (Scheme 4.1). The synthesis of the dansyl-substrates was designed to be short, robust, and modular for maximum ease and flexibility. A shift in Soret absorption (Figure 4.1) as well as greatly diminished dansyl luminescence attributable to Förster energy transfer to the heme⁵ (Figure 4.2) accompany probe binding. When D-4-Ad is displaced from the active site by camphor, fluorescence is restored (Figure 4.2a).⁶ Because a bright signal stands out against a dark background, substrate or inhibitor binding is readily detected. This assay, which is both simple and sensitive, can be employed to screen combinatorial chemical libraries.⁷

Scheme 4.1. (A) Dansyl-based fluorescent probe molecules used in this study. (B)

Synthesis of D-4-Ad.

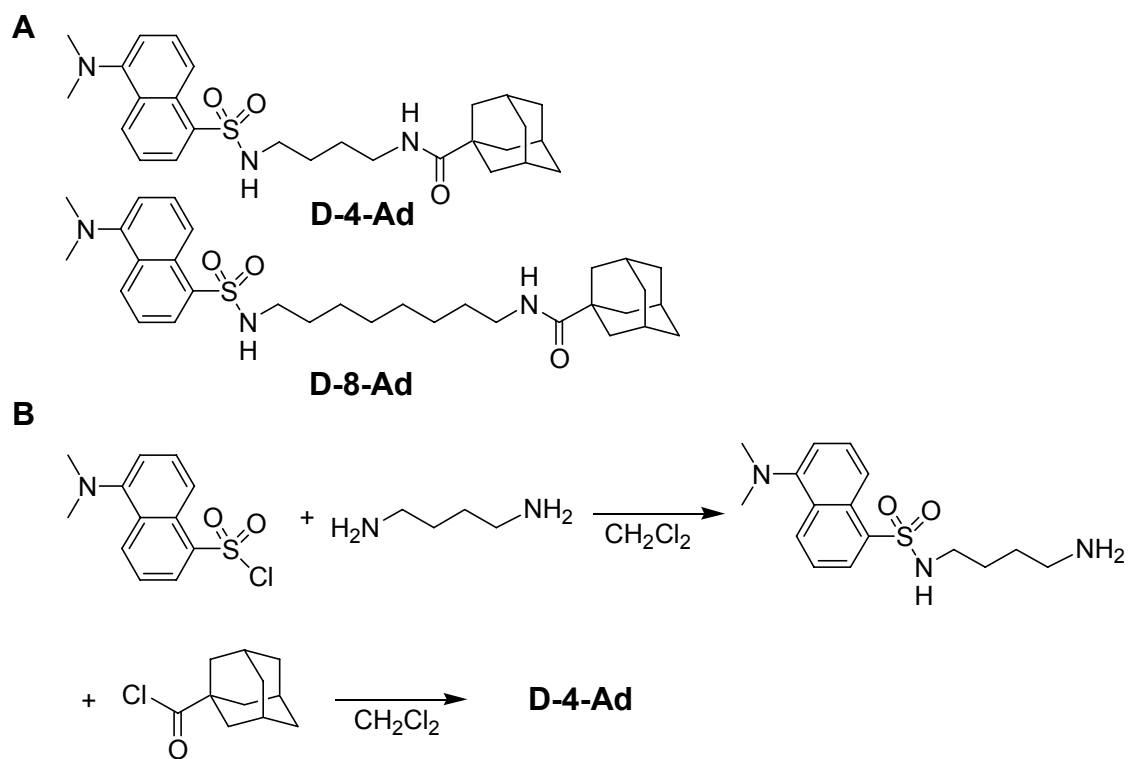


Figure 4.1. (A) Absorption spectra showing the binding of camphor to P450cam (4.9 μM) in the presence of 1 equivalent of D-4-Ad. The initial addition of D-4-Ad to P450cam results in a shift in the Soret from 416 to 414 nm. A fit of the data to a competitive binding model gives a dissociation constant of 0.83 μM . (B) The camphor-induced shift from low- to high-spin P450cam (5.7 μM) in the presence of 1 equivalent of D-8-Ad. Black, P450cam; purple, P450cam + 1 equivalent dansyl probe; blue to red, 0.5, 1, 2, 4, 8, 16, 32, and 64 equivalents camphor.

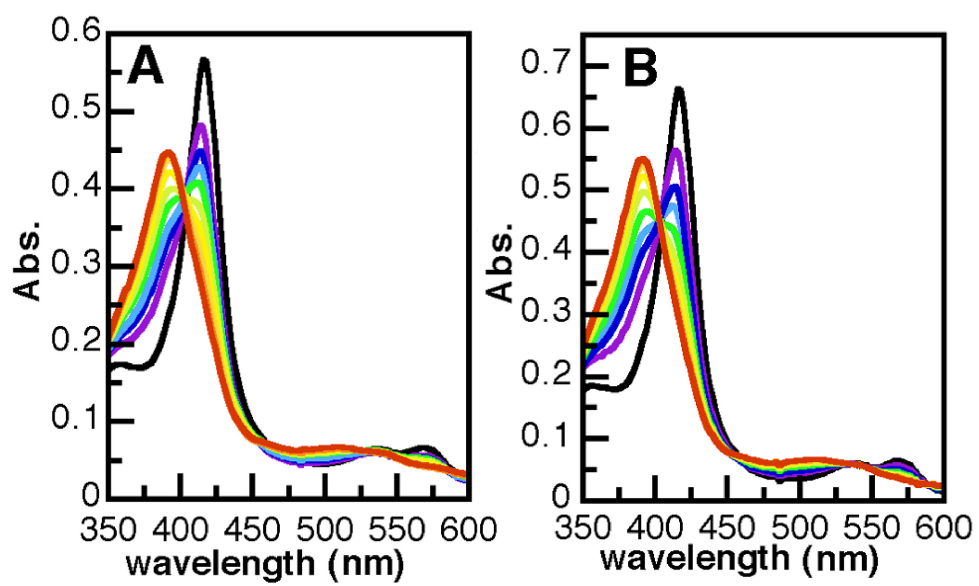
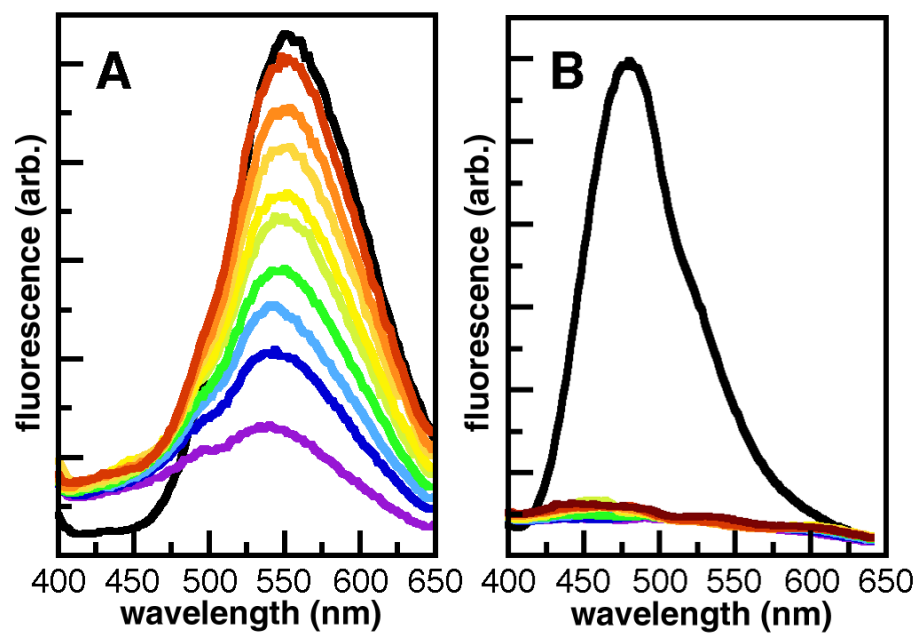


Figure 4.2. Fluorescence spectra of D-4-Ad (A) and D-8-Ad (B). Black, 2 μM D-8-Ad or D-4-Ad; purple, 2 μM dansyl probe + 1 equivalent P450cam; blue to red: 2 μM P450cam and dansyl probe + 0.5, 1, 2, 4, 8, 16, 32, and 64 equivalents of camphor ($K_d=1.6 \mu\text{M}$).⁸



MATERIALS AND METHODS

P450cam was expressed and purified as previously described.⁹ Steady-state UV-visible absorption spectra were measured on a Hewlett Packard 8452A diode array spectrophotometer. Steady-state fluorescence spectra were measured using an ISS K2 fluorometer ($\lambda_{\text{ex}} = 340 \text{ nm}$). Absorption and emission spectra were collected in quartz cuvettes using 50 mM potassium phosphate buffer (pH 7.4) containing 100 mM KCl. NMR spectra were collected on an Oxford Instruments 300 MHz NMR and analyzed with Varian VNMR 6.1B software. Electrospray mass spectra were collected on a Finnigan LCQ ion trap mass spectrometer. Buried solvent accessible surface area was calculated using the solvation module of InsightII (1.4 Å radius probe). All reagents were purchased from the Aldrich chemical company and used as received. DMF and N,N-diisopropylethylamine were anhydrous, and used as received.

RESULTS AND DISCUSSION

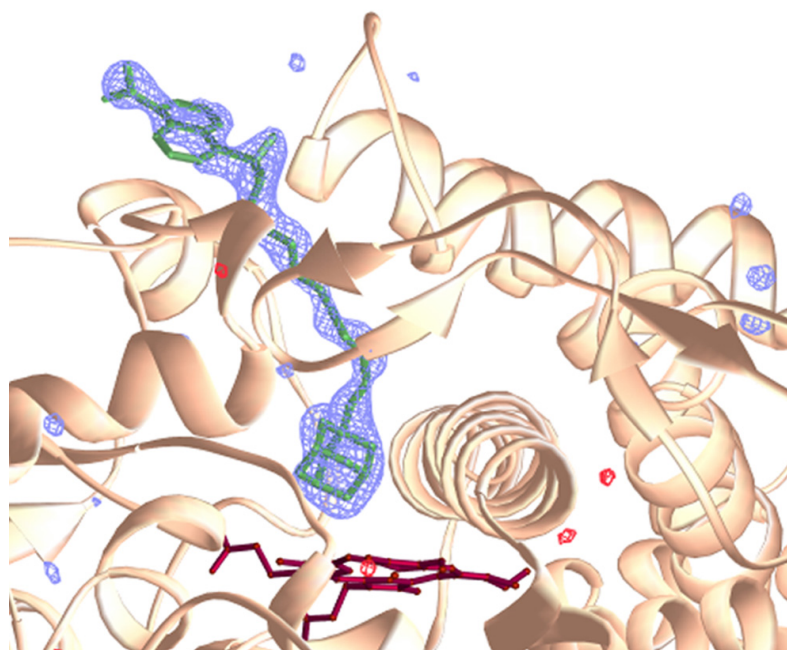
Both fluorescence and absorption spectra show that D-4-Ad binding to P450cam is competitive with camphor. The Soret shift (416 to 414 nm) induced by D-4-Ad indicates that it binds in the active site. With a K_d of 0.83 μM , D-4-Ad binds twice as strongly as the natural substrate. D-8-Ad also induces a shift in the Soret maximum from 416 to 414 nm: from the integrated D-8-Ad fluorescence in the presence and absence of P450cam, we estimate an upper limit $K_d \sim 0.02 \mu\text{M}$ for this probe.

Interestingly, the titration of a 1:1 mixture of D-8-Ad and P450cam with camphor also shows a shift in the Soret to 392 nm, and an *apparent* camphor K_d of $\sim 1 \mu\text{M}$ (Figure 4.1B). However, the steady-state luminescence titrations indicate that D-8-Ad remains bound to P450cam even when the absorption spectrum indicates that the heme has converted fully to its high spin, and presumably camphor-bound, form. The luminescence and absorption data are best reconciled by a model that includes simultaneous camphor and D-8-Ad binding. Given the low K_d of D-8-Ad, it is perhaps not surprising that camphor binding fails to expel the probe into solution.

The crystal structure of the P450cam:D-8-Ad complex shows that the probe binds in the same channel as $\text{Ru}^{\text{II}}(\text{bpy})_3$ -linker-Ad (bpy = 2,2'-bipyridine) analogs (Figure 4.3).^{9,10} The eight-carbon chain is nearly fully extended, allowing the dansyl moiety to bind at the surface of the protein. The good fit is attributable to conformational flexibility, that is, the F and G helices open just enough to allow the probe to enter and bind. The observed conformation is midway between the “closed” (camphor)¹¹ and “open” (Ru-linker-Ad)^{10c} structures.

The structure reveals a hydrogen bond between the amide carbonyl of the probe and Tyr96 in P450cam:D-8-Ad, mimicking the hydrogen bond between camphor and Tyr96 in the P450cam:substrate complex.¹¹ In addition, there are a great many hydrophobic interactions between the probe molecule and the enzyme; analysis of these

Figure 4.3. The 2.2 Å resolution structure of the D-8-Ad:P450cam cocrystal, with the omit electron density ($|F_{\text{obs}}| - |F_{\text{calc}}|$) contoured at 4.0 σ (blue positive, red negative).

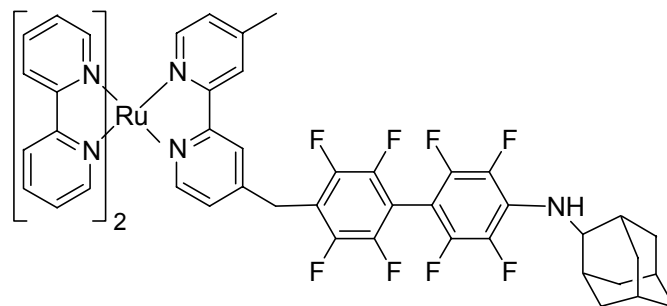
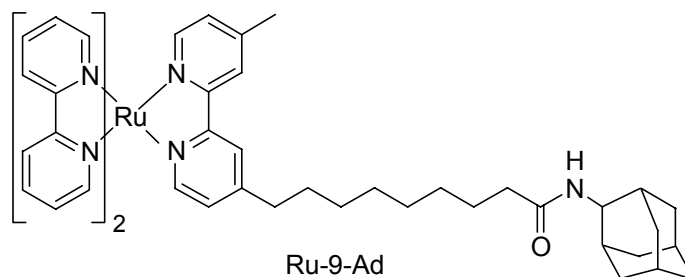


contacts shows that much of the solvent accessible surface area is buried. The estimated K_d of 0.02 μM corresponds to a binding energy of ~ 11 kcal/mol, or ~ 11 cal/mol \AA^2 (Figure 4.4). The $\text{Ru}(\text{bpy})_3^{2+}$ analogs (Ru-9-Ad and Ru-F₈bp-Ad) do not bind as tightly to P450cam, but the free energy changes per buried surface area are comparable.

The structure of the D-4-Ad:P450cam complex shows the enzyme in a conformation similar to that observed in the P450cam:Ru-wire conjugates (Figure 4.5). The shorter D-4-Ad hydrocarbon tether results in dansyl moiety occupying the relatively narrow “neck” of the substrate access channel, thus capturing the enzyme in a relatively more open conformation. This inferior steric fit as compared to the D-8-Ad:P450cam structure likely is responsible for the differences in binding constants observed for D-4-Ad and D-8-Ad.

In addition, a preliminary structure of the ternary P450cam:D-8-Ad:camphor complex has recently been determined. Initial analysis based on partial refinement of this data indicates that D-8-Ad remains bound in the active site and substrate access channel.¹² Importantly, the F and G helices adopt a opened conformation akin to the Ru-wire bound structures, and markedly different than that observed in the D-8-Ad:P450cam conjugate structure. In addition, the B' helix and loop form a greatly altered conformation somewhat analogous to that seen in the Ru-F₈bp-Ad:P450cam structure.

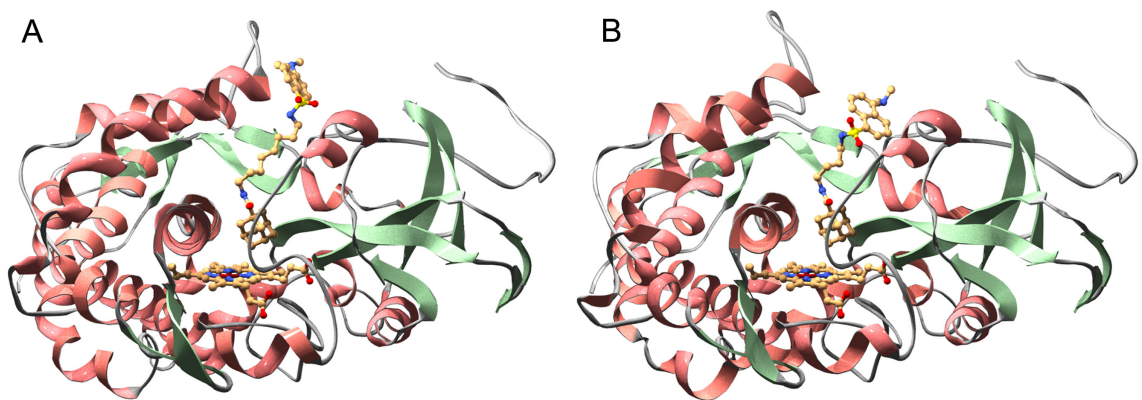
Figure 4.4. (top) Ruthenium *tris*-bipyridyl photosensitizers known to bind P450cam. The crystal structures of both compounds bound to P450cam have been determined to high resolution (Ru-9-Ad 1.55 Å, Ru-F₈bp-Ad 1.65 Å).^{10c} (bottom) Dissociation constants, binding energies, buried solvent accessible surface areas (SASA) and the binding energy per square angstrom of buried surface area for the P450cam:probe complexes. The Ru-9-Ad:P450cam crystal contains both Δ and Λ stereoisomers.

Ru-F₈bp-Ad

Ru-9-Ad

Compound	K _d (nM)	kcal mol ⁻¹	Buried SASA (Å ²)	cal mol ⁻¹ Å ⁻²
D-8-Ad	~20	~11	988	~11
Ru-9-Ad (Δ)	190	9.23	1097	8.4
Ru-9-Ad (Λ)	90	9.69	1042	9.3
Ru-F₈bp-Ad	74	9.80	1191	8.2

Figure 4.5. (A) Ribbon diagram of the D-8-Ad:P450cam crystal structure. (B) Ribbon diagram of the D-4-Ad:P450cam crystal structure; note the wider substrate access channel, and the deeper position of the dansyl moiety within the channel.



These provisional data demonstrate unambiguously that P450cam binds camphor and D-8-Ad simultaneously.

CONCLUDING REMARKS

Even though P450cam has evolved for a single, relatively small substrate, it has the ability to bind much larger molecules more tightly. The key to this ability is the mobility of the B', F, and G helices (Chapter 3).^{10c} Both solution¹³ and crystallographic¹⁴ studies of other P450s suggest that this feature is common to the P450 superfamily. The two probes described herein illustrate the usefulness of our methodology. D-4-Ad can be employed to screen potential P450 inhibitors, as it is easily displaced by other molecules with comparable or lower dissociation constants. In contrast, D-8-Ad binds extremely tightly: the conformational flexibility of the P450 fold allows the enzyme to close around the probe, thereby making a great many productive hydrophobic contacts. The insight gained from the D-8-Ad:P450cam structure could potentially lead to a more rational design strategy for P450 inhibitors.

ACKNOWLEDGEMENT

This work was supported by the Fannie and John Hertz Foundation (ARD), the National Science Foundation, and the National Institutes of Health (Metalloprotein Program Project Grant P01 GM48495; NRSA fellowship GM20703 to A-MAH).

REFERENCES AND NOTES

1. (a) Kagawa, N.; Waterman, M. R. In *Cytochrome P450: Structure, Mechanism and Biochemistry*; Ortiz de Montellano, P. R., Ed.; Plenum Press: New York, 1995, pp 419-442. (b) Capdevila, J. H.; Zeldin, D.; Makita, K.; Karara, A.; Falck, J. R. In *Cytochrome P450: Structure, Mechanism and Biochemistry*; Ortiz de Montellano, P. R., Ed.; Plenum Press: New York, 1995, pp 443-472. (c) Goss, P. E.; Strasser, K. *J. Clin. Oncol.* **2001**, *19*, 881-94. (d) Frye, L. L.; Leonard, D. A. *Crit. Rev. Biochem. Mol. Biol.* **1999**, *34*, 123-140. (e) Sheehan, D. J.; Hitchcock, C. A.; Sibley, C. M. *Clin. Microbiol. Rev.* **1999**, *12*, 40-79.
2. (a) Rendic, S.; DiCarlo, F. J. *Drug Metab. Rev.* **1997**, *29*, 413-580. (b) Guengerich, F. P. In *Cytochrome P450: Structure, Mechanism and Biochemistry*; Ortiz de Montellano, P. R., Ed.; Plenum Press: New York, NY, 1995, pp 473-536.
3. Otton, S. V.; Wu, D. F.; Joffe, R. T.; Cheung, S. W.; Sellers, E. M. *Clin. Pharm. Ther.* **1993**, *53*, 401-409.
4. Li, A. P. *Drug-drug interactions: scientific and regulatory perspectives*; Academic Press: New York, 1997; Vol. 21, pp 304
5. (a) Wu, P.; Brand, L. *Anal. Biochem.* **1994**, *218*, 1-13. (b) Selvin, P. R. *Nature Struct. Biol.* **2000**, *7*, 730-734.

6. The fluorescence of D-8-Ad (λ_{\max} 480 nm) is blue shifted from that of D-4-Ad (550 nm), indicating that the D-8-Ad environment is less polar [Li, Y.-H.; Chan, L.-M.; Tyer, L.; Moody, R. T.; Himel, C. M.; Hercules, D. M. *J. Am. Chem. Soc.* **1975**, *97*, 3118-3126]. One possible explanation is that the hydrophobic tail of D-8-Ad folds back in solution to partially cover the dansyl fluorophore, effectively lowering the local dielectric. Although the fluorescence maximum is not concentration dependent (data not shown), D-8-Ad aggregation cannot be ruled out.
7. Schobel, U.; Coille, I.; Brecht, A.; Steinwand, M.; Gauglitz, G. *Anal. Chem.* **2001**, *73*, 5172-5179.
8. Atkins, W. M.; Sligar, S. G. *J. Biol. Chem.* **1988**, *263*, 18842-18849.
9. Dmochowski, I. J.; Crane, B. R.; Wilker, J. J.; Winkler, J. R.; Gray, H. B. *Proc. Natl. Acad. Sci. USA* **1999**, *23*, 12987-12990.
10. (a) Wilker, J. J.; Dmochowski, I. J.; Dawson, J. H.; Winkler, J. R.; Gray, H. B. *Angew. Chem., Int. Ed. Engl.* **1999**, *38*, 90-92. (b) Dmochowski, I. J.; Crane, B. R.; Wilker, J. J.; Winkler, J. R.; Gray, H. B. *Proc. Natl. Acad. Sci. USA* **1999**, *23*, 12987-12990. (c) Dunn, A. R.; Dmochowski, I. J.; Bilwes, A. M.; Gray, H. B.; Crane, B. R. *Proc. Natl. Acad. Sci. USA* **2001**, *98*, 12420-12425.

11. Poulos, T. L.; Finzel, B. C.; Howard, A. J. *J. Mol. Biol.* **1987**, *195*, 867-700.
12. Anna-Maria A. Hays, personal communication.
13. (a) DiPrimo, C.; Hoa, G. H. B.; Deprez, E.; Douzou, P.; Sligar, S. G. *Biochemistry* **1993**, *32*, 3671-3676. (b) Prasad, S.; Mazumdar, S.; Mitra, S. *FEBS Lett.* **2000**, *477*, 157-160. (c) Lepesheva, G. I.; Strushkevich, N. V.; Usanov, S. A. *Biochem. Biophys. Acta* **1999**, *1434*, 31-43.
14. (a) Li, H.; Poulos, T. L. *Biochim. Biophys. Acta* **1999**, *1441*, 141-149. (b) Ravichandran, K. G.; Boddupalli, S. S.; Hasemann, C. A.; Peterson, J. A.; Deisenhofer, J. *Science* **1993**, *261*, 731-736. (c) Hasemann, C. A.; Ravichandran, K. G.; Peterson, J. A.; Deisenhofer, J. *J. Mol. Biol.* **1994**, *236*, 1169-1185. (d) Williams, P. A.; Cosme, J.; Sridhar, V.; Johnson, E. F.; McRee, D. E. *Mol. Cell* **2000**, *5*, 121-131. (e) Yano, J. K.; Koo, L. S.; Schuller, D. J.; Li, H.; Ortiz de Montellano, P. R.; Poulos, T. L. *J. Biol. Chem.* **2000**, *275*, 31086-31092.

Chapter 5

Ruthenium- and rhenium-diimine luminescent probes for nitric oxide synthase

Acknowledgements:

Experiments involving rhenium-diimine wires were performed in collaboration with Wendy Belliston.

ABSTRACT

Ruthenium- and rhenium-diimine based luminescent probes that bind to inducible nitric oxide synthase (iNOS) are described. The ruthenium probes have the structure $[\text{Ru}(\text{L}_2)\text{L}]^{2+}$, where L' is a perfluorinated biphenyl bridge connecting 4,4'-dimethylbipyridine to an enzyme substrate (adamantane, **1**), a heme ligand (imidazole, **2**), or F (**3**). Probe **2** binds in the active site of the murine iNOS truncation mutants $\Delta 65$ and $\Delta 114$, as demonstrated by a shift in the heme Soret from 422 to 426 nm. **1** and **3** also bind $\Delta 65$ and $\Delta 114$, as evidenced by biphasic luminescence decay kinetics. However, the heme absorption spectrum is not altered in the presence of **1** or **3**, Ru-wire binding is not affected by the presence of tetrahydrobiopterin or arginine, and the Ru to heme-Fe distances calculated from Förster energy transfer (FET) rates (~ 19 Å) are incompatible with binding in the iNOS dimer substrate access channel. These data suggest that **1** and **3** may instead bind to the distal side of the enzyme at the hydrophobic surface patch thought to interact with the NOS reductase domain. Novel rhenium-diimine probes with the structure $[\text{Re}(4,7\text{-dimethyl phenanthroline})(\text{CO})_3\text{L}]^+$, where L = imidazole- C_{12}F_8 -imidazole (**4**) or imidazole- C_{12}F_9 (**5**) are also described. Binding of **4** to $\Delta 114$ shifts the heme Soret to 426 nm, demonstrating that the terminal imidazole functionality ligates the heme iron. Steady-state luminescence measurements show that **4** binds $\Delta 114$ with a

dissociation constant of 6 nM. The Re-wire **5** binds $\Delta 114$ with a K_d of 3.4 μM , and causes a partial displacement of water from the heme iron. Compounds with properties similar to the Ru-diimine probes may provide a novel means of NOS inhibition by preventing electron transfer between the oxidase and reductase domains. The tight binding demonstrated by **4** and the surprising ability of **5** to bind in the NOS active site suggest novel designs for NOS inhibitors. Our results demonstrate the utility of time-resolved FET measurements in the characterization of small molecule-protein interactions that are otherwise difficult to observe.

INTRODUCTION

The enzyme nitric oxide synthase (NOS) is the major biological source of nitric oxide (NO), a secondary messenger acting in a myriad of circumstances that include neuronal development, regulation of blood pressure, apoptosis, neurotransmission, and immunological response.¹⁻⁷ Because of the central importance of NO, NOS has been implicated in septic shock, inflammation, a variety of neurodegenerative disorders, and heart disease.⁸⁻¹⁰

The NOS oxidase domain (NOSoxy) catalyzes the conversion of arginine and molecular oxygen to NO and citrulline.¹¹ The electrons necessary for this reaction are provided by a reductase domain, which is attached to the oxidase domain by a calmodulin-binding linker.^{12,13} NOS functions as a homodimer; the reductase domain from one half of the dimer reduces the oxidase domain of the other.^{14,15} Calmodulin binding is known to modulate electron transfer, and hence catalysis.¹⁶⁻¹⁸ Numerous crystal structures of NOSoxy have been determined,¹⁹⁻²¹ but the structure of the full-length enzyme remains elusive.

We have a long-standing interest in the high-valent intermediates thought to play key roles in heme-mediated oxidations.²²⁻²⁴ In order to observe these intermediates, we have designed Ru-diimine photosensitizers (Ru-wires) that bind to the mechanistically related enzyme cytochrome P450, and inject an electron into the active site upon

excitation with 470-nm light.²⁵ Energy transfer between the excited state of the Ru-wire and the heme also serves as a sensitive structural probe.^{22,26} Given the postulated mechanistic similarities between NOS and cytochrome P450, we have endeavored to develop similar probes for NOS.

MATERIALS AND METHODS

The synthesis and characterization of the Ru-wire probes is described in appendix A. Both time-resolved and steady-state spectroscopic measurements were performed as described in chapter 1. The Stuehr lab provided samples of murine inducible NOS_{oxy} with N-terminal truncations at residues 65 ($\Delta 65$) and 114 ($\Delta 114$). As provided, the protein samples contained millimolar concentrations of dithiothreitol, (DTT) which ligates the heme. Small aliquots of the protein solutions were exchanged into phosphate buffer (50 mM potassium phosphate, 100 mM potassium chloride) using a desalting column immediately before use. The presence of the heme Soret peak at 422 nm verified successful removal of the DTT.

High-spin, dimeric $\Delta 65$ iNOS was generated by incubating $\Delta 65$ with 1 mM tetrahydrobiopterin (H_4B) and 1 mM arginine (Arg) for 2 hours at 4 °C before diluting the sample to final concentrations of 0.1 mM H_4B and 1 mM Arg. Satisfactory Arg and H_4B binding was signaled by a shift of the Soret to 396 nm. NOS extinction coefficients were determined using the hemochromogen assay: 1 mL of NOS solution was diluted

with 0.125 mL 0.5 M NaOH and 0.125 mL pyridine, then reduced with several grains of sodium dithionite. The resulting ferrohemochromogen concentration was calculated using an extinction coefficient of $31 \text{ mM}^{-1} \text{ cm}^{-1}$ at 556 nm. The assays were calibrated using cytochrome P450cam ($\epsilon_{416} = 115 \text{ mM}^{-1} \text{ cm}^{-1}$). The NOS extinction coefficients calculated using this method are: $\Delta 65 \epsilon_{422} = 75 \text{ M}^{-1} \text{ cm}^{-1}$ (substrate free and bound); substrate-free $\Delta 114 \epsilon_{422} = 85 \text{ M}^{-1} \text{ cm}^{-1}$.

RESULTS

Ru-wires. In the initial stages of our investigation we tested previously developed Ru-wires (Figure 5.1) to see if any bound NOSoxy. The two murine inducible NOSoxy truncation mutants $\Delta 114$ and $\Delta 65$ were investigated in order to probe the effect of the monomer-dimer NOSoxy equilibrium. $\Delta 114$ is solely monomeric, while $\Delta 65$ exists in a monomer-dimer equilibrium, and forms a strong dimer in the presence of tetrahydrobiopterin (H_4B).²⁷

No change in the NOSoxy heme absorption spectrum was observed upon the stoichiometric addition of **1** or **3** to either $\Delta 114$ or $\Delta 65$. In contrast, the addition of excess **2** to $\Delta 65$ and $\Delta 114$ resulted in a heme Soret shift from 420 and 422 to 426 nm, consistent with imidazole ligation of the heme (Figures 5.2 and 5.3). The absorption spectrum of Arg- and H_4B -bound $\Delta 65$ is not altered in the presence of **1-3**, indicating that none of the Ru-wires displace Arg from the NOS active site.

Figure 5.1. Ru-wires. The interaction of these compounds with cytochrome P450cam is described in Chapter 2.

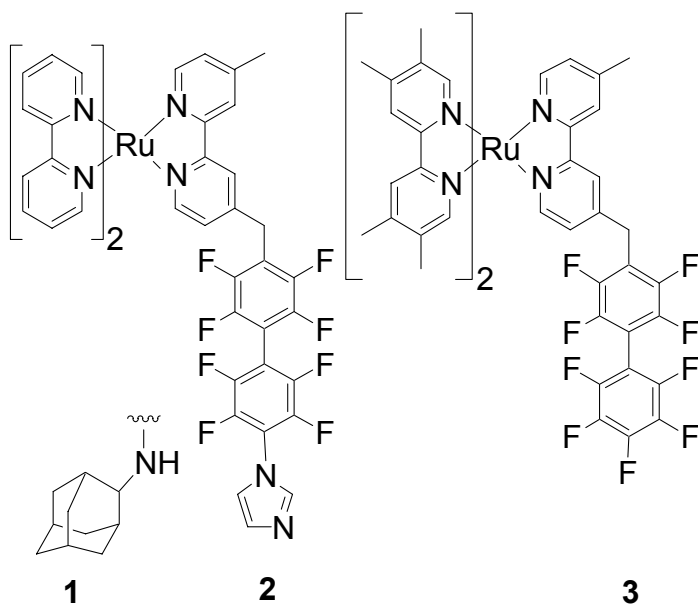


Figure 5.2. UV-visible absorption spectrum of $\Delta 114$ alone ($5.7 \mu\text{M}$; green) and bound to **2**, corrected for the absorption due to the Ru-wire ($+ 20.5 \mu\text{M}$ **2**; blue). The heme Soret peak shifts from 422 to 426 nm in response to Ru-wire binding.

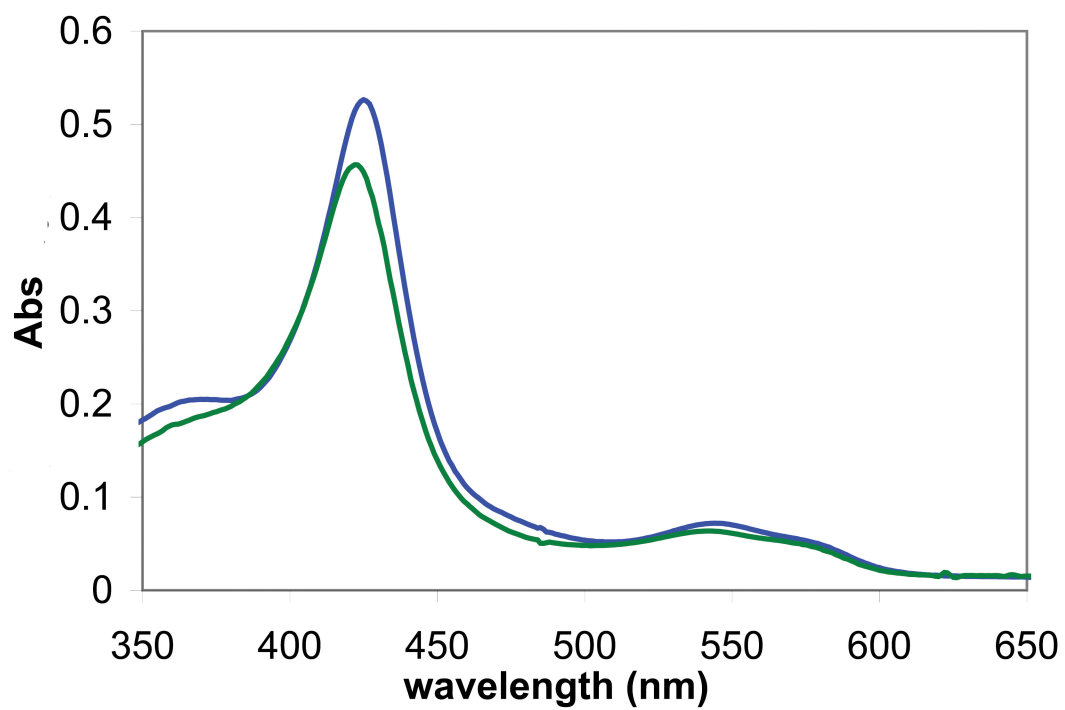
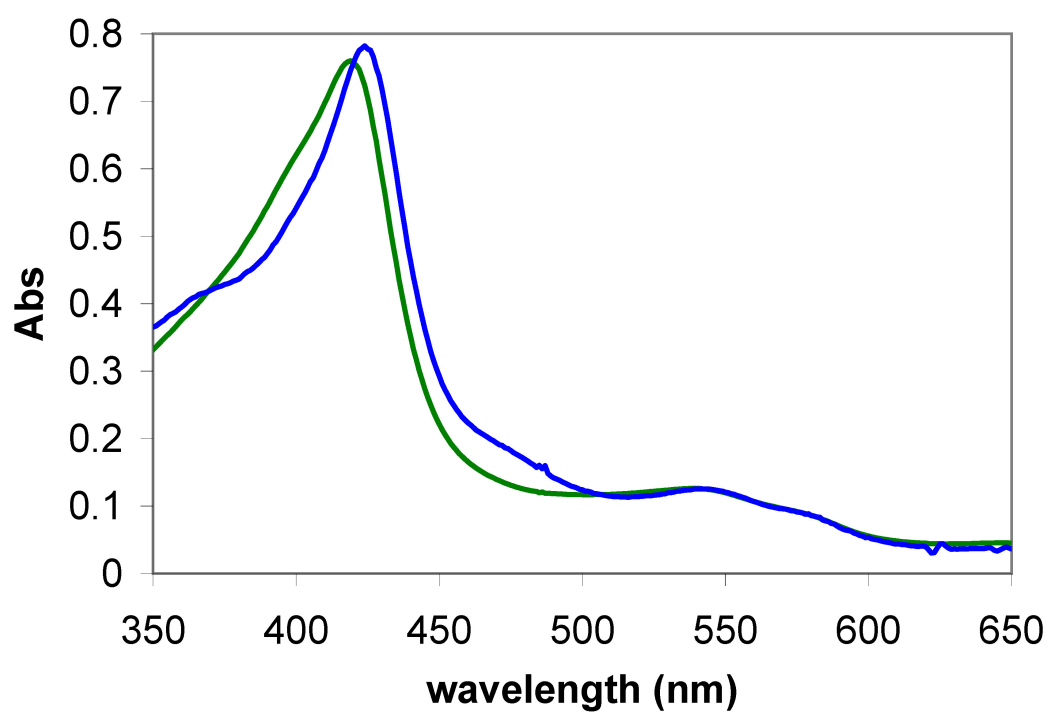


Figure 5.3. UV-visible absorption spectrum of $\Delta 65$ alone (10 μM ; green) and bound to **2** (+ 52 μM **2**; blue), corrected for absorption due to the Ru-wire. The heme Soret peak shifts from 418 to 426 nm in response to Ru-wire binding.



In all cases, biexponential Ru-wire luminescence decays are observed in the presence of quantities of stoichiometric $\Delta 114$ and $\Delta 65$, indicating that the Ru-wires bind to the enzyme (Figure 5.4). As described in Chapter 2, the weightings of the fast and slow phases were used to calculate dissociation constants, while the rates of energy transfer were used to calculate Ru-heme distances. Ru-Fe distances previously calculated for Ru-wire:P450cam conjugates match those observed in the corresponding crystal structures to within 0.4 Å (Chapter 1, ref. 22).

The Ru-wires bind with micromolar dissociation constants and Ru-Fe distances of 18-21 Å (Table 1). Interestingly, the Ru-wires bind $\Delta 114$, $\Delta 65$, and H₄B- and Arg-bound $\Delta 65$ with dissociation constants that are essentially identical. The Ru-Fe distances calculated for **1** and **3** are similar for $\Delta 114$ and $\Delta 65$, and are unaffected by the presence of H₄B and Arg (Table 1). In contrast, the Ru-Fe distance calculated for the **2**: $\Delta 144$ conjugate is 17.8 Å, and increases from 19.3 to 20.9 Å upon addition of H₄B and Arg to the **2**: $\Delta 65$ conjugate, suggesting displacement from the active site.

The shifts in the absorption spectra of $\Delta 65$ and $\Delta 114$ in the presence of **2** clearly indicate that the imidazole functionality of **2** ligates the heme. In contrast, the spectroscopic evidence suggests that **1** and **3** do not bind in the active site: The heme absorption spectrum is not altered in the presence of **1** or **3**, and the K_d's and Ru-Fe distances measured with these Ru-wires are not affected by the presence of H₄B and Arg.

Figure 5.4. Sample transient luminescence data for **1** (blue) and a 1:1 mixture of **1** and $\Delta 65$ (1.8 μM ; green). The fast component of the luminescence decay corresponds to **1** bound to $\Delta 65$.

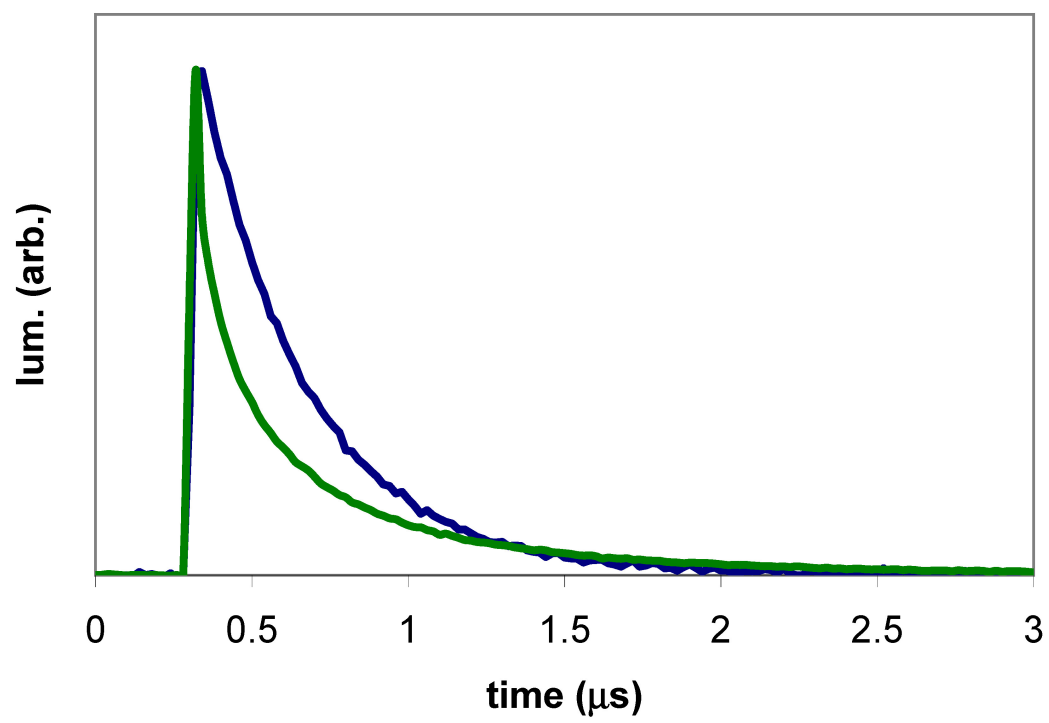


Table 1. Ru-wire dissociation constants and Ru-Fe distances calculated from FET.

Uncertainties are the root-mean-square deviations calculated from independent measurements (3 with $\Delta 114$, 2 with $\Delta 65$, 3 with $\Delta 65 + \text{Arg}$, + H_4B).

Compound	$\Delta 114$		$\Delta 65$		$\Delta 65 + \text{Arg}, +\text{H}_4\text{B}$	
	K_d (μM)	Ru-Fe (\AA)	K_d (μM)	Ru-Fe (\AA)	K_d (μM)	Ru-Fe (\AA)
1	0.88 ± 0.15	18.9 ± 0.1	0.54 ± 0.04	19.6 ± 0.2	1.7 ± 0.4	19.6 ± 0.4
2	7.1 ± 0.4	17.8 ± 0.5	6.5 ± 2.4	19.3 ± 0.6	7.2 ± 3.4	20.9 ± 0.8
3	0.71 ± 0.09	20.1 ± 0.1	0.58 ± 0.16	20.2 ± 0.4	0.89 ± 0.15	21.0 ± 0.3

Structural modeling suggests that while **2** can bind to the active site of $\Delta 114$ (Figure 5.5), the Ru-wires cannot fit down the substrate access channel of dimeric NOS due to the bulk of the ruthenium *tris*-bipyridyl moiety (Figure 5.6). Instead, the Ru-Fe distances suggest that the Ru-wires may bind on the distal side of the enzyme, at the binding site of the reductase domain. This binding model is consistent with the result that the dissociation constants and Ru-heme distances of **1** and **3** are unaffected by the addition of Arg and H₄B. In addition, 1.5 equivalents of **2** bind to $\Delta 65$ when the Ru-wire is present in 6-fold excess, suggesting that **2** may bind to both the active site and another portion of the protein.

Modeling of the proposed surface binding results in Ru-heme distances consistent with those calculated from experimental data (Figure 5.6). The proposed binding site is concave and hydrophobic. The Ru-wires present few opportunities for specific interactions with the protein surface. Instead, extensive hydrophobic contacts between the Ru-wire and the protein likely provide the free energy necessary for binding. Indeed, **1** binds most tightly, while **2** is the weakest binder. This interpretation is consistent with the previously observed binding of ruthenium-diimine complexes to cytochrome *c* oxidase at the surface patch known to bind cytochrome *c*.^{28,29}

Re-wires. The rhenium complexes $[\text{Re}(\text{CO})_3(\text{L}_2)(\text{L}')]^{1+}$, where L₂ is a 2,2'-bipyridyl or

Figure 5.5. Model of **2** bound to exposed heme of $\Delta 114$. The Ru-Fe distance in this model is 16.9 Å.

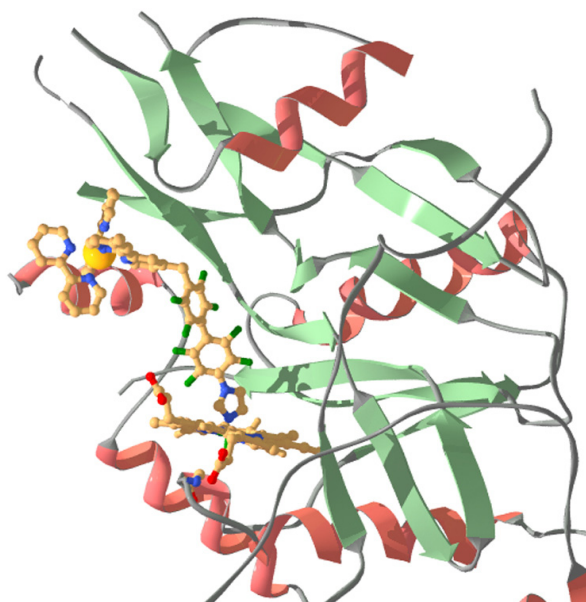
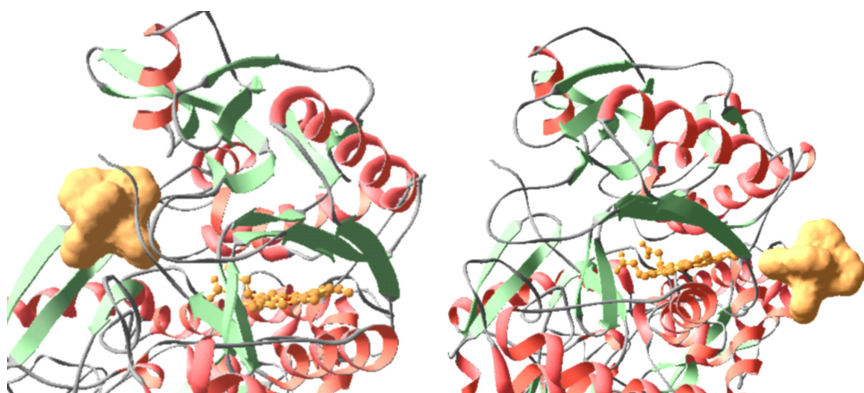


Figure 5.6. The NOS dimer, shown with Ru(bpy)₃ docked at the mouth of the substrate access channel (*left*), or at the proposed reductase binding site (*right*). The Ru-Fe distance is 24 Å when the Ru-diimine is bound in the substrate access channel, and ~18 Å when it is bound at the reductase domain recognition site.



phenanthryl derivative and L' is a nitrogen donor such as imidazole or pyridine, are in general luminescent compounds with microsecond excited state lifetimes and redox properties analogous to Ru(bpy)₃ compounds. The excited state is both a good oxidant (1.2 V NHE) and reductant (-0.7 V NHE).³⁰ In addition, the photochemically generated species [Re(CO)₃(L₂)(L')]²⁺ is an extremely strong oxidant (~1.8 V vs. SCE).³¹

In order to take advantage of rhenium photochemistry, compounds **4** and **5** were synthesized by Wendy Belliston (Figure 5.7). The compounds are structurally similar to **1** and **3**, but the rhenium chromophore has significantly smaller bulk. The absorption spectra of **4** and **5** are identical, and typical of Re-diimine complexes. Both are luminescent, with emission spectra centered at 560 nm and quantum yields of 0.055.

Upon addition of **4** to Δ114 murine iNOSoxy, the heme Soret absorption shifts from 422 to 426 nm, indicative of imidazole ligation to the heme iron (Figure 5.8). Time-resolved luminescence measurements indicate that **4** is almost completely bound to NOS in 1:1 micromolar solutions. A K_d could not be determined from the luminescence decay data due to the rapidity of the luminescence decay and the almost complete absence of a slow luminescence decay rate corresponding to **4** that is free in solution. Instead, a dissociation constant of 6 nM was calculated from a comparison of the steady-state luminescence spectra of **4** alone and bound to Δ114 iNOSoxy (Figure 5.9).

Figure 5.7. Re-wires. The fluorinated biphenyl bridging moieties were synthesized by reacting imidazole and perfluorobiphenyl in dimethylsulfoxide. The resulting mono- and disubstituted perfluorobiphenyl-imidazole ligands were separated by flash silica chromatography. $\text{Re}(\text{dimethylphenanthroline})(\text{CO})_3\text{Cl}$ was treated with silver triflate, and then reacted with either the mono- or disubstituted perfluorobiphenyl-imidazole ligand to form **4** and **5** as triflate salts.

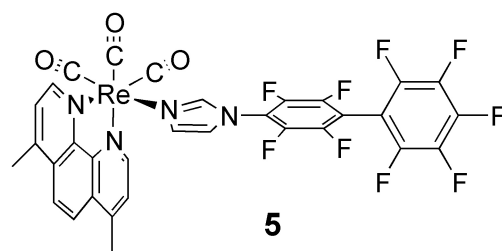
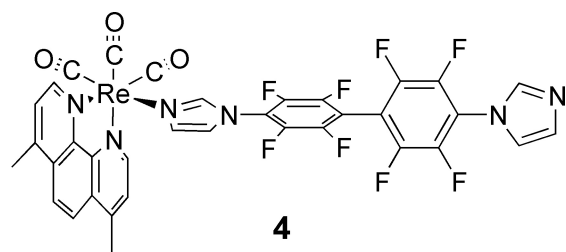


Figure 5.8. 10.2 μM $\Delta 114$ alone (green) and in the presence of 1 equivalent of **4**. The shift in the heme Soret is similar to that observed with **2**.

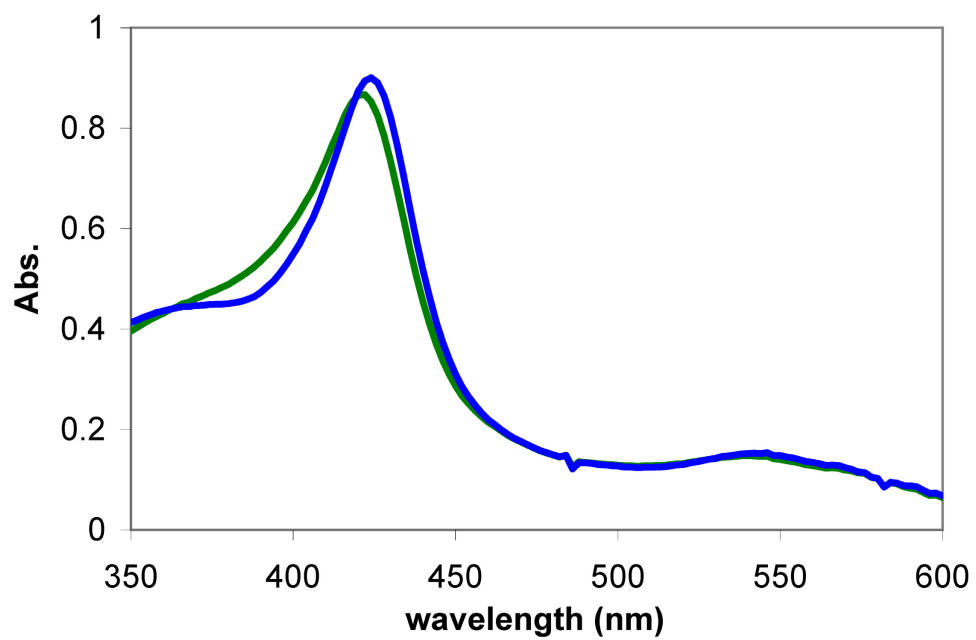
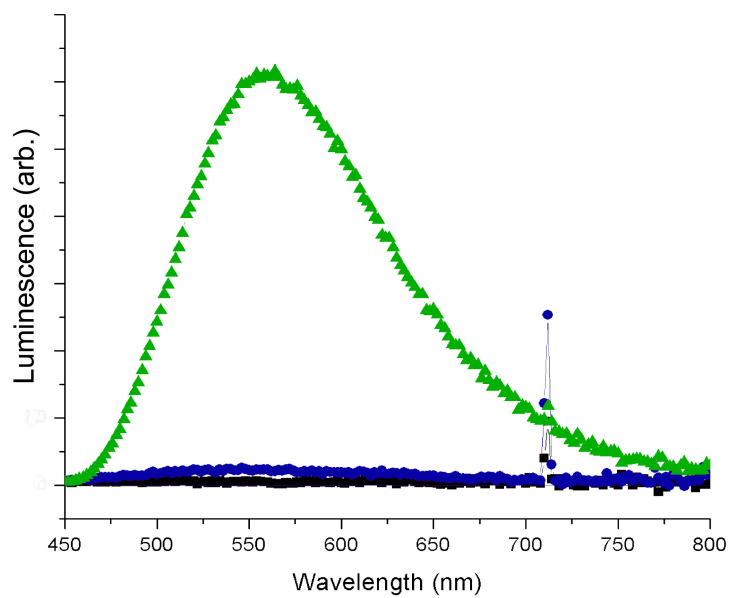


Figure 5.9. Steady-state luminescence spectra of 5.4 μM samples of $\Delta 114$ (black), **4** (green), and a 1:1 mixture of $\Delta 114$ and **4** (blue). The luminescence of **4** is almost completely quenched in the presence of $\Delta 114$, making it a sensitive indicator of the presence of the enzyme. Modified from a figure provided by Wendy Belliston.

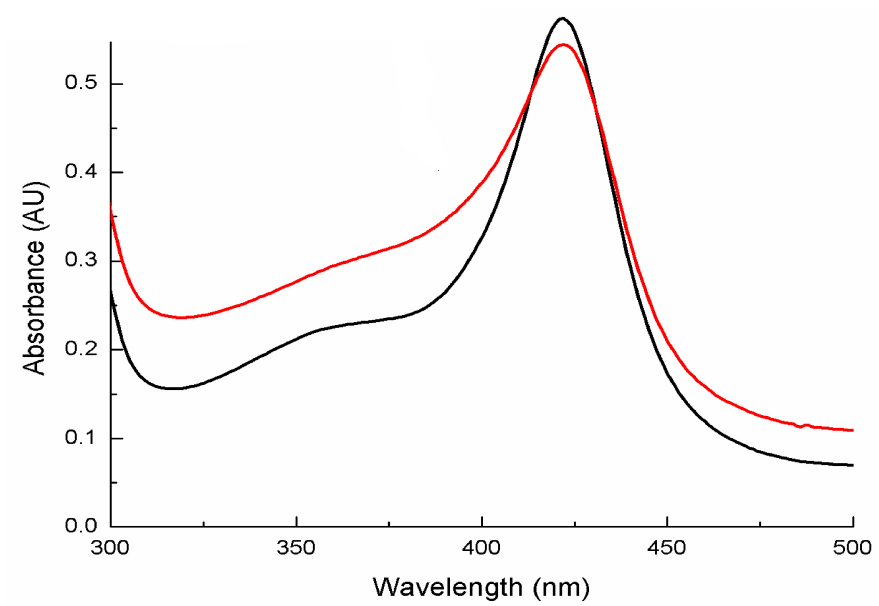


The compound **5** causes a blue-shift in the $\Delta 114$ heme Soret, indicating a partial conversion to high-spin, 5-coordinate heme (Figure 5.10). The time-resolved luminescence decay spectra indicate that **5** binds with a dissociation constant of $3.4 \mu\text{M}$ and a Re-heme distance of $\sim 18 \text{ \AA}$. Both the change in the Soret absorption spectrum and the calculated Re-Fe distance are consistent with **5** binding in the active site. However, H_4B binding is also known to sometimes result in a partial low- to high-spin conversion, so binding in the pterin pocket cannot be ruled out. The structural dissimilarities of **5** and Arg make it surprising that **5** binds at all. However, the relatively exposed active site of the monomeric $\Delta 114$ iNOSoxy provides good surface complementarity with the fluorinated biphenyl moiety.

DISCUSSION

Ru-wire binding to the distal side of iNOSoxy suggests a novel method for electron injection into the active site. As with cytochrome *c* oxidase, the Ru-diimine complex likely binds to the surface of the enzyme, leaving the active site free to bind the natural substrates arginine and N-hydroxyarginine. No photoreduction was observed in the present experiments, perhaps because of the weak electronic coupling provided by the protein matrix. Future investigations employing the bimolecular photochemical generation of reduced sensitizers may circumvent this difficulty.²³

Figure 5.10. UV-Visible absorption spectra of 6.6 μM $\Delta 114$ alone (black) and with a stoichiometric amount of **5** (red). The blue-shift in the absorption is indicative of a partial transition to high spin, five-coordinate iron.



NOS inhibitors are being investigated as potential treatments for several diseases.^{32,33} All currently known inhibitors bind in the active site of the enzyme. In contrast, Ru-wires or similar compounds may provide a novel means of NOS inhibition by preventing electron transfer (ET) between the reductase and oxidase domains. A NOS ET inhibitor would be a rare example of an inhibitor that works by preventing protein-protein interactions. Although such inhibitors are unusual, they are the subject of great interest due to the biological ubiquity and importance of transient protein complexes. These results, and other related studies (Chapter 4),²⁶ suggest that a conceptually simple and readily analyzed aspect of designing such inhibitors is the analysis of buried surface area in the inhibitor:protein complex.

The interactions of **2** and **4** with $\Delta 114$ are in many ways analogous to those observed with previously described inhibitors that prevent NOS holoenzyme dimerization.³⁴ Because only iNOS exhibits an appreciable monomer-dimer equilibrium *in vivo*, these inhibitors are highly isoform selective. The low dissociation constant of **4** makes it a useful lead compound for further iNOS inhibitor development. The three orders of magnitude difference in dissociation constants between **2** and **4** illustrates the steric influence of the Ru(bpy)₃ moiety.

The ability of **5** to bind in or near the NOSoxy active site is remarkable given its dissimilarity to Arg or known inhibitors. As with the Ru-wires, it seems likely that

binding is driven principally by hydrophobic interactions. Although **3** binds NOS more tightly than **5**, it does not produce a similar shift in the absorption spectrum, again demonstrating the importance of steric bulk in modulating probe-NOS interactions.

CONCLUDING REMARKS

Our results demonstrate the utility of FET measurements in characterizing small-molecule:protein interactions. Conventional UV-visible absorption measurements or competition binding assays would have overlooked the ability of **1** and **3** to bind NOSoxy. This study also shows that FET measurements can provide valuable structural information about the probe:enzyme conjugate. Similar luminescent probes may be useful in studying other heme enzymes, and more broadly proteins that emit or absorb light.

ACKNOWLEDGEMENT

This research was funded by the Fannie and John Hertz Foundation (ARD) and the National Science Foundation.

REFERENCES

- (1) Kendrick, K. M.; Guzman, R. G.; Zorrilla, J.; Hinton, M. R.; Broad, K. D.; Mimmack, M.; Okura, S. *Nature* **1997**, *388*, 670-674.
- (2) Huang, P. L.; Huang, H. H.; Mashimo, H.; Bloch, K. D.; Moskowitz, M. A.; Bevan, J. A.; Fishman, M. C. *Nature* **1995**, *377*, 239-242.
- (3) Ko, G. Y.; Kelly, P. T. *J. Neurosci.* **1999**, *19*, 6784-6794.
- (4) Luth, H. J.; Holzer, M.; Gertz, H. J.; Arendt, T. *Brain Research* **2000**, *852*, 45-55.
- (5) Mize, R. R.; Dawson, T. M.; Dawson, V. L.; Friedlander, M. J. *Nitric Oxide in Brain Development, Plasticity and Disease*; Elsevier, 1998.
- (6) Nathan, D. *J. Clin. Invest.* **1997**, *100*, 2417-2423.
- (7) Lancaster, J. *Nitric Oxide: Principles and Actions*; Academic Press: San Diego, CA, 1996.
- (8) Hobbs, A. J.; Higgs, A.; Moncada, S. *Annu. Rev. Pharmacol. Toxicol.* **1999**, *39*, 191-220.
- (9) Heales, S. J. R.; Bolanos, J. P.; Stewart, V. C.; Brookes, P. S.; Land, J. M.; Clark, J. B. *Biochim. Biophys. Acta-Bioenerg.* **1999**, *1410*, 215-228.
- (10) Hingorani, A. D.; Liang, C. F.; Fatibene, J.; Lyon, A.; Monteith, S.; Parsons, A.; Haydock, S.; Hopper, R. V.; Stephens, N. G.; O'Shaughnessy, K. M.; Brown, M. J. *Circulation* **1999**, *100*, 1515-1520.

- (11) Stuehr, D. J. *Biochim. Biophys. Acta* **1999**, *1411*, 217-230.
- (12) Cho, H. J.; Xie, Q. W.; Calaycay, J.; Mumford, R. A.; Swiderek, K. M.; Lee, T. D.; Nathan, C. J. *J. Exp. Med.* **1992**, *176*, 599-604.
- (13) Brecht, D. S.; Hwang, P. M.; Glatt, C. E.; Lowenstein, C.; Reed, R. R.; Snyder, S. H. *Nature* **1991**, *351*, 714-718.
- (14) Crane, B. R.; Rosenfeld, R. J.; Arvai, A. S.; Ghosh, D. K.; S.Ghosh; Tainer, J. A.; Stuehr, D. J.; Getzoff, E. D. *EMBO J.* **1999**, *18*, 6271-6281.
- (15) Siddhanta, U.; Wu, C. Q.; Abu-Soud, H. M.; Zhang, J. L.; Ghosh, D. K.; Stuehr, D. J. *J. Biol. Chem.* **1996**, *271*, 7309-7312.
- (16) Kobayashi, K.; Tagawa, S.; Daff, S.; Sagami, I.; Shimizu, T. *J. Biol. Chem.* **2001**, *276*, 39864-39871.
- (17) Panda, K.; Ghosh, S.; Stuehr, D. J. *J. Biol. Chem.* **2001**, *276*, 23349-23356.
- (18) Abu-Soud, H. M.; Yoho, L. L.; Stuehr, D. J. *J. Biol. Chem.* **1994**, *269*, 32047-32050.
- (19) Crane, B. R.; Arvai, A. S.; Gachhui, R.; Wu, C.; Ghosh, D. K.; Getzoff, E. D.; Stuehr, D. J.; Tainer, J. A. *Science* **1997**, *278*, 425-431.
- (20) Raman, C. S.; Li, H. Y.; Martasek, P.; Kral, V.; Masters, B. S. S.; Poulos, T. L. *Cell* **1998**, *95*, 939-950.

- (21) Poulos, T. L.; Li, H. Y.; Raman, C. S.; Schuller, D. J. In *Advances in Inorganic Chemistry, Vol 51*, 2001; Vol. 51, pp 243-293.
- (22) Dmochowski, I. J.; Crane, B. R.; Wilker, J. J.; Winkler, J. R.; Gray, H. B. *Proc. Natl. Acad. Sci. USA* **1999**, *96*, 12987-12990.
- (23) Wilker, J. J.; Dmochowski, I. J.; Dawson, J. H.; Winkler, J. R.; Gray, H. B. *Angew. Chem. Int. Ed. Eng.* **1999**, *38*, 90-92.
- (24) Dmochowski, I. J.; Dunn, A. R.; Wilker, J. J.; Crane, B. R.; Green, M. T.; Dawson, J. H.; Sligar, S. G.; Winkler, J. R.; Gray, H. B. *Methods Enzymol.* **2002**, *357*, 120-133.
- (25) Dunn, A. R.; Dmochowski, I. J.; Bilwes, A. M.; Gray, H. B.; Crane, B. R. *Proc. Natl. Acad. Sci. U. S. A.* **2001**, *98*, 12420-12425.
- (26) Dunn, A. R.; Hays, A. M. A.; Goodin, D. B.; Stout, C. D.; Chiu, R.; Winkler, J. R.; Gray, H. B. *J. Am. Chem. Soc.* **2002**, *124*, 10254-10255.
- (27) Ghosh, D. K.; Wu, C. Q.; Pitters, E.; Moloney, M.; Werner, E. R.; Mayer, B.; Stuehr, D. J. *Biochemistry* **1997**, *36*, 10609-10619.
- (28) Zaslavsky, D.; Sadoski, R. C.; Wang, K. F.; Durham, B.; Gennis, R. B.; Millett, F. *Biochemistry* **1998**, *37*, 14910-14916.
- (29) Zaslavsky, D.; Kaulen, A. D.; Smirnova, I. A.; Vygodina, T.; Konstantinov, A. A. *FEBS Lett.* **1993**, *336*, 389-393.

- (30) Connick, W. B.; DiBilio, A. J.; Hill, M. G.; Winkler, J. R.; Gray, H. B. *Inorg. Chim. Acta* **1995**, *240*, 169-173.
- (31) Sacksteder, L.; Zipp, A. P.; Brown, E. A.; Streich, J.; Demas, J. N.; Degraff, B. A. *Inorg. Chem.* **1990**, *29*, 4335-4340.
- (32) Salerno, L.; Sorrenti, V.; Di Giacomo, C.; Romeo, G.; Siracusa, M. A. *Curr. Pharm. Design* **2002**, *8*, 177-200.
- (33) Vallance, P.; Leiper, J. *Nat. Rev. Drug Discov.* **2002**, *1*, 939-950.
- (34) McMillan, K.; Adler, M.; Auld, D. S.; Baldwin, J. J.; Blasko, E.; Browne, L. J.; Chelsky, D.; Davey, D.; Dolle, R. E.; Eagen, K. A.; Erickson, S.; Feldman, R. I.; Glaser, C. B.; Mallari, C.; Morrissey, M. M.; Ohlmeyer, M. H. J.; Pan, C. H.; Parkinson, J. F.; Phillips, G. B.; Polokoff, M. A.; Sigal, N. H.; Vergona, R.; Whitlow, M.; Young, T. A.; Devlin, J. J. *Proc. Natl. Acad. Sci. U. S. A.* **2000**, *97*, 1506-1511.

APPENDIX A

Synthesis and characterization of Ru-wires

Syntheses

General: NMR spectra were taken on a General Electric QE300 or Varian Mercury 300. Electrospray mass spectral data were collected on a Finnigan LCQ quadrupole ion trap mass spectrometer.

$\text{Ru}(\text{tmbpy})_2\text{Cl}_2$ (tmbpy = 4,4',5,5'-tetramethyl-2,2'-bipyridine) was synthesized by a standard procedure.¹ THF was purified by refluxing over calcium hydride for at least 3 days followed by distillation under Argon onto activated 3 Å molecular sieves. Dimethyl sulfoxide (DMSO) was stored over calcium hydride and distilled under argon immediately before use. All other reagents were obtained from the Aldrich Chemical Co. and used as received unless otherwise noted.

4-perfluorobiphenylmethyl-4'-methyl-2,2'-bipyridine (5). 0.50 g 4,4'-dimethyl-2,2'-bipyridine (Me_2bpy) (2.7 mmol) was dissolved in 100 mL dry THF. 1.4 mL LDA (2M) in ether (Aldrich Chemical Co.) was added dropwise under an argon atmosphere. In a separate flask, 1.36 g perfluorobiphenyl (4.07 mmol) was dissolved in 30 mL dry THF. The deprotonated Me_2bpy solution was cannulated into the perfluorobiphenyl solution with fast stirring at room temperature over 20 minutes. After the reaction mixture had stirred for several hours the solvent was removed under vacuum. The residue was then dissolved in 150 mL 1:2 (v/v) $\text{CH}_2\text{Cl}_2/\text{Et}_2\text{O}$ and extracted with 150 mL brine. The aqueous layer was extracted with 2x150 mL Et_2O , and the combined organics were

concentrated to dryness under vacuum. The crude product was then purified by flash chromatography using a 20 to 50% ethyl acetate/hexanes gradient. The desired product was the second band that eluted from the column. Yield: 247 mg, 18.4%. ^1H NMR (CDCl_3 , 300 MHz) 8.57 (1H, d, $J=5$ Hz) 8.49 (1H, d, 5 Hz) 8.32 (1H, s) 8.14 (1H, s) 7.15 (1H, d, $J=4$ Hz) 7.10 (1H, d, $J=4$ Hz) 4.17 (2H, s) 2.39 (3H, s) ^{19}F NMR (CDCl_3 , 300 MHz) -137.62 (2F, m) -138.49 (2F, dd, $J=20$, 11 Hz) -141.78 (2F, dd, $J=22$, 12 Hz) -150.69 (1F, t, $J=28$ Hz) -160.95 (2F, m).

4-(4,4'-dimethyl-2,2'-bipyridine),4'-2-aminoadamantyl-octafluorobiphenyl (6). 100 mg **5** (0.200 mmol), 30.4 mg 2-amino-adamantane (0.200 mmol), and 32 mg K_2CO_3 were added to 0.2 mL dry DMSO. The reaction was heated under argon at 80 °C for 16 hours, then at 110 °C for 6 hours. The reaction mixture was diluted with 100 mL 1:2 v/v $\text{CH}_2\text{Cl}_2/\text{Et}_2\text{O}$, and extracted once with saturated aqueous Na_2CO_3 . The organic phase was concentrated to dryness under reduced pressure. The crude product was purified by column chromatography using 2% MeOH in CH_2Cl_2 as the eluent. Yield: 99 mg (76.4 %). ^1H NMR (CDCl_3 , 300 MHz) 8.55 (1H, d, $J=5$ Hz) 8.48 (1H, d, 5 Hz), 8.29 (1H, s) 8.14 (1H, s) 7.13 (1H, d, $J=5$ Hz) 7.08 (1H, d, $J=4$ Hz) 4.38 (1H, m) 4.19 (2H, s) 3.87 (1H, m) 2.43 (3H, s) 1.96 (2H, m) 1.83 (3H, m) 1.77 (1H, m) 1.69 (6 H, m) 1.61 (1H, m) 1.56 (1H, m) ^{19}F NMR (CDCl_3 , 300 MHz) -138.91 (2F, dd, $J=22$, 11Hz) -141.59 (2F, m) -143.01 (2F, dd, $J=21$, 13 Hz) -160.77 (2F, d, $J=19$ Hz).

4-(4,4'-dimethyl-2,2'-bipyridine),4'-N-imidazole-octafluorobiphenyl (7). 40 mg **5** (0.08 mmol), 5.7 mg imidazole (0.08 mmol), and 13 mg K_2CO_3 were dissolved in 0.08 mL dry DMSO. The reaction was stirred at room temperature for 3 days, after which the reaction mixture was diluted with 10 mL each CH_2Cl_2 and H_2O . The aqueous layer was washed three times with 10 mL CH_2Cl_2 . The combined organics were evaporated to dryness under reduced pressure, and the crude product was purified by column chromatography using 4% MeOH in CH_2Cl_2 as the eluent. Yield: 26.8 mg (61%) 1H NMR (CD_2Cl_2 , 300 MHz) 8.59 (1H, d, J=5 Hz) 8.50 (1H, d, J=5 Hz) 8.39 (1H, s) 8.26 (1H, s) 7.81 (1H, m) 7.29 (1H, m) 7.26 (1H, m) 7.22 (1H, d, J=5 Hz) 7.15 (1H, d, J=4 Hz) 4.25 (2H, s) 2.42 (3H, s) ^{19}F NMR (CD_2Cl_2 , 300 MHz) -135.38 (2F, dd, J=22, 11 Hz) -137.27 (2F, dd, 22, 11 Hz) -140.49 (2F, J=22, 11 Hz) -146.80 (2F, J=25, 11 Hz).

[Ru-F₈bp-Ad](NO₃)₂ (1). 24.5 mg $Ru(bpy)_2Cl_2$ (0.048 mmol) and 30 mg **6** (0.048 mmol) were dissolved in 3 mL 6:3:1 ethanol:chloroform:water. Oxygen was removed by three cycles of freeze-pump-thawing. The reaction mixture was heated to 80 °C for 14 h, after which the solvent was removed under vacuum. The desired product was isolated using flash chromatography, using 12:2:3 acetonitrile:water:ethanol saturated with KNO_3 as eluent. The fractions containing product were concentrated to dryness under reduced pressure, and the product was extracted from the resulting salt with CH_2Cl_2 . The resulting solution was filtered, then evaporated to dryness. The product was redissolved

in CH₂Cl₂ and filtered over a 0.45 μM teflon filter (Amicon). Removal of the solvent gave the product as a red, amorphous solid. Yield: 40 mg (70 %). ¹H NMR (CD₂Cl₂, 300 MHz) 8.56 (4H, m) 8.46 (1H, s) 8.37 (1H, s) 8.03 (4H, m) 7.74 (4H, m) 7.64 (1H, d, J=6 Hz) 7.57 (1H, d, J=6 Hz) 7.41 (4H, m) 7.28 (2H, t, J=5 Hz) 4.53 (1H, m) 4.38 (2H, s) 3.97 (1H, m) 2.56 (3H, s) 2.01 (2H, m) 1.85 (4H, m) 1.77 (2H, m) 1.73 (4H, m) 1.68 (1H, s) 1.63 (1H, s) ¹⁹F NMR (CD₂Cl₂, 300 MHz) -137.21 (2F, dd, J=22, 11) -140.71 (2F, dd, J=24, 11 Hz) -141.11 (2F, dd, J=22, 13) -159.18 (2F, d, J=15 Hz) ESI-MS m/z 521.7 (M+2).

[Ru-F₈bp-im](NO₃)₂ (2). This compound was synthesized in analogy to **1** from 26.8 mg **7** (0.049 mmol) and 25.5 mg Ru(bpy)₂Cl₂ (0.049 mmol). Yield: 15.3 mg (28.8%) ¹H NMR (CD₂Cl₂, 300 MHz) 8.61 (4H, m) 8.50 (1H, s) 8.50 (1H, s) 8.06 (4H, m) 7.79 (1H, d, J=6 Hz) 7.76 (1H, s) 7.74 (4H, m) 7.64 (1H, d, J=6 Hz) 7.54 (1H, d, J=6 Hz) 7.49 (4H, m) 7.29 (1H, m) 7.25 (1H, s) 4.45 (2H, s) 2.58 (3H, s) ¹⁹F NMR (CD₂Cl₂, 300 MHz) -135.43 (2F, dd, J=22, 11) -136.51 (2F, d, J=22, 11 Hz) -139.74 (2F, dd, J=22, 11 Hz) -146.55 (2F, dd, J=22, 10.0 Hz) ESI-MS m/z 480 (M+2).

[tmRu-F₈bp-im](Cl)₂ (3). 17.6 mg Ru(tmbpy)₂Cl₂ (29.8 μmol) and 15.2 mg **7** (29.8 μmol) were dissolved in a mixture of 1mL THF, 1mL EtOH, and 0.25 mL water. The reaction mixture was deaerated using 3 freeze-pump-thaw cycles and heated to 60 °C under argon for 12 h. The reaction mixture was concentrated under reduced pressure,

and purified using flash chromatography with a mixture of 18:1:1 acetonitrile:EtOH:water saturated with KNO_3 as eluent. The fractions containing product were pooled and concentrated to dryness, then extracted with CH_2Cl_2 to yield the product. Yield: 10.4 mg (30%). The nitrate counterion was exchanged for chloride using a CM Sepharose cation exchange column (2x13 cm) and 1M NaCl as eluent. The fractions containing product were diluted by 1/3 with brine and extracted with two 100-mL portions of CH_2Cl_2 . The CH_2Cl_2 solutions were pooled and concentrated to dryness. ^1H NMR (acetone D_6 , 300 MHz) 9.58 (1H, s) 9.27 (1H, s) 9.08 (2H, s) 9.07 (1H, s) 9.06(1H, s) 8.03 (1H, s) 7.83 (1H, d, J=6 Hz) 7.80 (1H, d, J=6 Hz) 7.66 (1H, s) 7.61 (1H, s) 7.59 (1H, s) 7.58 (1H, m) 7.48 (1H, s) 7.37 (1H, d, J=7 Hz) 7.35 (1H, d, J=7 Hz) 7.25 (1H, m) 4.63 (2H, s) 2.56 (3H, s) 2.49 (6H, s) 2.48 (6H, s) 2.10 (12H, m) ^{19}F NMR (acetone D_6 , 300 MHz) -139.85 (2F, dd, J=22, 11 Hz) -140.52 (2F, dd, J=22, 11 Hz) -142.68 (2F, dd, J=19, 11 Hz) -149.72 (2F, dd, J=22, 11 Hz) ESI-MS m/z 536.2 (M+2).

[tmRu-F₉bp(Cl)₂ (4). 20 mg $\text{Ru}(\text{tmbpy})_2\text{Cl}_2$ (31.6 μmol) and 16.5 mg **5** (33.2 μmol) were dissolved in a mixture of 1mL THF, 1mL EtOH and 0.25 mL water. Oxygen was removed using three freeze-pump-thaw cycles. The reaction was then heated to 65 °C under argon for 16 h. The reaction mixture was diluted with 50 mL CH_2Cl_2 , and washed with 50 mL sat. NaCl solution. The aqueous phase was washed with 3 25-mL portions of CH_2Cl_2 , and the combined CH_2Cl_2 solutions were concentrated to dryness under vacuum.

The product was purified by flash chromatography using 83:10:7 acetonitrile:ethanol:water saturated with KNO_3 as eluent. The fractions containing product were pooled and concentrated under reduced pressure until only water remained, diluted with 15 mL saturated NaCl solution, and washed with 3 25-mL portions of CH_2Cl_2 . The CH_2Cl_2 solutions were combined and concentrated under reduced pressure to give the red, luminescent product. Yield was > 90 %. ^1H NMR (acetone D_6 , 300 MHz) 9.20 (1H, s) 9.11 (1H, s) 8.95 (1H, s) 7.85 (4H, s) 7.84 (1H, d, $J=4$ Hz) 7.81 (1H, d, $J=6$ Hz) 7.68 (1H, s) 7.61 (1H, s) 7.60 (1H, s) 7.47 (1H, s) 7.37 (1H, d, $J=7$ Hz) 7.35 (1H, d, $J=7$ Hz) 4.60 (2H, s) 2.55 (3H, s) 2.48 (6H, s) 2.47 (6H, s) 2.09 (12H, m) ^{19}F NMR (acetone D_6 , 300 MHz) -140.05 (2F, m) -140.63 (2F, m) -142.82 (2F, m) -143.92 (1F, t, $J = 21$ Hz) -153.82 (2F, m). ESI-MS m/z 512 ($M+2$).

REFERENCES

1. Mines, G. A.; Bjerrum, M. J.; Hill, M. G.; Casimiro, D. R.; Chang, I.-J.; Winkler, J. R.; Gray, H. B. *J. Am. Chem. Soc.* **1996**, *118*, 1961-1965.

Appendix B

Dansyl probe syntheses and characterization and D-8-Ad:P450cam structure determination

Acknowledgements. The structure of the D-8-Ad:P450cam conjugate was determined by Anna-Maria A. Hays.

Syntheses.**Adamantane-1-carboxylic acid [4-(5-dimethylamino-naphthalene-1-sulfonylamino)-**

butyl]-amide (1): (D-4-Ad) 0.100 g (0.312 mmole) **3**, 74.5 mg (0.37 mmole) 1-adamantyl carbonyl chloride, and 0.11 mL (0.62 mmole) N,N-diisopropylethylamine were dissolved in 5 mL dry DMF under Ar and stirred overnight at ambient temperature.

The reaction mixture was diluted with 25 mL CH₂Cl₂, washed twice with water, and the organic phase concentrated under reduced pressure. The crude product was purified via flash chromatography using 9:1 MeOH:CH₂Cl₂ as eluent to give the product as a pale yellow-green solid. Yield 35.6 mg (24 %) ¹H NMR (CDCl₃) 8.53 (1H, d, J=8.4 Hz) 8.31 (1H, d, J=8.4 Hz) 8.22 (1H, dd, J=0.9, 7.2 Hz) 7.55 (1H, dd, J= 7.5, 8.4 Hz) 7.51 (1H, dd, J= 7.2, 8.4 Hz) 7.18 (1H, d, J=7.5 Hz) 5.63 (1H, m) 5.30 (1H, t, J=6.0 Hz) 3.11 (2H, m) 2.89 (2H, m) 2.88 (6H, s) 2.00 (3H, m) 1.77 (6H, m) 1.68 (6H, m) 1.42 (4H, m) ¹³C NMR (CDCl₃) 178.43, 152.16, 134.95, 130.58, 130.06, 129.81, 128.57, 123.44, 119.07, 115.41, 45.68, 43.10, 40.77, 39.45, 38.73, 36.72, 28.33, 26.99, 26.90. ESI-MS (m/z) 484.3 (M+H⁺).

Adamantane-1-carboxylic acid [4-(5-dimethylamino-naphthalene-1-sulfonylamino)-

octyl]-amide (2): Was prepared from **4** and 1-adamantyl carbonyl chloride in a manner identical to **1**. Yield 45%. ¹H NMR (CDCl₃) 8.53 (1H, d, J=8.4) 8.29 (1H, d, J=8.7) 8.24 (1H, dd, J=7.5, 1.2 Hz) 7.56 (1H, dd, J=7.5, 8.7 Hz) 7.52 (1H, dd, J=7.2, 8.4 Hz) 7.18

(1H, d, J=7.2 Hz) 5.58 (1H, m) 4.77 (1H, t, J=5.7 Hz) 3.17 (2H, m) 2.88 (6H, s) 2.87 (2H, m) 2.02 (3H, m) 1.90 (3H, m) 1.82 (3H, m) 1.70 (6H, m) 1.38 (4H, m) 1.14 (8H, m)) ^{13}C NMR (CDCl_3) 178.17, 152.20, 134.98, 130.57, 130.07, 129.86, 123.45, 118.98, 115.40, 45.67, 43.48, 40.77, 39.50, 38.83, 36.75, 36.65, 29.73, 29.17, 28.99, 28.36, 28.06, 26.86, 26.50. ESI-MS (m/z) 540.3 ($\text{M}+\text{H}^+$).

5-Dimethylamino-Naphthalene-1-sulfonic acid (4-amino-butyl)-amide (3):

Following the preparation by Ikunaga *et al.*,² 200 mg (0.75 mmole) dansyl chloride and 1.49 mL 1,4-diaminobutane (14.8 mmole) were dissolved in 5 mL CH_2Cl_2 and stirred for 2 hours under argon. The reaction mixture was loaded directly onto a flash silica column, and eluted using 4:1:1 CH_2Cl_2 :MeOH:Et₃N to give the product as a pale yellow-green oil. Yield 0.104 g (44 %) ^1H NMR (CDCl_3) 8.49 (1H, d, J=8.4 Hz) 8.36 (1 H, d, J=8.7 Hz) 8.20 (1H, d, J=7.5 Hz) 7.49 (1H, dd, J= 7.5, 8.7 Hz) 7.48 (1H, dd, J = 7.2, 8.4 Hz) 7.13 (1H, d, J=7.2 Hz) 5.3 (3H, overlapping m) 2.85 (6H, s) 2.84 (2H, m) 2.73 (2H, t, J=6.3 Hz) 1.52 (4H, m) ^{13}C NMR (CDCl_3) 152.00, 135.28, 130.25, 130.02, 129.81, 129.49, 128.32, 123.39, 119.28, 115.31, 45.61, 43.01, 40.61, 28.36, 27.22. ESI-MS (m/z) 322.2 ($\text{M}+\text{H}^+$).

5-Dimethylamino-naphthalene-1-sulfonic acid (4-amino-octyl)-amide (4):³ Was

prepared from 1,8-diaminooctane and dansyl chloride in an identical fashion to **3**. Yield 66%. ^1H NMR (CDCl_3) 8.49 (2H, d, J=8.4 Hz) 8.32 (2H, d, J=8.4 Hz) 8.20 (2H, dd,

J=0.9, 7.2) 7.52 (2H, dd, J=8.4, 7.5 Hz) 7.48 (2H, dd, J=7.2, 8.4 Hz) 7.14 (2H, d, J=7.5 Hz) 5.5 (3H, overlapping m) 2.85 (6H, s) 2.82 (2H, m) 2.75 (2H, t, J=7.2 Hz) 1.49 (2H, m) 1.33 (2H, m) 1.11 (8H, m) ^{13}C NMR (CDCl_3) 152.09, 135.25, 130.42, 130.05, 129.87, 129.60, 128.51, 123.43, 119.18, 115.36, 45.65, 43.39, 40.99, 30.44, 29.64, 28.95, 28.82, 26.51, 26.35. ESI-MS (m/z) 378.3 ($\text{M}+\text{H}^+$).

P450cam:D-8-Ad Crystallization and Data Collection. The C334A P450cam:D-8-Ad complex was formed at a molar ratio of 1:1 (400 μ M) at room temperature and crystallized by hanging drop vapor diffusion at 4° C. Crystals were obtained under 0.1 M citrate (pH 5.5), 200 mM KCl, 13% (wt/vol) polyethylene glycol (PEG; molecular weight = 8,000). For diffraction experiments, crystals were soaked in a solution containing 0.75 M citrate (pH 5.5), 150 mM KCl, 10% (wt/vol) PEG 8000, and 25% (wt/vol) PEG 400 for 1 minute and flash frozen in liquid nitrogen. Data were collected on an Raxis IV detector equipped with Osmic confocal mirrors and Xstream cryo-device (100K) using CuK_α radiation ($\lambda = 1.5418 \text{ \AA}$) from a Ru200 X-ray generator operated at 50 kV, 100 mA. Data were processed using DENZO and SCALEPACK.⁴ The space group was $P2_12_12_1$ with cell dimensions: $a = 64.95$, $b = 75.31$, $c = 93.17 \text{ \AA}^3$ (Matthews coefficient (V_M) = 2.50; solvent content = 49.9%).

Structure Determination. The structure was solved by molecular replacement using the program AMoRE⁵ with camphor-bound P450cam (PDB code 2cpp) as the initial model. After initial rigid body refinement in CNS,⁶ further refinement was carried out by iterative cycles of simulated annealing and B factor refinement using CNS and manual fitting using XFIT.⁷ The heme and D-8-Ad were located in $|F_o|-|F_c|$ electron density omit maps and further refined by simulated annealing and manual fitting. The difference

electron density map ($|F_{\text{obs}}| - |F_{\text{calc}}|$) of the D-8-Ad is well defined and continuous, and the average B-factor for D-8-Ad is moderately low (38 \AA^2) confirming the high occupancy of the ligand. The final model, which includes residues (11 – 414) of P450cam, D-8-Ad, heme, and 301 waters, gave $R_{\text{factor}}/R_{\text{free}}$ values of 20.2 and 24.7.

Table B.1. Diffraction and Refinement Statistics for P450cam complexed with D-8-Ad

Diffraction Data:	
PDB code	
Resolution (Å)	20 - 2.2
Unit Cell (Å)	a=64.95, b=75.31, c=93.17
Space Group	P2 ₁ 2 ₁ 2 ₁
Reflections (Total/Unique)	115720 / 21045
Multiplicity	5.2
Completeness (%)	93.3 (63.8)*
R _{sym}	0.102 (0.266)*
I/σ(I)	13.9 (2.5)*
Refinement Statistics:	
R _{factor} [§]	20.2 (28.5)*
R _{free} [¶]	24.7 (33.0)*
Average B (from Wilson plot, Å ²)	26.2
No. of protein atoms and Ave B, (Å ²)	3200, 25.4
No. of waters and Ave B, (Å ²)	301, 34.0
No. of heme atoms and Ave B, (Å ²)	43, 16.5
No. of D-8-Ad atoms and Ave B, (Å ²)	38, 38.9
Rms bonds, angles [†]	0.006 Å, 1.3°

* Outer shell statistics (2.30 – 2.20 Å)

[§] $R = \frac{\sum ||F_{obs}| - |F_{calc}||}{\sum |F_{obs}|}$ for all reflections (no σ cutoff).

[¶] Free R calculated using 4.8% as test set.

[†] rms deviations from ideal bond and angle restraints.

REFERENCES

1. Dmochowski, I. J.; Crane, B. R.; Wilker, J. J.; Winkler, J. R.; Gray, H. B. *Proc. Natl. Acad. Sci. U.S.A.* **1999**, *96*, 12987-12990.
2. Ikunaga, T.; Ikeda, H.; Ueno, A. *Chem. Eur. J.* **1999**, *5*, 2698-2704.
3. Macchia, M.; Salvetti, F.; Barontini, S.; Calvani, F.; Gesi, M.; Hamdan, M.; Lucacchini, A.; Pellegrini, A.; Soldani, P.; Marini, C. *Bioorg. Med. Chem. Lett.* **1998**, *8*, 3223-3228.
4. Otwinowski, Z.; Minor, W. *Methods Enzymol.* **1997**, *276*, 307-326.
5. Navaza, J. *Acta Crystallogr., Sect. A* **1994**, *50*, 157-163.
6. Brunger, A. T.; Adams, P. D.; Clore, G. M.; DeLano, W. L.; Gros, P.; Gross-Kunstleve, R. W.; Jiang, J. S.; Kuszewski, J.; Nilges, M.; Pannu, N. S.; Read, R. J.; Rice, L. M.; Simonson, T.; Warren, G. L. *Acta Crystallogr., Sect. D* **1998**, *54*, 905-921.
7. McRee, D. E. *J. Struct. Biol.* **1999**, *125*, 156-165.

Appendix C

Matlab deconvolution scripts

Introduction

The optical absorption kinetics discussed in Chapter 2 occur on the same timescale as the instrument response. Thus, it was necessary to deconvolute the instrument response from the observed kinetics. This appendix presents the Matlab scripts used for this purpose. While they were developed specifically for the kinetics observed in Chapter 2, these scripts can be easily modified to accommodate a wide variety of kinetics equations.

The process used is one of deconvolution by iterative reconvolution. A model of the kinetics is convolved with the response function, and the resulting convolved model is compared to the data. The model is then modified, and the process repeated until the fit between the data and the convolved model cannot be improved. This method has the advantage of working with an arbitrary response function. It is, however, slow compared to methods that assume a Gaussian response function.

Time and space limitations make a full discussion of deconvolution algorithms impractical. For an excellent discussion of deconvolution as related to time-resolved spectroscopy, see *Excited State Lifetime Measurements* by Demas.¹

This is the main module, optical_decon4.m

% fits OD data by first converting it into intensity and then deconvoluting the response
 % function by iterative reconvolution. Data are loaded as .txt single columns. The file
 % names are then converted over to the internal names resp (response) and int (intensity)

```

global time
global t_r
global interp
global interp_resp
global t_0_data
global t_0_resp
global kr
load bt_420_long.txt;           %CHANGE name of the raw OD data file
load bt_resp.txt;             %CHANGE name of the response function
                               %(intensity)
resp = bt_resp;               % CHANGE
int = 10.^(-(bt_420_long));    %CHANGE converts OD input into intensity
t = 5*(1:(length(int)));      %define a time axis 'time' with 5 ns spacing
time_resp = 5*(1:(length(resp))); %define a time axis for response function
                               %'time_resp'
time = 1:(5*length(int));     %define time a axis t with 1 ns spacing
t_r = 1:(5*length(resp));     %define a time axis t_r with 1 ns spacing
interp = spline(t, int, time); %interpolate data to 1 ns spacing using cubic spline
interp_resp = spline(time_resp, resp, t_r); %interpolate resp function
m = trapz(interp_resp);
interp_resp = interp_resp/m;   %normalizes the interpolated response function
% _____
%input guesses at parameters
% note: this version is for when the decay rate of the excited Ru* is known
c = -0.014;                    %CHANGE input guess for preexponential

```

```

kr = 0.037;          %CHANGE input measured Ru* decay exponential
kb = 0.19;          %CHANGE input guess for 2nd exponential
ksep = 0.0154;     %CHANGE input guess for rate of charge separation
t_0_data = 41 ;    % CHANGE input time 0 of data function 41
t_0_resp = 7.4 ;   % CHANGE input time 0 of response function 6
%_____
parameters = [c, kb, ksep];
[x,fval]= fminsearch('rutmim2',parameters) % rutmim2 is a function that contains the
                                           % kinetics equation specific to this system
                                           % fminsearch minimizes rutmim2 with
                                           % respect to the parameters in 'parameters'
out = rutmim_out2(x);                    % out is the non-convolved kinetics model
con_out = convolver2(interp_resp, out, 5*t_0_resp); %con_out is the convolved
                                                %kinetics model
resid = interp'-con_out;                  % calculates residual

```

This function, `rutmim.m`, contains the specific model to be fit.

```
function f = rutmim(p)
% this function returns the kinetics of an A->B->C process,
% given the parameters c, ka, kb, and the time vector t
% note in this version it is assumed that the decay rate of Ru* (kr) is known
global time
global t_0_data
global interp
global t_0_resp
global interp_resp
global kr
w = length(time);
temp = zeros(w,1);
for i = 0 : (w-(5*t_0_data))
    temp(i+(5*t_0_data)) = (p(1)/(p(2)+p(3)-kr))*((1-(p(3)/kr))*exp(-kr*i) - (1 -
(p(3)/(p(2)+p(3))))*exp(-(p(2)+p(3))*i) + (p(3)/kr) - (p(3)/(p(2)+p(3))));
end
% change the equation in the line above to fit a different kinetics model
% the parameters that are passed to this function will also have to modified accordingly
ideal = 10.^(-temp); %converts OD into intensity so that it can be convolved with the
                    %resp function
convolved = convolver2(interp_resp, ideal, 5*t_0_resp); % convolves interp_resp and
                    % ideal
f = sum(abs(convolved'-interp)); % function returns the sum of the absolute differences
                                % between the model (convolved) and the data (interp)
                                % this sum is what is minimized by fmimsearch
```

This function, `convolver2.m`, convolves one vector with another, in this case, the response function with the model.

```

function f = convolver(a,b,za)      % a is short vector, b is long one
n = length(b);                    % za is the zero point of a
flip = rot90(a);                  % flip = the resp. funct. run in reverse; row vector
m = length(a);
shift = -(m-za):1:(za-1);         % shifts t_0 to t_0 of resp. funct.
f = b;      % initially set conv product=obj (takes care of end effects)
for i = (m-(za-1)):(n-za)         % with t=0 at t_0_resp
    chunk = b(i + shift);        % define chunk of obj to be conv. w/resp
    int = flip.*chunk;           % define the integrand
    f(i) = trapz(int);           % point-wise convolution
end

% This function convolves two vectors. Beware of the conv. function
% built into Matlab, which is another thing entirely. Both a and b should
% be column vectors

```

This function, `rutmim_out.m`, produces a column vector containing the kinetics model.

```
function f = rutmim(p)
global time
global t_0_data
global interp
global t_0_resp
global interp_resp
global kr
w = length(time);
temp = zeros(w,1);
for i = 0 : (w-(5*t_0_data))
    temp(i+(5*t_0_data)) = (p(1)/(p(2)+p(3)-kr))*((1-(p(3)/kr))*exp(-kr*i) - (1 -
(p(3)/(p(2)+p(3))))*exp(-(p(2)+p(3))*i) + (p(3)/kr) - (p(3)/(p(2)+p(3))));
    end
f = 10.^(-temp);

% this function returns the kinetics of an A->B->C process,
% given the parameters c, ka, kb, and the time vector t
% note in this version it is assumed that the decay rate of Ru* (kr) is known
```

REFERENCES

1. Demas, J. N. *Excited State Lifetime Measurements*; Academic Press: New York, 1983.